Università degli Studi di Padova

Department of Information Engineering

Master Thesis in Master's Level Degree in Bioengineering

Application of spatial and temporal ICA on resting state fmri data to remove motion-related noise

Supervisor
Prof Alessandra Bertoldo
Università di Padova

Co-supervisor
PhD Erica Silvestri
Università di Padova

Master Candidate
Irene Piotto

Abstract

For over two decades resting state functional Magnetic Resonance Imaging (fMRI) has become an extremely popular area of research for neuroimaging as it measures spontaneous, low frequency fluctuations in the BOLD signal (Blood Oxygenation Level Dependent) to investigate the functional architecture of the brain. However fMRI data are influenced by non-neural processes that affect the results of any task-based or resting state fMRI experiment. Such processes arise from a variety of sources including subject motion, subject cardiac and respiratory cycles, and MRI scanner hardware artefacts.

One of the most problematic source of noise in resting state fMRI data (rs-fMRI) is subject head motion during scans: it causes image intensity to reflect not only blood oxygenation but also motion-related artefact. In this way signal intensity could change in fMRI data, causing peaks presence or drop of the signal. Compensating motion effects has always been an important issue in both resting state and task fMRI data analysis, and pre-processing steps as motion correction are not complete. Numerous correction methods for head motion artefact in rs-fMRI were developed, for example Power [1] has been the first researcher to find out a relation between motion and functional connectivity of rs-fMRI; moreover as possible solution of movement problem he proposed the *scrubbing* method which still remains one of the solutions more adopted. Recently methods have also been developed to automatically and selectively remove structured noise, so not only motion related, from fMRI data using for example machine learning classifiers and spatial Independent Components Analysis (sICA). For instance in 2014 Griffanti and colleagues developed a new method to identify artefactual components which include the application of single-subject ICA, followed by automatic component classification with FMRIB's ICA-based X-noiseifier (FIX) [2].

Noise is still an unresolved problem and no methods currently exist to selectively and completely remove global structured noise while retaining the global signal from neural activity. To solve this problem, last year Glasser and colleagues [3] published a new method which use the combination of the standard spatial ICA approach with the temporal ICA (tICA).

The aim of the present study is to implement Glasser's method, in particular the focus of this thesis is to select and remove motion-related noise sources.

In order to evaluate the effectiveness of implemented method on motion problem on rs-fmri data, it will be compared the results before and after tICA cleanup in terms of motion traces and functional connectivity.

Contents

Abstract **iii**

List of figures **vii**

List of tables **ix**

1 **Introduction** **1**

2 **Materials and Methods** **9**
2.1 **Dataset** . . . 9
2.1.1 **Pre-processing** . . . 10
2.2 **rs-fMRI data Processing** . . . 12
2.2.1 **Independent Component Analysis** . . . 13
2.2.2 **Denoising of Single Subject rs-fMRI** . . . 16
2.2.3 **Implementation of Glasser method** . . . 21
2.3 **Evaluation of Motion-Related Noise Reduction Procedure** 34
2.3.1 **DVARS Comparison** . . . 35
2.3.2 **QC-RSFC** . . . 35

3 **Results** **45**
3.1 **Denoising of Single Subject rs-fMRI** . . . 45
3.2 **Group spatial ICA** . . . 49
3.3 **Temporal ICA** . . . 53
3.4 **Indices** . . . 55
3.4.1 **Normalized Difference in Amplitude for DVARS dips** 55
3.4.2 **Variability between subjects:** $\boldsymbol{Variability}_{\mathbf{Amp}}$, $\boldsymbol{Diff}_{\mathbf{AmpDVARS}}$ . . . 63
3.5 **Identification of noise-related components** . . . 64
3.5.1 **Outlier Detection** . . . 66
3.5.2 **Thresholds selection** . . . 73
3.6 **Evaluation of Motion Related Noise Reduction Procedure** 79
3.6.1 **DVARS Comparison** . . . 79
3.6.2 **QC-RSFC** . . . 85

4 **Discussion** **93**
4.1 **Relation with the state-of-the-art** . . . 99

5 **Conclusions** **103**

Appendix A **FastICA Algorithm** **107**

Appendix B **Infomax Algorithm** **109**

Appendix C **ICASSO** **111**

References **114**

Listing of figures

2.1 Scheme of individual sICA step 12
2.2 Visual representation of sICA and tICA of fMRI 16
2.3 Illustration of PICA model [4] 18
2.4 Scheme of the procedure 21
2.5 Group-ICA procedure in GIFT 25
2.6 Example od DVARS trace with a chosen threshold 30
2.7 Connectivity matrix 37
2.8 Subjects connectivity matrix 39
2.10 Overview of FC matrices 42

3.1 Signal components from Melodic 46
3.2 Noise components from Melodic 47
3.3 Comparison Melodic-GIFT 50
3.4 Comparison on GIFT between different pre-processing. 51
3.5 Comparison Melodic-GIFT(Intensity normalization) 51
3.6 Comparison on GIFT between different algorithms. 51
3.7 Group Spatial ICA components from GIFT 53
3.8 Index quality group-ICA 54
3.9 Group temporal ICA components 55
3.10 Comparison between $DVARS_0$ and $nDVARS_0$ 56
3.11 DVARS de-meaned normalized with threshold $\pm$ 25 58
3.12 Histogram of higher 75 values of each subject's DVARS 59
3.13 Demeaned and normalized DVARS with thresholds 60
3.14 Difference in component amplitude between frames with DVARS dips/non-dips 62
3.15 Comparison between $Variability_{Amp}$ and $diff_{Amp}$ metrics 63
3.16 Difference between the maximum subject's component amplitude and the next highest one 64
3.17 Temporal ICA components identified as noise 65
3.18 $nDVARS_0$ traces of subject 5 66
3.19 $nDVARS_0$ with thresholds calculated with and without subjects 5 68
3.20 Distribution of concatenated DVARS without considering subjec 5 69
3.21 Histogram of distribution of concatenated DVARS 70
3.22 Example of DVARS traces with 2 Σ threshold 70

3.23 Comparison between DVARS Difference in component amplitude with and without subject 5 72
3.24 Representation of subject 5 influence on $diff_{Amp}$ plot 72
3.25 Comparison between $diff_{Amp}$ computed with and without subject 5 73
3.26 Difference in component amplitude between frames with DVARS dips/non-dips excluding subject 5 from tICA 74
3.27 Difference between the maximum subject's component amplitude and the next highest one excluding subject 5 from tICA 74
3.28 Representation of $diff_{AmpDVARS}$ and $diff_{Amp}$ computed without subject 5 in tICA analysis and with a new threshold 76
3.29 Representation of $diff_{AmpDVARS}$ and $diff_{Amp}$ computed without subject 5 in tICA analysis and with a new threshold 76
3.30 Group temporal ICA components to be removed 77
3.31 Examples of comparison of DVARS traces pre and post s-sICA . . 79
3.32 Examples of comparison of DVARS traces post s-sICA and post tICA 81
3.33 Examples of comparison of DVARS traces pre subjectwise sICA, post subjectwise sICA and post tICA 82
3.34 Sum of DVARS peaks difference 84
3.35 Structure of FC matrix 85
3.36 FC and p-values matrices resulting from QC-RSFC measure 86
3.37 FC matrices of subject 6 87
3.38 FC matrices of subject 10 87
3.39 Mean FC matrices among subjects 88
3.40 T-Tests on first comparison 89
3.41 T-Tests on second comparison 90
3.42 T-Tests on third comparison 90
3.43 FC and p-values matrices resulting from QC-RSFC measure 91

Listing of tables

3.1 Results coming from the application of Melodic to each subject individually 48
3.2 Comparison between MELODIC and GIFT for group-ICA analysis 49
3.3 Table of values of DVARS traces computed after s-sICA 57
3.4 Thresholds' values 61
3.5 Table of peaks over threshold 67
3.6 Thresholds' values excluding subject 5 67
3.7 Table of peaks over threshold without subject 5 71
3.8 Table of components number to remove after tICA with and without subject 5 and with different thresholds 75
3.9 Final choices to develop the entire procedure 78
3.10 Table of values of mean value of DVARS traces computed after s-sICA 83
3.11 Table of values of standard deviation of DVARS traces computed after s-sICA 83

1 Introduction

Functional magnetic resonance imaging (fMRI) is a powerful neuroscientific tool for non-invasively mapping brain activity and for estimating the functional interactions between brain areas. Its fundamental principle is based on the capacity of revealing the neuronal activity through cerebral hemodynamic. Through magnetic fields fMRI allows to observe variation of signal depending on metabolic and hemodinamic change present during cerebral activation induced by external or internal stimuli. An increment of synaptic activity provides at the beginning a reduction of oxygen concentration that requires a raise of blood flow due to an increased demand of oxygen. This bring to a reduction of deoxyhaemoglobin concentration (determined from the incrementation of cerebral activity), resulting in an unbalance between deoxy and oxy-hemoglobin concentrations. This physiological condition was demonstrated in 1890 from study results of Roy and Sherrington [5]. The difference of concentrations between deoxy and oxy-hemoglobin causes a variation of the signal that can be measured using fmri imaging methods such as echo-planar sequences. First experiments on fmri were performed by Ogawa et al. [6] on animals and it has been proved that, through magnetic fields with intensity grater that 1.5T and weighted $T2^*$ images, is possible to measure a signal depending on the level of deoxyhemoglobin present in different cerebral regions, the so called BOLD signal (Blood Oxygenation Level Dependent). It is not a direct measure of nervous tissue activity, but is an neuronal activity index since

it is associated to hemodinamic effects.

The acquisition of bold signal can be obtained submitting the subject to a particular task or in absence of any stimulus. The first method requires that the subject performs a certain task, but this results a limiting factor for subjects/patients that are unable to make even easy instructions, becoming thus not analysable cases. The latter method, called resting state fMRI (rs-fMRI), was first described by Biswal et al. in 1995 [7] which found out structure, organization, correlations among groups of brain regions that were known to function together, so even at rest the brain's different functional networks spontaneously fluctuate in their activity level. In particular he demonstrated highly correlated low frequency (<0.1 Hz) changes in BOLD signal between sensorimotor and supplementary motor cortices bilaterally in subjects at rest.
As opposed to task-based studies which model evoked activity from many trials or blocks of trials, rs-fmri occurs in the absence of a task or stimulus and investigates in synchronous activations between regions that are spatially distinct to identify resting state networks (RSNs): they are a set of brain regions that shows similarities in their BOLD timeseries obtained during rest, so when the brain is aware, conscious but there aren't any specific stimulus. Rs-fMRI can be used to inform about the inherent organization and functioning of the brain. Gaining a better understanding of the brain's intrinsic architecture and the level of communication that supports is an important basic neuroscience aim and may help understand how the brain enables complex information processing.
One of the benefits of rs-fMRI is that it requires only the MRI scanner for data acquisition: there is no need to present the subjects with any information or record any behavioural responses during the scan, individuals are instructed to simply rest. Rs-fMRI application has been growing in the research and clinical setting for the past 2 decades, since the absence of a task makes this technique particularly attractive because it is easy to acquire and it is feasible for patients who may have difficulty or are unable to perform tasks, such as pediatric patients or those with neurologic, neurosurgical and psychiatric conditions [8].

Resting state fMRI has rapidly emerged as a powerful and reliable approach to explore the human brain architecture. First approaches performed on brain functional studies exploit the so called functional segregation: it focuses on the local function of specific brain regions, is mainly used for brain mapping with the aim to

identify and isolate region functionally specialized in carrying out certain tasks. Then the interest focused on functional integration that studies the functional relationships or connectivity between different brain areas. For an assessment of functional integration features and so analyse rs-fmri, several methods were performed such as seed-based functional connectivity analysis, functional connectivity density analysis (FCD) and independent component analysis (ICA). One of the first ones employed in numerous studies [9] [10] is the seed-based analysis whose aim is to identify seed regions or regions of interest (ROIs) and correlate the average BOLD time course of voxels within these ROIs with each other and with the time courses of all other voxels in the brain. The computation of seed-based analysis is simple and the interpretation of the results is intuitive, but requires a priori selection of ROIs and because of its dependence on the selection of seeds, makes it vulnerable to bias.

FCD method was proposed recently in 2010 by Dardo Tomasi [11] as a data-driven method to overcome the limitations of seed-based approaches for the identification of highly connected areas, called hubs, in the human brain. It calculates the correlation of the BOLD time-series between each voxel and all the other voxels in the brain, showing the importance of functional hubs of brain connectivity. It is a data-driven method and not need any model assumptions to be performed.

Among different data-driven methods, one of the most popular rapidly developed in '90s and used in recent researches is the Independent Component Analysis (ICA): it was introduced at first in the '80s by J. Hérault and colleagues [12] [13] for a model of the encoding of movement in muscle contraction, but only in the '90s it started to receive attention from a portion of the scientific community, with first publications of ICA as fmri analysis method. Since then, ICA has become a well establish area of research. One of the first works on ICA application in fmri data has been published in 2003 [14] and focused on studying the separation of physiological signal sources of the brain in anaesthetized patients.

Using ICA application on fmri is possible to acquire signals related to brain neural activity, to highlight signals co-variations in networks of brain regions and to separate networks. Independent component analysis uses multivariate decomposition to disentangle the measured BOLD signal into several independent components. In particular fMRI data is decomposed into a set of timecourses and associated spatial maps. To identify the components number that compose fmri signal, ICA

assumes that these components are mutually and statistically independent in space (sICA) or time (tICA). Several methods exist to estimate this number and will be discussed later in this thesis work.
For fMRI dataset analyses, sICA is preferred because temporal points (few hundreds, corresponding to each occurrence of a functional image acquisition) are small compared to spatial ones (more than 10^5, corresponding to the number of voxels contained in a functional image), leading tICA to a computationally intractable mixing matrix. In contrast to seed-based method which extracts only the regions functionally connected to the chosen ROI, ICA uses a whole-brain approach.

Results of fMRI experiments not only reflect neural activity, but also are affected from the contribution of non-neuronal fluctuations [15]. In case of task-based fMRI the timing and intensity of the task is known a priori and the responses of many trials are averaged to eliminate or reduce noise due to non-neuronal sources and increase statistical significance. Instead in rs-fMRI the absence of a priori hypothesis of activation and externally triggered temporal references and the inability of performing averaging process make the problem of artefact identification and removal more difficult [16].
Noise sources are the major obstacle for resting state analysis because they can strongly influence the computation of temporal correlation of fMRI signal changes between different parts of the brain and, if not dealt with appropriately, it is possible for such noise sources to drive findings, leading to erroneous interpretations of fMRI results [17].
Non-neuronal fluctuation derives from a variety of sources, including subject motion, subject physiology and MRI scanner hardware artefacts. About the last one, recording devices and their accessories can affect MR image quality [18]. Some of artifacts, such as radio-frequency (RF) noise from interfering equipment, can be reduced or avoided altogether by careful acquisition; others instead are more difficult to avoid and need to be addressed during preprocessing, for example distortion of gradient magnetic fields and of the RF electromagnetic field, *drift*, which is a very slow change in the baseline BOLD signal over time, and *drop out* which is the loss of signal in certain areas. An important noise source in fMRI data is physiological in nature and his effects on resting state data occur through a variety of complex mechanisms caused by breathing and cardiac pulsations. In

particular the effects of breathing and of heart rate include pulsation in the brain causing local motion, changes in blood pressure and in blood oxygenation [17].
One of the most problematic cause of noise in resting state fMRI data is subject head motion which, during scans, causes brain matter position shifts in space and disrupts the establishment of magnetic gradients and subsequent readout of the BOLD signal. This problem has been highlighted starting from 2012 [1].
Motion effects can also be related to partial volume effects, spin history and field inhomogeneities variations. The first one derives from the fact that, because of the relatively coarse spatial resolution of fMRI, voxels at boundaries between tissue types sampled during fMRI are often made up of a combination of gray and white matter, and/or cerebrospinal fluid [17]. When head motion occurs, the relative contribution of the tissues may change because the same voxel represents a different position in the brain; hence further errors are introduced in BOLD signal measure because the peak of the true BOLD activation can be mismatched from the location of any voxels, decreasing the detection of the signal.
Regarding spin history effects, they appears when slice-selective RF pulses are used for excitation [19]. As it is known, an excitation MR pulse sequence is applied for acquisition of BOLD signal and it is based on the application of RF pulses. When a slice is acquired, in the case of no motion, regions of that slice excited by all pulses overlap resulting in the desired signal evolution. In the case of out-of-plane motion between pulses, movement influences the desired evolution: as consequence there is a reduction of desired signals and the generation of undesired resulting in artifacts.
Finally field inhomogeneities in the static magnetic field occur close to cavities of air, such as around the nasal sinuses, and cause signal drop.

Compensating motion effects has always been an important issue in resting state and task fMRI data analysis since the '90s with Friston et al. [20] which regressed out the 6 rigid body realignment parameters (translations and rotations), as well as their temporal derivatives, additionally including time-shifted and/or squared versions of these motion parameters.
Movement artefact is undesirable in fMRI studies and it is impossible to avoid it entirely despite movement reduction through appropriate padding and pillows. To solve this problem some pre-processing steps can be useful to remove part of signal related to motion, for example motion correction allows to deal with the

spatial misalignment from one volume to the next, in this way motion-related noise is partially removed.
Various correction methods for head motion artefact in rs-fMRI were developed in the last years starting from 2011 when three groups reported that small head movements produced spurious but structured (non-gaussian) noise in brain scans, bringing to distance-dependent changes in signal correlations [21]. In particular Power in 2012 [1] proposed a scrubbing method, called also censoring, that identifies motion-induced spikes in rs-fMRI time series. These data are removed with a temporal mask, and adjacent time points are temporally concatenated.
Since than, lots of researcher proposed several methods for structured noise removal from rs-fMRI data with regression models more and more complex. An important progress has been made through the development of automated methods for removing spatially specific structured temporal noise, using ICA as technique for detecting spatial components and separating signal from noise. In particular taking advantage of sICA and machine learning classifier, FMRIB's ICA-based Xnoiseifier (FIX) [2] and ICA-AROMA [22] were performed as automated approaches for cleaning fMRI data of various types of artefact. However also these methods incompletely removed noise sources because, according to Glasser [3], sICA is unable to segregate global temporal fluctuation in spatially signal and noise components. Hence a gold standard has not jet been achieved to selectively and completely remove global structured noise while retaining the global signal from neural activity.

To solve the problem recently Glasser and colleagues [3] proposed a fMRI data clean-up method based on ICA: temporal ICA (tICA) was used as additive procedure, after the standard sICA, to identify noise components in both task-based and resting state fMRI data coming from Human Connectome Project (HCP).
Until now tICA was rarely used because it is known that ICA works in input data matrix looking for the orthogonality along one of the axis (time or space), based on its orientation: because generally voxels number is superior compared to timepoints one, sICA is generally the chosen method. However sICA method is restricted precisely by the fact that estimated components must be spatially orthogonal and sparse effectively, and global components are difficult to make spatially uncorrelated with other global/non-global components, so sICA can't succeed at removing global artifacts. On the other hand, temporal ICA, which is

performed by transposing the fMRI data matrix used in sICA, allows to obtain temporally independent timeseries components and a mixing matrix constituted by spatial maps not orthogonal to each other. For this reason tICA should be capable to find global spatial maps.
Glasser et al. used the combination of spatial and temporal ICA to obtain independent component maps and timecourses, then taking into account some noise measure metrics they managed to classify and remove noise components. In particular their work exploited the acquisition of physiological data, obtained during scan through a respiratory belt and a heart rate monitor, and converted them into 14 physiological regressors: 4 cardiac, 4 respiratory and 4 interaction regressors, a heart rate regressor and a Respiration Volume per Time regressor (RVT). These physiological measures were then compared with component timeseries of tICA, showing a particular strong relationship between the tICA components and respiration. Another parameter used as index of task and resting state fMRI component classification is the measure of derivative of root mean square variance over voxels DVARS (D referring to temporal derivative of timecourses, VARS referring to root-mean-square variance over voxels) as modelling subject motion [1]. DVARS is a measure of how rapidly signal changes from volume to volume and so it is used to identify those volumes that are affected by excessive motion. Glasser and colleagues focused on the identification of spikes in the timeseries DVARS traces of each subject because these peaks and dips should reflect image intensity changes and so represent some movement of subject during the acquisition.

In this work of thesis attempts have been made to replicate Glasser procedure, implemented ex novo, to evaluate and quantify the capability of the proposed method in removing motion influence on rs-fMRI data and functional connectivity FC. Current method will be applied on a different dataset, characterized by rs-fMRI data. Hence the entire analysis will focus on removing motion-related noise components through application of spatial and temporal ICA. To do that some of the measures proposed by Glasser will be implemented, others instead will be introduced to evaluate the applied procedure. In particular the effectiveness of Glasser procedure for removal of motion sources will be evaluated at first using DVARS as measure of the change rate of BOLD signal at each time point. In particular for each patient several DVARS measures will be computed in different

steps of entire procedure to analyse if DVARS traces improve after spatial and temporal ICA, reducing their peaks. Another metric used is QC-RSFC (QC referring to quality control, measured by mean FD in the present example, RSFC denoting resting state functional connectivity) developed by Power [21]: the aim is to quantify the impact of motion on functional connectivity correlations, so analyse how connections between the obtained networks are related to movement.

2
Materials and Methods

2.1 Dataset

Data are part of a multi-modal studio on the impact of glioma on cognitive functions, composed of 13 patients 25 to 83 years of age with high-low grade glioma. At University-Hospital of Padova, Department of Medicine, Nuclear Medicine Unit both anatomical and functional images were acquired through Biograph mMR PET-MR system of Siemens. Anatomical images will need for the identification and definition of tumours, whereas functional ones were obtained asking patients to stay still, relaxed and with open eyes.Images were acquired following MR brain imaging protocol. Structural images:

- A three-dimensional T1-weighted Magnetization-Prepared Rapid Gradient-Echo (MPRAGE) sequence covering the whole brain was performed with time of repetition (TR) /time of echo (TE) 2400/3.2 ms, voxel dimension of 1x1x1mm^3 , field of view (FOV) of 256 mm and 160 slices;
- A three-dimensional T2-weighted with TR/TE 3200/536ms, voxel dimension of 1x1x1mm^3, FOV of 256 mm and 160 slices;
- A three-dimensional T2-weighted Fluid Attenuated Inversion Recovery (FLAIR) sequence with TR/TE 5000/395 ms, voxel dimension of 1x1x1mm^3, FOV of 250 mm and 160 slices.

Resting State fmri data:

- Echo-planar Imaging (EPI) sequence and SMS (CMRR, R014) 2 were performed with the following parameters: TR/TE of 1260/30 ms, FA of 68° (set by Ernst Criteria), voxel dimension of 3x3x3mm^3, FOV of 204 mm, 40 slices, anterior-posterior (AP) phase encoding direction and 750 dynamic scans lasting a total of about 15 minutes.

- Two fMRI geometrically matched spin echo (SE) EPI, two-fold acceleration with Generalized Autocalibration partial parallel Imaging (GRAPPA), SMS 1, AP and posterior-anterior (PA) phase encoding direction.

The fMRI SMS-EPI pulse sequences included in the acquisition protocol were provided by University of Minnesota's Center for Magnetic Resonance Research (CMRR) through a master research agreement (MRA) with Siemens and then a Core Competence Partnership (C2P) agreement with CMRR.

2.1.1 Pre-processing

Software used for pre-processing were Advanced Normalization Tools software (ANTs [23]), FMRIB Software Library (FSL [24]), MATLAB and ITK-SNAP [25].

Anatomical Images Pre-processing

The tumor extent was manually delineate by an expert physician using the FLAIR as well as the T2w image by means of ITK-SNAP tool. A normalization to MNI152 2009 symm space [26] is performed through patients T1w.

Functional Images Pre-processing

Data analysis follows state-of-the-art standard pipelines:

- Slice Timing: the aim of this step is to correct for the slight difference in the time at which each slice of BOLD was acquired (i.e. some slices are acquired at the start of the TR, whereas others are acquired later). All slices related to a same volume are temporally realigned in order to actually consider them sampled at the same temporal instant .

- Readout distortion correction (using the two SE images) used to reduce or eliminate magnetic field inhomogeneities.
- Motion correction using affine transforms and as reference the functional single band image. The aim of this process is to correct the effect of subject head motion in the scanner.
- Co-registration: In order to perform group-level analyses it is essential to re-sample all subjects to a common "standard" space. In this case subjects' images are registered to MNI152 2009 symm space.

The main aim of preprocessing is to prepare the resting state data for subsequent functional connectivity analysis by reducing the influence of artifacts and other types of structured noise. The reported pre-processing steps are in line with the pipeline followed by Glasser et al., i.e. distortion correction, motion correction and image alignment.

2.2 rs-fMRI data Processing

The denoising method developed by Glasser uses as input the pre-processed data previously cleaned individually by sICA+FIX method [2] which allows to denoise spatially specific temporal artefacts. FIX algorithm automatically classifies the resulting sICA components as signal or noise using training weights previously established with the FIX machine learning classifier.
To obtain similar initial data condition, the available dataset has to be cleaned individually, this will be performed through Melodic (Multivariate Exploratory Linear Decomposition Into Independent Components) toolbox [27] that allows to identify independent components. Then the independent component spatial maps will be manually classified into signal or noise, according to [28] and [29]. Noise components were removed in order to clean subjects data, resulting new cleaned images for each subject. All this first step can be seen in figure 2.1 and it will be discussed in more detail in the next three paragraphs. In particular an introduction of basic theory of ICA will be explained, then the Melodic functioning will be introduced, finally the process of identification and removal of noise components will be described.

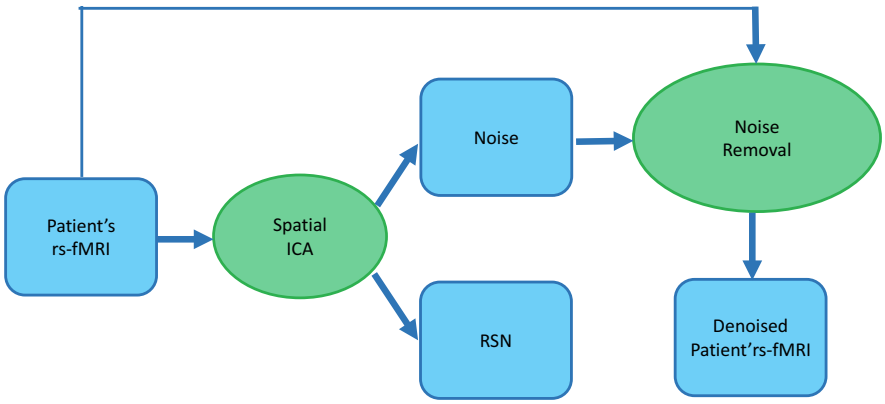

Figure 2.1: Scheme of individual sICA performed through Melodic toolbox. Data are blue and algorithms are green. *Spatial ICA* is performed individually on *Patient's rs-fMRI* data, obtaining independent components. Noise one are manually identified and removed from original rs-fMRI data, resulting *Denoised Patient's rs-fMRI*

Finally in the last paragraph of this sub-chapter the Glasser method will be described, as well as the implementation of that method developed in this work.

2.2.1 Independent Component Analysis

Independent component analysis (ICA) is a statistical technique whose aim is to recover hidden underlying source signals from an observed mixture of these sources.
In standard ICA the mixture is supposed to be linear and the hypothesis made is that the sources are statistically mutually independent and are not Gaussian. The observed signal in a certain voxel is described as the sum of the contributions of all independent sources present in dataset.
Assuming M zero mean signals/sources $s_1, s_2, ..., s_M$, N linear combinations of these sources are observed. The j-th observed variable can be written as:

$$x_j = a_{j1}s_1 + a_{j2}s_2 + \cdots + a_{ji}s_i \qquad \text{with} \qquad i = 1, \ldots, M \qquad j = 1, \ldots, N$$

that in matrix format:

$$X = AS \tag{2.1}$$

representing the generative linear instantaneous noise-free mixing ICA model [30], where X is the mixture, i.e. the observed data, A is the unknown square mixing matrix ($N \times M$) which has to be estimated and S represents the unknown source signals to be recovered. The aim of ICA is to estimate an unmixing matrix W so that $C = WX$ is a good approximation to the true sources S. W is the weight matrix which allows to project the original space X into a new space that characterized the sources S.
To reduce problem complexity, typical pre-processing procedures are performed. First one is *centering* which consists of subtract mean value of X, $m = E[X]$, since it doesn't bring any useful information on the signal variance. The result is X as a null mean variable and therefore C as well. Once the mixing matrix A has been computed, the mean values will be reintroduced, adding to the estimate of C its mean value given by $A^{-1}m$.
Another important step is the so called *whitening* or *sphering*, used to whiten the observed variables resulting in uncorrelated data and with unity variances, and allows narrow the search of A to orthogonal matrices. Then it has to be

identified a V matrix, so that:

$$Z = VX \qquad \text{with} \qquad E[ZZ^t] = 1 = I \tag{2.2}$$

Defining P as square and symmetric matrix, computed as:

$$P = E[XX^t] \tag{2.3}$$

and

$$V = P^{-1/2} \tag{2.4}$$

and substituting:

$$E[ZZ^t] = I = E[VXX^tV^t] = P^{-1/2}PP^{-1/2} \tag{2.5}$$

After that the result is:

$$Z = VX = VAS = \widetilde{A}S \tag{2.6}$$

The new mixing matrix now is $\widetilde{A} = VA$ which is orthogonal ($\widetilde{A}\widetilde{A}^T = I$); once it has been estimated, the sources can be computed as $S = \widetilde{A}^T Z$. Hence the i-th independent source/component is computed as: $s_i = (\widetilde{a}_i)^T z$.
Equation 2.6 represents a linear combination of independent components. This sum is "more gaussian" than original components (sources). In fact under the hypotesis of non-gaussianity of sources, thanks to Limit Central Theory, the mixture given by the linear combination of sources will have a probability distribution surely more gaussian than that of sources [30]. $\widetilde{A}$ has to be chosen in order to maximize the non-gaussianity of $S = \widetilde{A}^T Z$.
There are several measures of non-gaussianity, such as Kurtosis index, mutual information and negentropy. The first one measures the dispersion of a statistical distribution around its mean value. The kurtosis of a general aleatory variable y is classically defined by:

$$Kurt(y) = E[y^4] - 3(E[y^2])^2 \tag{2.7}$$

Being null for gaussian variables, $Kurt(y)$ has to be maximized.
A second measure of non-gaussianity is given by negentropy which is based on

entropy variation, in order to be null for gaussian variables and not negative in the other cases:

$$J(y) = H(y_{gauss}) - H(y) \tag{2.8}$$

where $H(\cdot)$ is the entropy, y_{gauss} is a gaussian variable. As kurtosis, the aim is to maximize $J(y)$. This index is used in many algorithms of sources separation, such as FastICA [31].
Another approach for ICA estimation is the minimization of mutual information which measures the grade of statistic dependence between random variables. It is calculated through entropy as:

$$I(y_1, \ldots, y_M) = \sum_i H(y_i) - H(\mathbf{y}) \tag{2.9}$$

where $\mathbf{y}$ is the joint variable. It is a non-negative equation and it is null in case of independent variables because the second term overlaps with the first one. Therefore the mutual information has to be minimize in order to maximize the non-gaussianity of sources.

Two kind of ICA can be carried on: spatial (sICA), when ICA assumes that sources are statistically independent in space, or temporal (tICA) in which sources are assumed to be statistically independent in time [32]. The two ICA types are illustrated in fig. 2.2.

Spatial ICA is represented at the top row of the figure 2.2: known data X is a $N \times N_V$ matrix, where N is the number of time points, N_V the number of voxels. The sICA decomposition can be described as $C = \hat{W}X$, where C is an $M \times N_V$ matrix containing the M independent components, and $\hat{W}$ is the $M \times N$ estimated unmixing matrix found using ICA. The starting fMRI data can then be written as $X = \hat{W}^{-1}C$, where the spatially independent components are located in the rows of C and the associated spatially independent time courses are in the columns of $\hat{W}^{-1}$.
In tICA, which is represented at the bottom row of the figure 2.2, the dimensions of X original data matrix are reversed so that the rows of C represent the temporally independent timecourses and the associated temporally independent maps are in the columns of $\hat{W}^{-1}$.

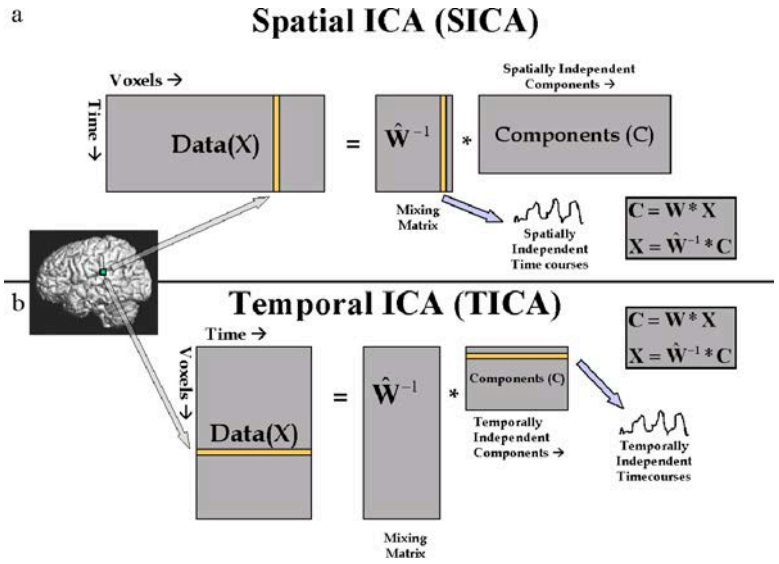

Figure 2.2: Visual representation of sICA and tICA of fMRI [32]. In the first one, the algorithm attempts to find spatially independent components with associated time courses, in the latter one the algorithm attempts to find temporally independent time courses with associated spatial maps.

2.2.2 Denoising of Single Subject rs-fMRI

Melodic is a FSL toolbox [33] that implements the ICA. Tradition ICA models are based on deterministic methods which ignore process uncertainties caused by a contamination of random noise [34]. A more natural expression for the process data can be obtained using a probabilistic model structure. This is the model implemented in Melodic, it is called "Probabilist Independent Component Analysis" (PICA) [4].

Probabilistic Independent Component Analysis

The Probabilist Independent Component Analysis (PICA) allows for a non-square mixing process and assumes that the data are confounded by additive Gaussian noise, so it models the observations as mixtures of spatially non-Gaussian signals plus Gaussian noise [24]. This latter one is the assumption that differentiates traditional ICA described in 2.2.1 and PICA.
This model manages to overcome the over-fitting problem (fragmentation of signal across multiple component maps, reducing the ability to identify the signals of in-

terest) of the classical ICA: fitting a noise-free model to noisy observations causes a no control over what is signal and noise and precludes any test of statistical significance on single voxels.

The PICA model equation is:

$$x_i = As_i + \mu + \eta_i \qquad \forall i \in \mathcal{V} \tag{2.10}$$

where x_i is a N-vector of individual measurements relatively to the voxel location i, s_i is a M-vector of non-Gaussian source signals contained in the data, A is the $N \times M$ mixing matrix of rank M, μ is a vector which defines the mean of x_i, η_i represents a gaussian noise, so $\eta_i \sim \mathcal{N}\ (0,\ \sigma^2\Sigma_i)$ and $\mathcal{V}$ is the set of all voxel locations. It is assumed that $M < N$. To find statistically independent sources, a matrix $W\ (M \times N)$:

$$W = A^{-1} \tag{2.11}$$

has to be identified such that:

$$\hat{s} = Wx \tag{2.12}$$

where $\hat{s}$ is a good approximation to the true source signals s [4].

PICA is composed of several steps, as illustrated in fig 2.3.

Assuming sources with unit variance, the original data are demeaned and normalized to variance through the knowledge about the noise covariance Σ_i at every voxel location. Possible available spatial prior information is encoded in the estimation of the covariance matrix of observations R_x which is used by probabilistic PCA (PPCA) to estimate the model order so to choose the unknown number of sources. It is possible to use several criteria for the selection of model order for PPCA. The one chosen as default estimation technique in Melodic is Laplacian approximation (LAP) which is a way of approximating Bayesian parameter estimation and Bayesian model comparison. It is based on a second-order Taylor approximation of the log posterior around the maximum a posteriori probability estimate. Once the model order is selected, as output PPCA returns a noise estimate and a set of spatially whitened observations. From obtained residuals Σ_i is re-estimated in order to voxel-wise (temporally) pre-whiten and re-normalise the data and iterate the entire cycle. Through the spatially whitened observations,

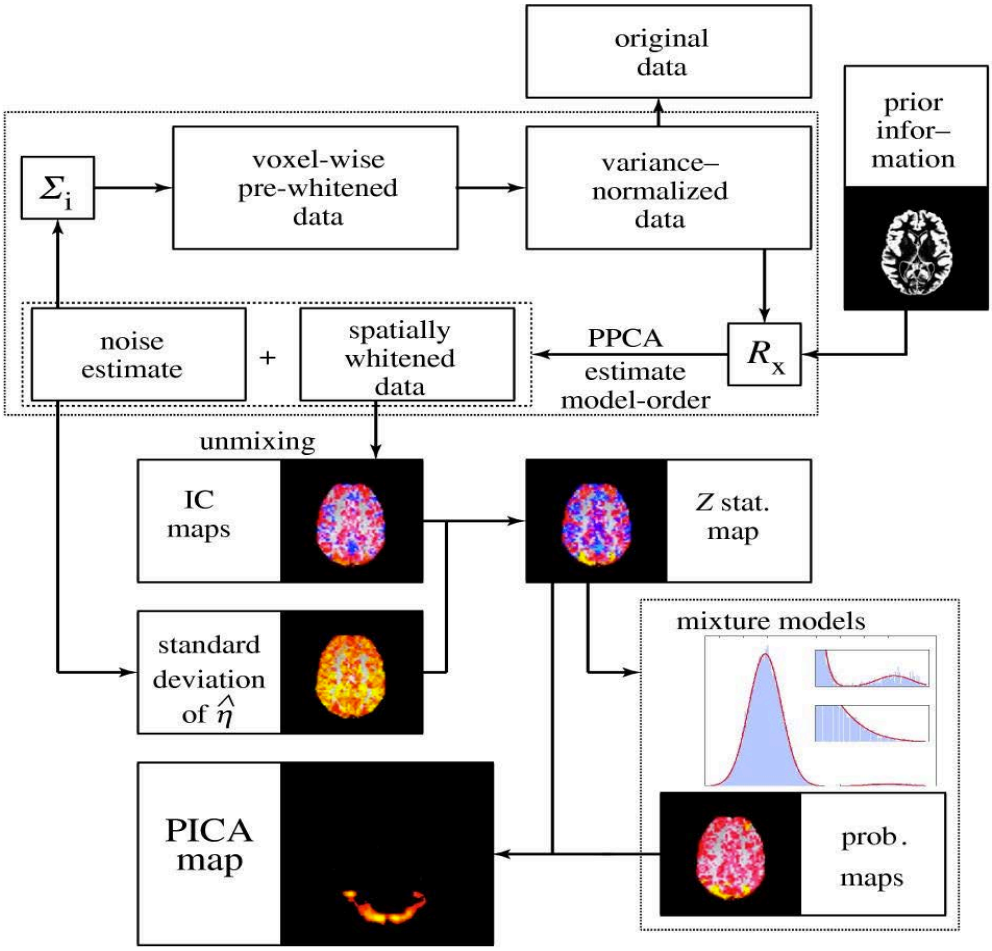

Figure 2.3: Illustration of PICA model [4]

the individual component (IC) maps are obtained using the fixed point iteration scheme FastICA [31] which optimised for non-Gaussian sources estimates by maximising the negentropy [Appendix A]. To obtain statistical significance from results, Z-score maps are formed by dividing IC maps by the voxel-wise estimated standard deviation of the noise: these new maps depend on the amount of variability explained by the entire decomposition at each voxel location. In the final steps Gaussian Mixture Model (GMM) is applied to probability density of individual Z-score maps to highlight regions or voxels in which statistically significant levels of activation or correlation occur. GMM models the distribution of spatial intensity values of each Z-maps by K mixture of mono-dimensional

Gaussian distributions:

$$p(Z_r \mid \theta_k) = \sum_{l=1}^{K} \pi_{r,l} \mathcal{N}_{z_r}[\mu_{r,l}, \sigma^2_{r,l}] \tag{2.13}$$

where θ_k represents the vector of parameters $\{\pi_K,\mu_K,\theta_k\}$ which are respectively the vectors of the K mixture coefficients, mean and variances. GMM is crucial in order to infer voxel locations that are significantly modulated by the associated time course. As results from GMM probability maps are otabined and the final PICA maps.

Application of Melodic

In this work of thesis Melodic has been used to perform individually single subject sICA.
Several tests for the setting-up of Melodic parameters have been run. Melodic allows to compute, the number of components which will be estimated through a criterion of model order selection or to set fixed the number by the user. The latter option has been chosen in this work and a same number has been fixed for all data.
Once independent component spatial maps and relative timecourses are obtained, components will be classified in signal or noise and these last ones will be removed from subject pre-processed data.

Identification and removal of noise components

Unlike initial data of Glasser which has been previously cleaned through the automatic FIX classifier, the components labelling has been made manually due to the limited number of subjects, leading not feasible training the classifier.
Manual classification is based on visual inspection of the components. According to [17], [29] and [28], three complementary pieces of available information were evaluated: spatial maps, time-courses, and the frequency spectrum of time-courses.

As suggest in [29], spatial maps of signal components are characterized by a relatively low number of relatively large clusters while the presence of small and scattered clusters suggests the presence of a noise component. The signal com-

ponents are represented by spatial maps which span for the most part the gray matter, with their peaks located within this area. On the other hand, noise components should mainly be located in the white matter, cerebrospinal fluid and blood vessels.
Spatial maps that show a characteristic ringing around the brain represent motion and so indicate a noise component. The presence of non-physiological patterns, such as positive/negative stripes or clusters visible only in a single slice or alternating slices are usually related to the MRI sequence (e.g. interation between EPI susceptibility and multiband) or hardware artefacts (e.g. RF interference), or interactions of the acquisition with head motion (e.g. interleaved slice acquisitions).

In terms of temporal features, timeseries of signal components are typically stable with no presence of sudden isolated spikes which can suggest motion, and no significantly changes in the oscillation pattern of the timecourse.
From a physiological point of view resting state signal is the result of a convolution between the neuronal spiking and haemodynamic response. It is known from literature that BOLD signal is characterized by low frequency fluctuations, with power between 0.01 - 0.1 Hz. The physiological noise caused by cardiac and respiratory cycle can also appear as low-frequency fluctuations, hence in these cases it may be difficult to identify and separate neural activity-related BOLD signals from noise ones.

Exploiting those three characteristics, lots of noise components can be easily identified, but some of them can appear very similar to signal components in one of the three information types or it is possible that a component contains a mixture of signal and noise and this is often reflected in all three pieces of information. In these cases it has been a conservative approach, so those components are not considered as noise because the aim is to preserve all of the neuronal-related signal present in the dataset.
Once classification is completed for each subject, noise components are removed through the FSL command *fsl_regfilt*.

2.2.3 Implementation of Glasser method

The entire procedure is represented in fig.2.4: the upper part (yellow background) represents the first step of thesis processing described in section 2.2.2, while the bottom one reflects the Glasser procedure and includes the following steps:

a. Spatial ICA through Group ICA of FMRI Toolbox (GIFT [35])

b. Temporal ICA through Fastica [31] included in Matlab

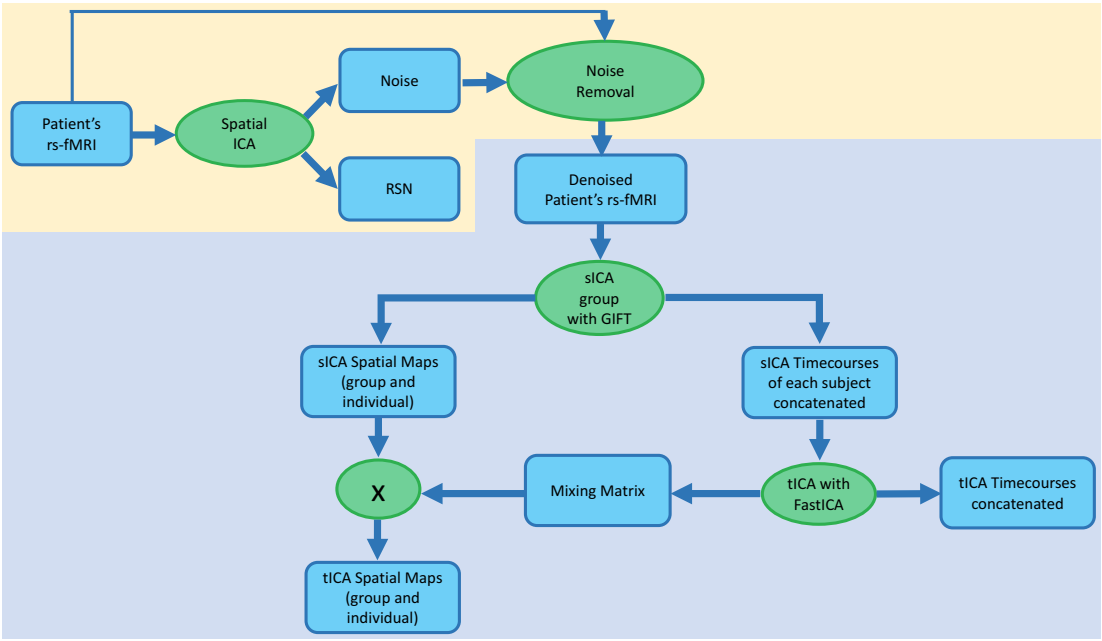

Figure 2.4: Overview of the denoising procedure, adapted from figure 1 in [3]: data are blue and algorithms are green. The scheme is divided into two parts: in the upper part (yellow background) *Denoised Patient's rs-fMRI* are obtained through Melodic toolbox, whereas the bottom one reflects Glasser method and it describes two steps. In the first one the use of spatial-ICA (sICA) with GIFT toolbox, obtaining as results *group and individual Spatial Maps* and *sICA Timecourses of each subject concatenated*; in the second step, through FastICA algorithm, temporal-ICA (tICA) is applied on sICA timecourses and the final results are *tICA Timecourses* and *group and individual tICA Spatial Maps*

The aim of Glasser method is to utilize the combination of spatial ICA (step *a*) and temporal ICA (step *b*) to identify global spatial and temporal structured noise and remove it from subjects data.
Step *a* represents the group sICA performed from data after cleaning-up of

sICA+FIX. This process can be described by the following equation:

$$Data = sICA\_Maps \ * \ sICA\_TCS + Error \tag{2.14}$$

in which:

- $Data \in \mathbb{R}^{\ voxel \times time}$ represents all subjects' cleaned data
- $sICA\_Maps \in \mathbb{R}^{\ voxel \times comp_s}$ are the sICA spatial maps
- $sICA\_TCS \in \mathbb{R}^{\ comp_s \times time}$ defines the sICA timecourses
- $Error$ is the unstructured noise subspace left over after dimensionality reduction to N_c

where *voxel*, *time* and $comp_s$ define respectively the number of voxels, of timecourses and of components estimated with group sICA. After obtaining group spatial maps and timeseries, it is possible to derive the individual subject ones through weighted spatial regression [36]. So the final results are a timecourse for each of the group-ICA components for each subject and a subject-specific spatial map for each component.

Step *b* consists in the application of temporal ICA on the cross-subject concatenated individual sICA component timecourses, using the FastICA algorithm implemented in Matlab. The FastICA parameter settings used by Glasser were *tanh* as nonlinear function and *symm* as estimation method. Another important parameter is the number of components to be estimated: to identify the optimal dimensionality, in Glasser procedure binary search and ICASSO software package [37] are developed. In particular the final dimensionality is the number of components with the index quality $I_q > 0.5$. Temporal ICA is implemented through the equation:

$$sICA\_TCS_{concat} = Mixing\_Matrix \ * \ tICA\_TCS \tag{2.15}$$

where:

- $sICA\_TCS_{concat} \in \mathbb{R}^{\ comp_s \times (time \ \times \ N_s)}$ are the subjects concatenated sICA timecourses, where N_s is the number of subjects

- $Mixing\_Matrix \in \mathbb{R}^{\,comp_s \times comp_t}$ represents the tICA mixing matrix, where $comp_t$ defines the number of components estimated through tICA.
- $tICA\_TCS \in \mathbb{R}^{\,comp_t \times (time \,\times\, N_s)}$ are the concatenated tICA timecourses which can be deconcatenated later to obtain tICA single subject timecourses.

So $sICA\_TCS$ of each subject is temporally concatenated and then fed into FastICA algorithm, obtaining as results the temporal mixing matrix and the new concatenated sources timecourses. To get tICA spatial maps of group and of individual subjects, the equation 2.15 is substituted into equation 2.14 :

$$\begin{aligned} Data &= sICA\_Maps \;*\; sICA\_TCS + Error \\ &= sICA\_Maps \;*\; Mixing\_Matrix \;*\; tICA\_TCS + Error \\ &= tICA\_Maps \;*\; tICA\_TCS + Error \end{aligned}$$

so tICA spatial maps are calculated as :

$$tICA\_Maps = sICA\_Maps \;*\; Mixing\_Matrix \tag{2.16}$$

In particular, tICA spatial maps of each single subject are obtained with the product between sICA spatial maps of that subject and the mixing matrix resulting from FastICA, tICA spatial maps of group are obtained with the product between sICA group spatial maps and the mixing matrix, as it reported in equation 2.17 and 2.18 :

$$tICA\_Maps_{ss} = sICA\_Maps_{ss} \;*\; Mixing\_Matrix \tag{2.17}$$

$$tICA\_Maps_{group} = sICA\_Maps_{group} \;*\; Mixing\_Matrix \tag{2.18}$$

Group spatial ICA

Independent component analysis can be applied to data from a single subject, as previously seen with the first step of the procedure through Melodic, or at the group level. When performing a group-ICA, the inputs are the preprocessed and cleaned resting state fMRI data from all subjects, so the components extracted

in the single-subject ICA decomposition performed by Melodic are not needed. In order to extract group-level components, data from all subjects has to be combined. There are two kind of available group ICA: spatial and temporal concatenation. In the first one data are combined in order to allow for unique maps assuming common timecourses, so considering each subject data as a matrix $time \times voxels$, data of different subjects will be concatenated side by side resulting a final matrix $time \times (voxels_1 ... voxels_{Ns})$, where $voxels_i$ is the number of voxels of i-th subject. The latter one, i.e. the temporal concatenation, allows for common group maps and unique time courses for each subject, therefore considering the example described before, subjects data will be concatenated under each other resulting a final matrix of dimensions $(time_1 ... time_{Ns}) \times voxels$, where $time_i$ is the number of time points of i-th subject. For resting state group-ICA the temporal concatenation approach is generally used:the dataset from subject $i+1$ is stacked after the last time point of the dataset of the i-th subject and so on, creating one long dataset. This concatenated dataset from all subjects is then fed into the ICA and components are extracted using data all subjects. The output from a concatenated group-ICA gives for each component a spatial map which represents the group map and the concatenated timeseries.

To carry on group-ICA two different implementations were evaluated: Melodic and Group ICA of FMRI Toolbox (GIFT) [35] that are the current state-of-the-art packages broadly used for group level rs-fMRI analysis [38].
GIFT is an application developed in Matlab. As Melodic, it can be used to run both single subject analysis as well as group. To perform group-ICA, in both softwares the temporal concatenation approach [39] is implemented, allowing for unique time courses for each subject and assumes common group maps. Unlike Melodic, GIFT software additionally implements a back-reconstruction step which produces subject specific maps and timecourses. So it applies multiple data reduction steps by PCA following data concatenation to reduce the computational load, along with the back-reconstruction.
Figure 2.5 illustrates a graphical representation of the GIFT approach: it involves a mixing matrix estimate which has unique partitions to each subject. Once the mixing matrix is estimated, the back-reconstruction step starts: components for each subject are obtained by projecting the single subject data onto the inverse of the partition of the mixing matrix which corresponds to that specific subject.

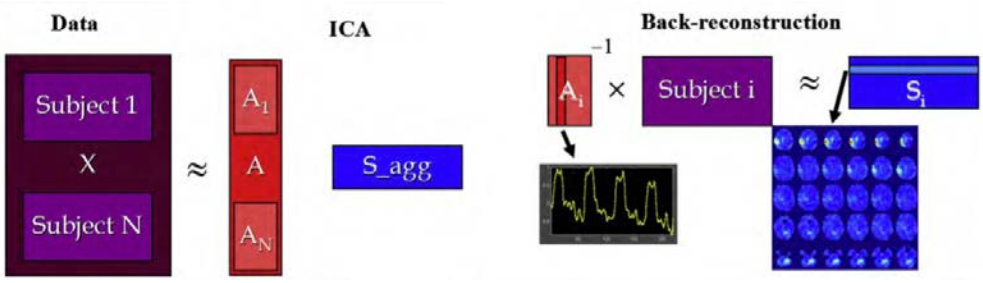

Figure 2.5: Graphical Illustration of Group ICA as implemented in GIFT. On the left group-ICA is represented: all subjects are concatenated to form one unique input data which is used by ICA of GIFT to estimate the mixing matrix (the red matrix) of all subjects and the group spatial maps. On the right the back reconstruction is explained: the inverse of the partition of the mixing matrix for subject i is computed and then it is multiplied by i-th subject data, obtaining component spatial maps specific for that subject [39]

GIFT procedure can be described mathematically as follow. The PCA reduced data matrix of i-th subject ($i = 1, 2, \ldots, N_s$) can be represent through the following equation:

$$X_i = F_i^{-1} Y_i \tag{2.19}$$

where X_i is a $L \times N_V$ matrix, Y_i is the $N \times N_V$ matrix which contains the preprocessed data and F_i^{-1} is the $L \times N$ reducing matrix computed by PCA decomposition, with N_V the number of voxels, N the number of fMRI time points and L the size of time dimension following reduction. All X_i matrix are then concatenated into a $LN_s \times N_V$ matrix and pre-multiplied by the $M \times LN_s$ reduction matrix G^{-1} (calculated by PCA decomposition), resulting a new reduced, concatenated matrix for the N_s subjects:

$$X = G^{-1} \begin{bmatrix} F_1^{-1} Y_1 \\ \vdots \\ F_{N_s}^{-1} Y_{N_s} \end{bmatrix} \tag{2.20}$$

where X is the $M \times N_V$ matrix, with M the number of components to be estimated. Multiplying previous equation for both sides by G of and using ICA

model equation $X = AS$, the following expression is obtained:

$$G\hat{A}\hat{S} = \begin{bmatrix} F_1^{-1}Y_1 \\ \vdots \\ F_{N_s}^{-1}Y_{N_s} \end{bmatrix} \tag{2.21}$$

where A is the $M \times M$ mixing matrix, S is the $M \times N_V$ component map. Partitioning the matrix G by subject equation 2.21 can we written as:

$$\begin{bmatrix} G_1 \\ \vdots \\ G_{N_s} \end{bmatrix} \hat{A}\hat{S} = \begin{bmatrix} F_1^{-1}Y_1 \\ \vdots \\ F_{N_s}^{-1}Y_{N_s} \end{bmatrix} \tag{2.22}$$

So for i-th subject:

$$G_i\hat{A}\hat{S}_i = F_i^{-1}Y_i \tag{2.23}$$

From equation 2.23 the single subject maps (S_i) can be calculated:

$$\hat{S}_i = (G_i\hat{A})^{-1}F_i^{-1}Y_i \tag{2.24}$$

Multiplying both sides of equation 2.23 by the reducing matrix F_i the decomposition of data from ns-th subject contained in the matrix Y_i is represented:

$$Y_i \approx F_iG_i\hat{A}S_i \tag{2.25}$$

where S_i describes M sources spatial maps and $F_iG_i\hat{A}$ is the $N \times M$ mixing matrix of single subject containing the timecourses of respective M components.

The choice of which implementation between Melodic and GIFT is more appropriate depends on available data, generally Melodic is more demanding from a computational point of view, in particular the required execution times in resting state data are much slower.
A comparison between Melodic and GIFT about their characteristics and setting parameters is described below.
Regarding the pre-processing, while Melodic applies voxel-wise de-meaning of the data and normalisation of the voxel-wise variance, in GIFT several pre-processing

types are available (remove mean per timepoint, remove mean per voxel, intensity normalization and variance normalization) and some tests on data were performed with *variance normalization* and *intensity normalization*: in the first one time-series are lineary de-trended and converted to Z-score at each voxel, the latter involves voxel-wise division of the timeseries mean. After a visual inspection on spatial components intensity normalization was used as data pre-processing type.
The choice of independent components number represents the problem of selection of model order. In Melodic the default technique of dimensions estimation is LAP (Laplace Approximation), but there are available also the other methods. GIFT instead provides only MDL method (Minimum Description Length). This difference of criteria may cause a different estimated number of components.
In this case to perform different comparisons between Melodic and GIFT, the number of estimated component was fixed. One of the differences between the two tools is that GIFT gives the opportunity to use ICASSO toolbox [37] which allows to determine the algorithmic reliability or stability and so do a better components' estimation [Appendix C]: reliable estimates correspond to tight clusters and unreliable ones do not point to any cluster. In order to apply ICASSO, a certain number of runs has to be selected: more runs are used, more reliable will be the results. In this case ICA algorithm was run 10 times.
GIFT allows also to run group-ICA in parallel mode which is a very useful option for analysing large data because it allows to exploit more cores and so speed up the computation.
About ICA algorithm while Melodic uses FastICA, GIFT gives several options, in particular in this work FastICA and Infomax [40] algorithms were explored.Both algorithms are based on maximization of an objective function, they use a fixed non-linearity so their performances tend to be biased towards certain types of probability density functions *pdfs*, in that they provide better estimate for certain classes of sources and hence cannot maximally optimize independence [35]. FastICA maximizes the negentropy of the output to maximize the non-gaussianity of the estimated sources using fixed point iterations. Infomax uses a fixed sigmoid non-linearity as the score function and hence emphasizes the estimation of sources that are super-Gaussian, i.e., have pdfs that are heavier-tailed and more peaky than the Gaussian [Appendix B].

Once GIFT has been selected as toolbox, group sICA can be performed.

It start with the Setup-ICA analysis, in which all parameters are chosen. Among them one important is the dimensionality of ICA decomposition that can be estimated from GIFT or be set. In this case the dimensionality has been fixed. To obtain an appropriate number of components, Melodic was taken into account again: data obtained after single-subject clean-up were used individually as input in Melodic, which estimated for each subject data the components number more appropriate. As result 13 values were obtained, one for each subject, then they were average obtaining the value of dimensionality.
Once the number of components has been selected, all input parameters for group-ICA are fed into GIFT. In this case the steps involved into group-ICA analysis are listed below:

1. Initialize Parameters

2. Group data reduction: Each subject's data is individually reduced through PCA. The outputs are concatenated into groups and put through another PCA data reduction step.

3. Calculate ICA: The reduced data from the data reduction stage is plugged into the ICA algorithm.

4. Back-Reconstruction: Individual subject image maps and time courses are computed.

Temporal ICA

The temporal ICA (tICA) is implemented in Matlab and developed following Glasser article procedure described at the beginning of subsection 2.2.3. After group-ICA approach, sICA timecourses of each subject obtained from the back-reconstruction of GIFT are concatenated into the matrix $sICA\_TCS_{concat}$ which will be used by FastICA. As in Glasser article using ICASSO the components with an index-quality measure $I_q > 0.5$ define how many of them have to be estimated. The tICA concatenated timecourses $tICA\_TCS$ obtained as output by FastICA are de-concatenated to get the individual subjects' ones. Then through the equation 2.16 implemented in Matlab group and individual independent component maps are calculated.

Indexes for identification of noise components

In order to remove noise components related to motion, three quantitative component-wise measures described in Glasser's paper are considered and they will be named as $diff_{AmpDVARS}(j)$, $Variability_{Amp}(j)$ and $diff_{Amp}(j)$.

First index is based on DVARS: it represents the rate of change of BOLD signal across the entire brain at each frame of data [1] and it is calculated for each subject starting from the intensities difference of consecutive volumetric images and root-mean-square:

$$\mathrm{DVARS}(\Delta I_i) = \sqrt{\left\langle \left[\Delta I_i(\vec{x})\right]^2 \right\rangle} = \sqrt{\left\langle \left[I_i(\vec{x}) - I_{i-1}(\vec{x})\right]^2 \right\rangle} \tag{2.26}$$

where $I_i(x)$ is the image intensity at locus x on frame i and the angle brackets $\langle\ \rangle$ denote the spatial average over the whole brain. This index is used as proxy of subject motion during time and measures how much brain image intensity has changed from one frame to the next one. According to Power [1] such image intensity changes often show up as "spikes" in the original timeseries DVARS trace. Generally after a data motion correction, it is expected that spikes disappear, returning the DVARS to its baseline level, whereas it often results that some spikes remain and other become dips (negative peaks) which, according to Glasser et al. [3], means that probably an excessive signal denoising was applied. Therefore the aim is to identify DVARS spikes or dips remaining after the first clean-up procedure (sICA single subject with Melodic) and to analyse tICA components' timeseries corresponding to peaks' instants/frames.
In order to identify spikes/dips in DVARS, a band has to be identified and its width is chosen through a threshold applied symmetrically to the mean value of DVARS trace. To better understand this concept, figure 2.6 has been reported. It is an example of DVARS trace in which the band is represented as the coloured part limited by two symmetric thresholds: what is outside of this band is called spike/dip.

To identify peaks representative of motion, Glasser and colleagues used a single

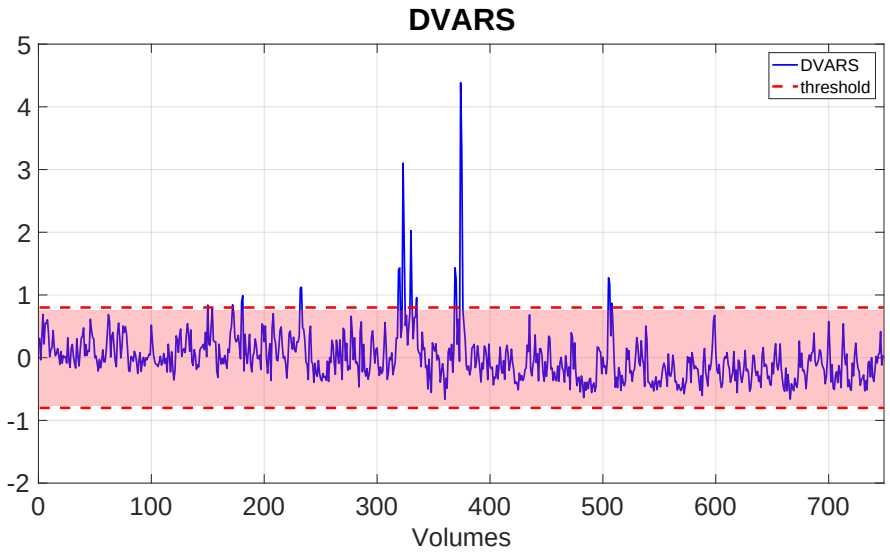

Figure 2.6: Example od DVARS trace with a chosen threshold. The symmetric thresholds define a band, represented colored: what is outside of this band is called spike/dip

subject approach and for each one of them they identified the maximum value of DVARS signal, normalized the signal for this peak value and then set the threshold equals to the $\pm$ 25% of this value: all that is over the 25% of distribution of that subject has been considered motion.
This proposal of thresholds selection has been applied also to available dataset: firstly subject DVARS has been calculated through equation 2.26 considering images obtained after sICA clean-up with Melodic, then DVARS have been individually normalized to their maximum value, as in Glasser's paper, and demeaned to be able to compare DVARS of different subjects each other.
Observing obtained results, this kind of threshold can't be adaptable with available dataset which has been showed varied: there are subjects which move a lot, others move less. Regarding the latter kind of subjects, once each DVARS has been normalized for their respective maximum value, the obtained threshold has led to an amount of data over the range excessively high, removing therefore too much values which in reality aren't significant peaks and so representative of movement.
For this reason several kind of thresholds are explored. The idea is use a group approach and not single subject to identify the band defined by a threshold: therefore it is considered DVARS of all subjects together and only one thresh-

old is found for all. Several thresholds are performed on subjects DVARS traces. Thresholds are described below:

- The first one is obtained considering the histogram of 10% of higher values of each subject DVARS: having 750 volumes of acquisition for each subject, this means to take into account the 75 grater peaks of each DVARS. Then these peaks selected for each subject are sorted in descent order and their distribution is observed. The threshold is set as the value from all order peaks corresponding to 10 percentile which can be defined as the value of a variable below which a certain percentage of the observation occurs (in this case 10 percentile is the value under which 10% of observation are situated). It is calculated as:
$$k\text{-}percentile = \left[\ 0.5 + \frac{n \cdot k}{100}\ \right] \tag{2.27}$$
where n is the number of data and k represents k-percentile so in this case $k = 10$.

- Under the hypothesis that subjects DVARS come from a Gaussian distribution, the other thresholds are calculated based on standard deviation σ of concatenated DVARS. In particular are considered as thresholds σ, 1.64σ and 2σ which reflects the fact that data has the probability respectively of 68%, 90% and 95% to fall inside the band derived from threshold.

After the computation of all thresholds just described, for each of them it has been observed the number of outliers and how it is distributed among all subjects.

Once the identification of DVARS peaks has been completed, $diff_{AmpDVARS}$ can be computed for each component. To do that, first the concept of amplitude has to be introduced: for each i-th subject, the amplitude of j-th tICA component was defined by Glasser [3] as the standard deviation of the component timeserie values:

$$Amp(i,j) = std\ \left[tICA\_TCS(i,j)\right] \qquad \text{with} \quad i = 1,\ldots,N_s \quad j = 1,\ldots,M \tag{2.28}$$

where $tICA\_TCS(i,j)$ is the tICA timeseries of i-th subject and j-th component. This definition was used to calculate the amplitude of each component through

the concatenation of tICA timecourses across all subjects:

$$Amp_{tot}(j) = std\left[tICA\_TCS_{concat}(j)\right] \qquad \text{with} \quad j = 1, \ldots, M \tag{2.29}$$

Next step is to calculate the difference in component amplitudes during periods of DVARS Dips compared to the non-DVARS Dips periods and the result is normalized by the component amplitude across all frames, obtaining the first index for noise classification:

$$diff_{AmpDVARS}(j) = \frac{Amp_{DVARS}(j) - Amp_{non-DVARS}(j)}{Amp_{tot}(j)} \tag{2.30}$$

where $Amp_{DVARS}(j)$ is the amplitude j-th IC corresponding to frames with DVARS peaks/dips, i.e. all the frames which lie outside the band produced by the chosen DVARS threshold. $Amp_{non-DVARS}(j)$ is the amplitude relative to frames without DVARS peaks/dips, so all frame which stay within the band, instead $Amp_{tot}(j)$ is the amplitude relative to all frames of current component.
Equation 2.30 represents hence the first computed index; each component will have a respective value of this measure and will be identify as signal or noise on the basis of a chosen threshold: all components under threshold will be classified as signal, on the contrary those above will be considered noise components. According to Glasser this threshold will be that value which "best discriminates between components that had already been clearly identified as signal or noise based on spatial patterns" [3]. There is no clear indication, in the paper, of how the threshold selection has been carried out, therefore this problem has been dealt with in three different ways: three kind of thresholds have been tested. Since the threshold should discriminate between signal and noise, the idea at the base of the three threshold approaches is to compute a mean value between signal and noise components. In particular to obtain a more reliable value, 3 signals and 3 noise components have been manually identified among all components.
In order to make the next equations more clear and readable, two variables are introduced and defined as:

$$m_{3signals} = mean[diff_{AmpDVARS}[s_1], diff_{AmpDVARS}[s_2], diff_{AmpDVARS}[s_3]]$$
$$m_{3noises} = mean[diff_{AmpDVARS}[n_1], diff_{AmpDVARS}[n_2], diff_{AmpDVARS}[n_3]]$$

where $diff_{AmpDVARS}[s_i]$ and $diff_{AmpDVARS}[n_i]$ are respectively the differences in component amplitude of i-th signal and i-th noise. The variables $m_{3signals}$ and $m_{3noises}$ represent respectively the mean value of the three signal and noise components.
The computation of all thresholds will be based on $m_{3signals}$ and $m_{3noises}$. The first threshold is computed as the mean of the two previous results:

$$th_{DVARS} = mean\ [m_{3signals}\ ,\ m_{3noises}] \tag{2.31}$$

The second one takes into account not only the mean value between $m_{3signals}$ and $m_{3noises}$, but also the standard deviation of the 6 chosen components:

$$th_{DVARS} = mean\ [m_{signal}\ ,\ m_{noise}] + std_{6components} \tag{2.32}$$

where the second term is obtained as the standard deviation of all the six identified components as described below:

$$std_{6components} = std\ [diff_{AmpDVARS}[3signals]\ +\ diff_{AmpDVARS}[3noises]]$$

The last threshold is similar to the second one, but considers the standard deviation of the two group separately:

$$std_{3signals} = std\ [diff_{AmpDVARS}[3signals]]$$
$$std_{3noises} = std\ [diff_{AmpDVARS}[3noises]]$$

and uses the mean of this two values inside threshold's formula:

$$th_{DVARS} = mean\ [m_{signal}\ ,\ m_{noise}] + mean[std_{3signals}\ ,\ std_{3noises}] \tag{2.33}$$

The second and third metric are based on an analysis of variability of component amplitudes across subjects.

Regarding the second metric, for each component j it is computed as:

$$Variability_{Amp}(j) = \frac{std\ [Amp(1,j),\ Amp(2,j),\ \cdots\ ,\ Amp(i,j),\ \cdots\ ,\ Amp(N_s,j)]}{Amp_{tot}(j)} \tag{2.34}$$

Then another standard deviation is calculated on these N_s values, obtaining one value for each component. This result is then normalized for $Amp_{tot}(j)$ computed as for the previous index.

In $diff_{Amp}$ the focus was on the two highest subject's component amplitudes. For each j-th component the index is calculated as:

$$diff_{Amp}(j) = \frac{Amp_{max}(j) - Amp_{2max}(j)}{Amp_{tot}(j)} \tag{2.35}$$

where $Amp_{max}(j)$ is the maximum amplitude across all subjects for j-th component, $Amp_{2max}(j)$ is the next highest amplitude across all subjects always for j-th component. The difference between them is normalized by $Amp_{tot}(j)$.

After the computation of indexes $Variability_{Amp}$ and $diff_{Amp}$, a robust threshold needs to be searched, in order to best discriminate between noise and signal. The threshold is computed as for $diff_{AmpDVARS}$ index.

Once all the three metrics described in equations 2.30, 2.34 and 2.35 are computed, for each of them it is obtained as result which components are above the respective thresholds and so could be considered as noise. Next step is now to compare results: the components which will be above all the thresholds, will be identified as noise components.
The selected components were then removed from each subject always through the FSL command *fsl_regfilt*, resulting new clean subject data.

2.3 Evaluation of Motion-Related Noise Reduction Procedure

To evaluate if the entire procedure represented in fig. 2.4 can be a valid method of cleaning-up rs-fMRI data from motion-related noise, two different indexes have

been employed.
The first one is the comparison between DVARS traces computed after steps of procedure: the focus is to check if possible peaks/dips of subjects DVARS has been lowered or even disappeared after the application of the entire procedure.
The second index, introduced by Power [21], is the QC-RSFC measure (QC referring to quality control, RSFC denoting resting state functional connectivity), in this work it is used to find out if motion is still much present in cleaned data after spatial and temporal ICA. In particular it is used to assess a possible relationship between head motion and resting state function connectivity (rsFC) estimates.

2.3.1 DVARS Comparison

For each subject three different DVARS traces are computed using equation 2.26:

1. DVARS of pre-processed fMRI data (*DVARS pre s-sICA*)
2. DVARS of data after single subject cleaning through Melodic (*DVARS post s-sICA*)
3. DVARS of fMRI data after the entire cleaning procedure (*DVARS post tICA*)

For each subject three different DVARS measures are compared to each other to evaluate if peaks/dips which are in the first DVARS (i.e. that without any ICA correction) are reduced or even disappeared after sICA+tICA procedure.

2.3.2 QC-RSFC

QC-RSFC metric was used by Power to quantify the impact of motion on functional connectivity correlations. To explain QC-RSFC calculation and how it can be exploited in this work, first an introduction of functional connectivity is needed, as well as the computation of connectivity matrices necessary for the metric, then QC-RSFC application is described.

Functional Connectivity

Functional connectivity (FC) is typically defined as the observed temporal correlation (or other statistical dependencies) between two electro or neuro-physiological

measurements from different parts of the brain [17]. For resting state fMRI this definition means that functional connectivity reveals the relationship between BOLD signals obtained from two separate regions of the brain: the hypothesis behind this method is that if two regions show similarities in their BOLD signals over time, they are functionally connected.

Many different methodological approaches are available to investigate functional connectivity, generally for rs-fMRI analysis the node/atlas-based approach is used [17]. Several steps characterize node-based connectivity analysis and they are represented in figure 2.7:

1. Definition of the nodes, i.e. grouping voxels together into areas that are to be considered as functionally homogeneous regions.

2. Extraction of each node timeseries.

3. Calculation of the connectivity between all pairs of nodes through the extracted timeseries.

4. Building of a connectivity matrix in which each element (i, j) describes the strength of functional connectivity between node i and node j.

Regarding the first step, identification of nodes is generally obtained through parcellation. In this work because an ICA-based approach is implemented, functional connectivity isn't computed at node based with parcellation, but at network-level. Therefore calculating connectivity between pairs of nodes means to do that between networks. The networks used in this thesis for FC computation are chosen through visual inspection of all spatial maps of ICA components from rs-fMRI, hence they will named as resting state networks (RSNs).
To obtain a connectivity matrix, IC sources timeseries of RSNs obtained using group ICA are used: each pair of timeseries is correlated, through Pearson's correlation coefficient, to investigate their similarity. Correlation ranges from -1 to +1, where 0 indicates no relationship on average between two signals. FC matrices of this work are obtained by computing Pearson correlation coefficients between the associated timecourses of any paired networks, resulting a symmetric matrix with a number of rows and columns equals to the number of the chosen networks. Pearson correlations were also transformed using the Fisher Z in this analysis

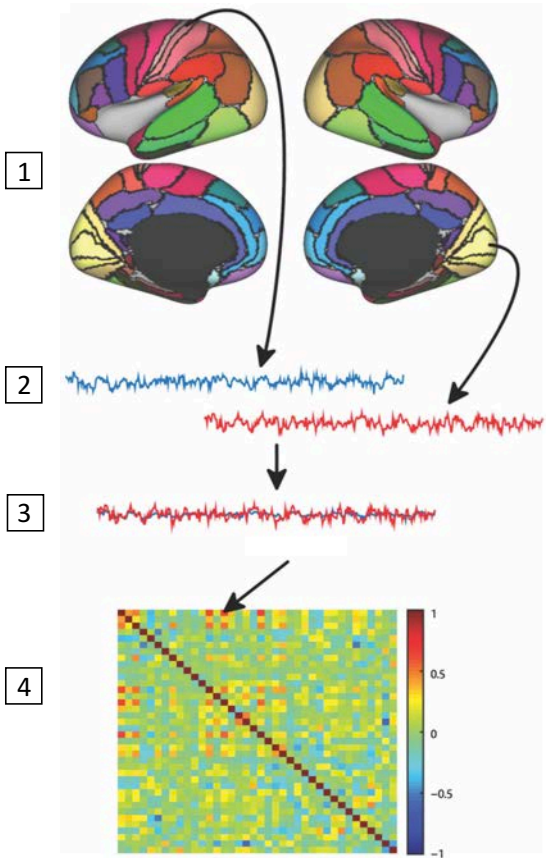

Figure 2.7: Steps of node-based connectivity analysis [17]. The first one represents the parcellation of brain in different areas, showed with different colours, in order to define nodes. The second one reflects the extraction of timeseries from areas. In the third step timeseries are considered in pairs and the correlation between them is computed. The last step involves the construction of connectivity matrix through the values of previous correlations. The entries of the matrix with a higher value equal to a stronger correlation and are represented with a shade into the red. Slight correlations will appear with colour near blue

because it allows to transform the sampling distribution of Pearson's correlation coefficients into an almost normally distributed measure [41].

QC-RSFC Application

According to Power [1], subjects' motion produces substantial changes in the time-courses of resting state functional connectivity MRI (rs-fcMRI) data, in particular many long-distance correlations could be increased or decreased by subject motion, whereas short-distance correlations increased.
The aim is to understand the additive step of temporal ICA compared to the

standard sICA has been successful in the detection and removal motion-related components. If tICA has effectively removed motion artefacts, then the paired correlations between RSNs illustrated in FC should change after tICA application; more precisely the relation between FC and subject motion should decrease.
This relation is what QC-RSFC measure computes: it allows to correlate, across subjects, subject motion with the observed correlation values of FC.
Before explaining how QC-RSFC is computed, it is important to noticed that QC-RSFC takes into account a measure of subject motion: the Frame-wise displacement (FD) which is calculated, for each i-th volume/frame, by combining the six motion parameters estimated during motion correction into a single measure of displacement [1]:

$$FD_i = \mid \Delta d_{ix} \mid + \mid \Delta d_{iy} \mid + \mid \Delta d_{iz} \mid + \mid \Delta \alpha_i \mid + \mid \Delta \beta_i \mid + \mid \Delta \gamma_i \mid \tag{2.36}$$

where $\Delta d_{ix} = d_{(i-1)x} - d_{ix}$, and similarly for the other rigid body parameters $[d_{ix}\ d_{iy}\ d_{iz}\ \alpha_i\ \beta_i\ \gamma_i]$.

Considering of having N_s subjects, for each of them there is a FD trace from which a mean value can be computed. There will be hence a vector of N_s FD mean values that can be correlated with each entries of FC, across subjects, in order to determine how that entries of all subjects is modulated by subject motion. Therefore the idea is to compute two kind of correlation matrices FC, one pre-tICA (FC_S) and one post-tICA (FC_{T+G}) for all N_s subjects. Then QC-RSFC is applied to relate the obtained FC_S with the mean values of subjects' FD. At this point the same approach is done for FC_{T+G} and the results of both will be observed.
Now it will be described how the FC_S of subjects have been computed. For each subject component spatial maps, obtained from back-reconstruction of group sICA with GIFT, are considered and of these only credible components have been chosen as the resting state (rs) networks for next steps, through visual inspection. The sources (i.e timeseries) of these networks are taken into account to compute FC_S. As result of this step N_s connectivity matrices pre-tICA are obtained.
To better explain the step which involves QC-RSFC metric, figure 2.8 is showed. As it can be seen the subject network matrices are combined into one large (num-

ber of subjects N_s by number of edges i.e connectivities) matrix: this is done by discarding one half of the network matrix (which contains the same information as the other half because the matrix is symmetric), and then reassembling half of the node by node matrix of edges from each subject into one long row, resulting a large subjects-by-edges matrix. This resulting matrix is then correlated with

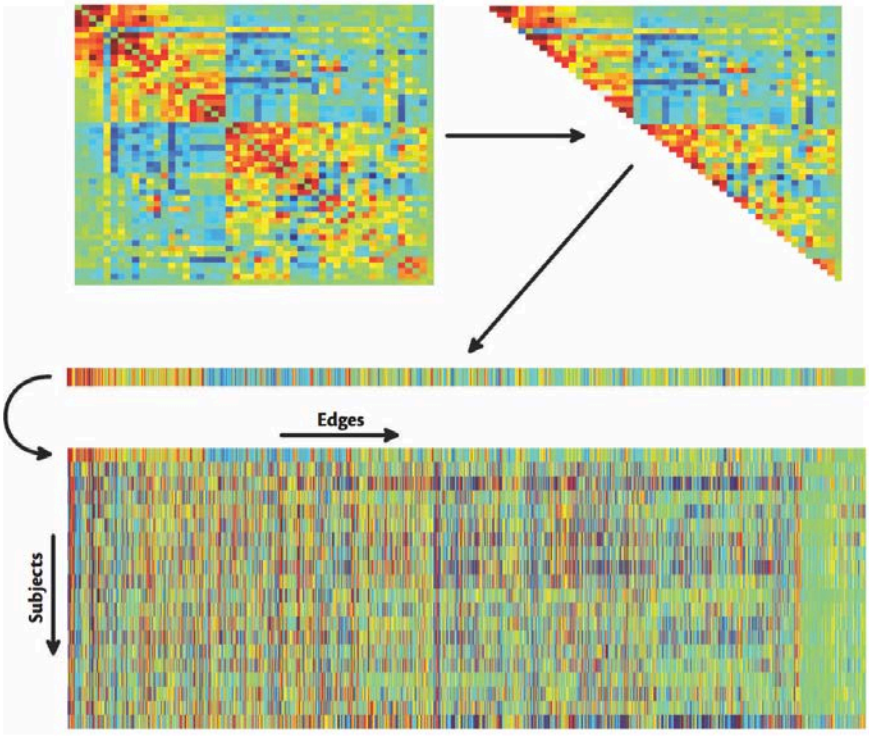

Figure 2.8: A network matrix from a single subject can be mapped into one line by removing the redundant part of the symmetric matrix and unwrapping it so that all edges are next to each other. Subjects can then be stacked below each other to form a matrix ready for group-level analysis [17]

the vector of mean values of subject's FD. As output a correlation matrix and a p-value matrix are obtained.

The same calculation is now applied starting from correlation matrices FC_{T+G} of all subjects. These correlation matrices are generated from timecourses derived from back-reconstruction of sICA components through group-information guided ICA (GIG-ICA) of GIFT applied on the clean data after tICA. In GIG-ICA, group information captured by standard ICA on the group level is used as guidance to estimate individual subject specific Independent Components (ICs), using

a multi-objective optimization strategy which simultaneously optimizes the independence among multiple ICs of each subject and the correspondence between each group-level IC and the associated subject-specific IC [42].
Hence GIG-ICA method involves the use of a spatial prior, which are the group spatial maps and represents the starting point of the minimization of cost function used by an ICA algorithm.
GIG-ICA process is applied individually for each subject; as input GIFT toolbox gets clean data from tICA and the group aggregate component spatial maps, producing component spatial maps and timeseries of that subject as output.

Statistical analyses

To evaluate the effect of tICA application, an important instrument is the statistical analysis applied to FC computed before and after tICA. Figure 2.9 shows the procedure of how get the two groups of FC to be compared. To evaluate whether and how FC of the RSNs change after the procedure, it is possible to work at statistical level. This means that t-tests will be performed between two FC groups to check whether there is a statistically significant difference between the two groups. The FC groups which will take into account are showed in figure 2.9: FC_{T+G}, which are obtained starting from tICA results (the right part of figure), and FC_{S+C}, obtained with the state of art in rs-fMRI (subject-wise cleaning data and group sICA).

In particular this latter FC group have been computed not correlating RSNs' sources, but considering only the clean and reliable part of sources, characterized by no motion. Doing that equals to apply the so called *censoring*: it leads to FC matrices devoid of volumes in which a subject movement occurred that hasn't been corrected but has remained despite the usage of the classical technique of *motion correction*. Applying censoring to a subject data allows to remove the part referring to motion of each timecourses of RSNs. In order to identify time frames corrupted by motion, censoring applies a threshold to a measure of movement, in this case to FD. Censoring works by simply removing volumes at time points where the FD was higher than the chosen threshold. Because motion has an impact on signal not only when it is above the threshold, but also on nearby volumes, also one volume before and two volumes after are also removed in addi-

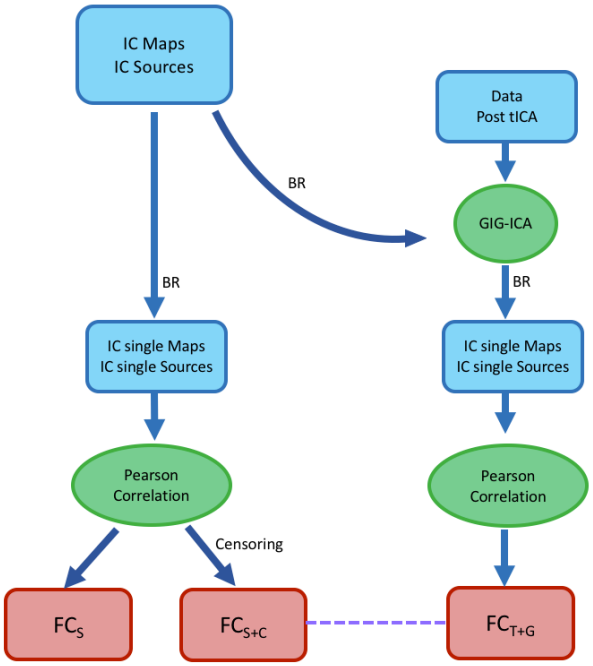

Figure 2.9: Illustration of how to compute functional connectivity (FC) matrices. FC_S are get through sICA timecoures of single subjects. FC_{S+C} are obtained from sICA timecourses after censoring. FC_{T+G} are calculated after applying GIG-ICA on data post tICA and correlation of selected networks timeseries. The dotted line represents comparisons between pairwise matrices, through t-tests.

tion to the volume corresponding to FD above threshold [21].
Observing any changes between FC_{T+G} and FC_{S+C} allows to understand if tICA managed to reduce motion impact on signal compared to what is done traditionally through group sICA and censoring.

Before describing in detail how t-tests are performed, it is noticed that the comparison is done between two FC groups computed with different methods: unlike FC_{S+C}, FC_{T+C} is obtained starting from GIG-ICA methodology which could have a strong impact on result and so the eventually statistically significant differences between the two matrices groups could only due to GIG-ICA application to only one of them. For this reason t-tests between FC_{S+C} and FC_{T+G} could not be suitable.

To verify if GIG-ICA method controls the results of the comparison between FC_{S+C} and FC_{T+G}, statistical analysis has been expanded compared to that described in figure 2.9: a second part has been added, resulting the computation

of more FC groups and so more t-tests between FC matrices in pairs.

This can be seen on figure 2.10 in which statistical analyses is performed between

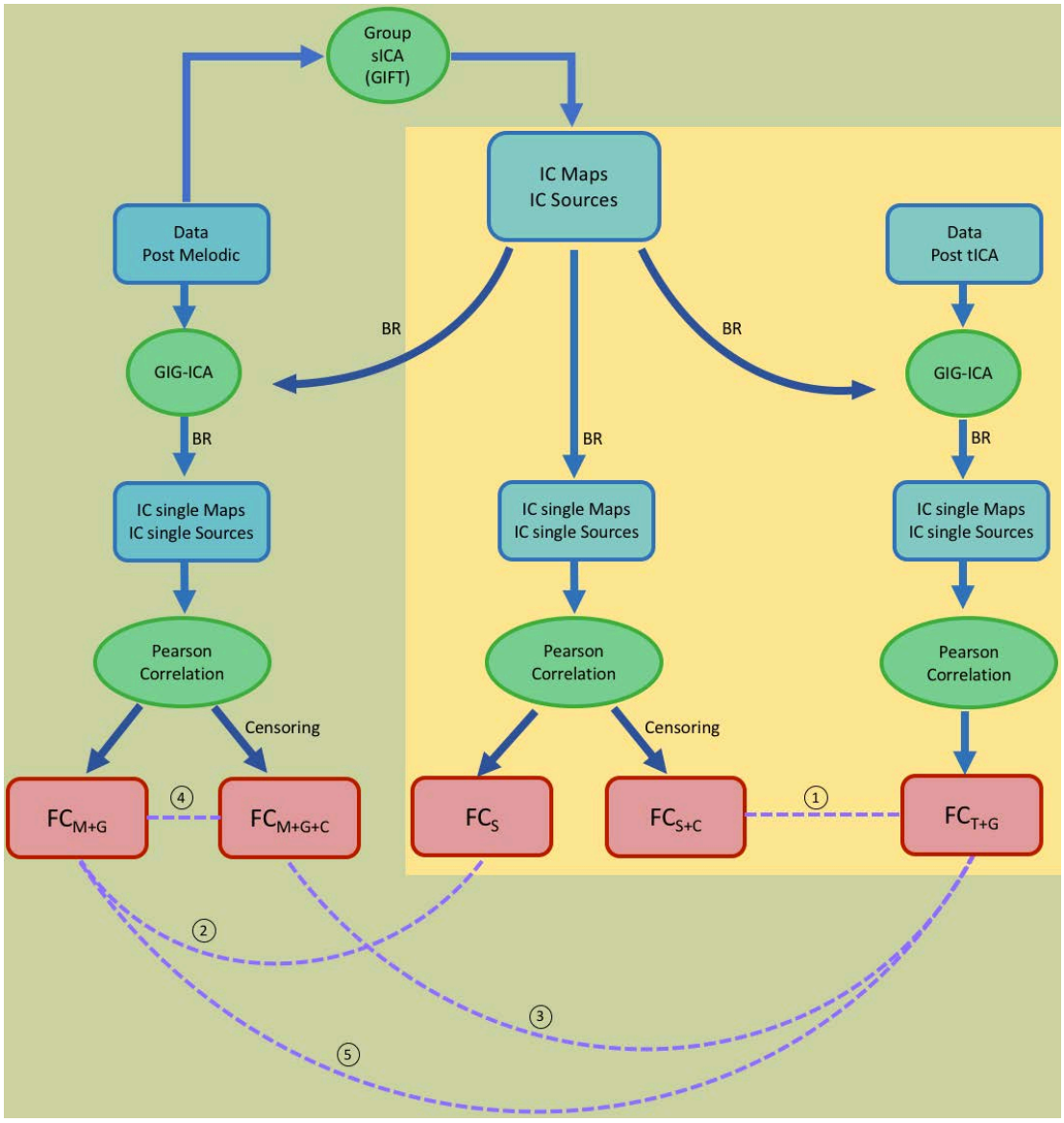

Figure 2.10: Illustration of all computed FC matrices. The yellow block represents the comparison between two FC groups FC_{S+C} and FC_{T+G} is performed. The other block instead is the new adding part which includes the computation of other FC and new t-tests. FC_{M+G} are computed after clean-up of Melodic and GIG-ICA application. FC_{M+G+C} are obtained after Melodic, GIG-ICA and censoring. The dotted lines represent all comparisons between pairwise matrices through t-tests

correlation matrices calculated in all phases of cleaning procedure (after Melodic

clean-up, after group sICA, after tICA), examining if there are some variations between components' connections:

- FC matrices obtained starting from cleaning data of Melodic: GIG-ICA of GIFT is used individually on single subject cleaned data, using as prior the spatial maps coming from group sICA. The results are new independent spatial maps and timecourses of individual subjects. Of these timecourses, only those referring to the rs-networks are taken into account and used to obtain initially the FC matrices (FC_{M+G}) and, after applying censoring, the other FC matrices FC_{M+G+C}.

- FC matrices starting from group sICA: rs-networks timecourses of single subjects obtained from back-reconstruction of group sICA are correlated to each other to create a FC matrix for each subject, FC_S. Applying censoring to timeseries before their correlation produces FC_{S+C} matrix, one for each subject.

- FC matrices derived after tICA: Clean data obtained with the entire cleaning procedure are used as input, along with spatial maps of group sICA, to perform GIG-ICA method. Of the new subject's data resulting, timecourses of the rs-networks are used to obtain FC_{T+G} matrices.

The idea behind the implementation of the new part represented in figure 2.10 is that it is expected that FC_{M+G} and FC_S are very similar, hence if they are significantly different, this will mean that all the difference is due to the usage of GIG-ICA in the computation of FC_{M+G}. In this case then comparison ① in figure isn't plausible because it compares matrices obtained with not comparable methods and therefore it would be more appropriate comparison ③ to verify the effects of tICA.
Other comparisons have been performed, resulting five tests:

① $FC_{S+C} \longleftrightarrow FC_{T+G}$

② $FC_{M+G} \longleftrightarrow FC_S$

③ $FC_{M+G+C} \longleftrightarrow FC_{T+G}$

④ $FC_{M+G} \longleftrightarrow FC_{M+G+C}$

⑤ $FC_{M+G} \quad \longleftrightarrow \quad FC_{T+G}$

Regarding the application of t-test, for each pairwise comparison two FC groups are considered. For each FC matrix group involved in a comparison only strictly upper triangular is taken into account and for each element (i, j) of these strictly upper triangular matrices the values in (i, j) position of all subjects are stacked: so for each pixel (i, j) a vector of subjects' values of (i, j) is obtained. Then a difference between respective vectors of the two FC groups is computed in each position (i, j): to see if each difference vector is significantly different from zero and so there was an effect between the two matrix groups, the difference vector of position (i, j) is used as input for t-test: there will be as much statistical tests as the total number of elements in the strictly upper triangular. From these t-tests the findings will be a connectivity matrix representing the comparison of two group connectivity matrices of interest, and a p-value matrix representing the possible significance of results.
This computation is done for each of the pairwise comparison, resulting after all statistical tests five matrix connectivities and as many p-value matrices.

In all t-tests the significance value is fixed to 0.05.All t-tests were corrected to multiple comparisons through false discovery rate correction (FDR) [43].

3
Results

3.1 Denoising of Single Subject rs-fMRI

The application of Melodic to individual subjects data was performed fixing the number of components (IC) to be estimated.
Current dataset is heterogeneous because of a high motion for some subjects and slow motion for others: the first type of subjects requires an high number of estimated components to explain the variance of rs-fMRI signal, the latter type instead needs a low number of components. In case of this study, there are 2 subjects that moved a lot during images acquisition (subject 5 and 8) and applying Melodic on them without a fixed number of estimated components, the number of independent components was respectively 127 and 140. Instead for subjects which moved less, the number estimated by the tool was lower (for the first 3 subjects it was respectively 96, 73, 64). So several ICA tests with Melodic were performed on subjects' data to look for the optimal ICA dimensionality which best explains data: through visual inspection the parameter is then set to 100. Hence for each subject 100 independent spatial maps and relative timecourses are obtained.
The classification in noise or RSN components has been done manually based on visual inspection of spatial maps, timecourses and power spectrums, exploiting the advices and the informations given in the articles of [29] and [28].

Figure 3.1 shows some examples of these three pieces of informations, fundamental for components identification, in case of signal IC. On the left side 3 signal

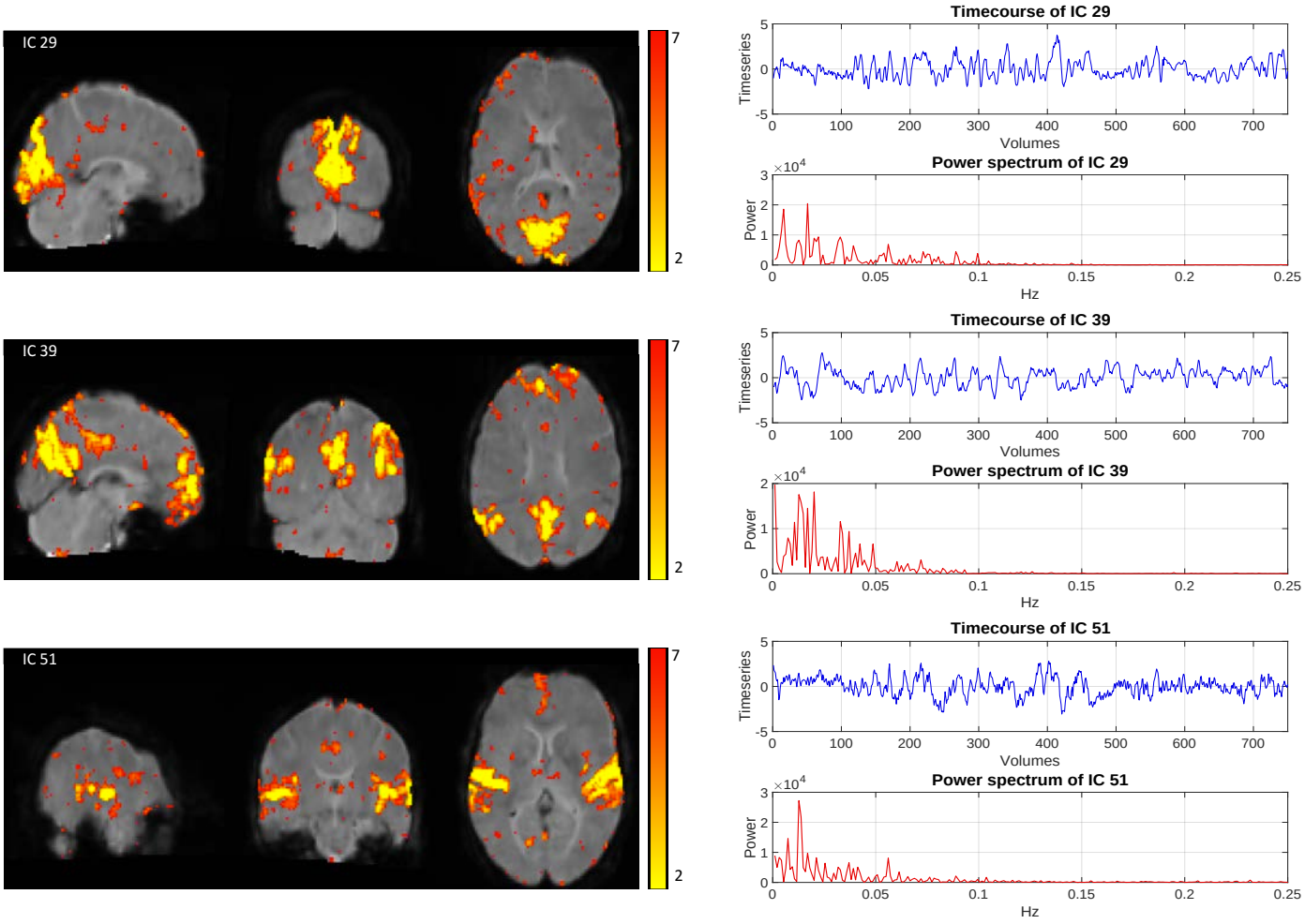

Figure 3.1: Graphic representation of some signal independent components coming from Melodic single subject. All three pieces of information are illustrated: on the left side, three spatial maps of subject 1 are showed, instead on the right the respectively timecourses and power spectrum are presented.

component spatial maps are showed and they represent respectively a visual, default and auditory RSNs. From maps on all three planes (sagittal, coronal and axial), clusters which define the components are big and well defined.
Timecourses of figure are characterized from a regular/oscillatory pattern, which

is typical of most of signals components. Power spectrum of signal sources is predominantly at low frequency (at least one strong peak within 0.01 - 0.1 Hz) as it is showed for all 3 signal IC in figure.

Figure 3.2 illustrates the three measures relative to some noise components. Compared to signals spatial maps, noise ones are characterized by smaller and sparse clusters which dispose mostly on the edges of the brain.

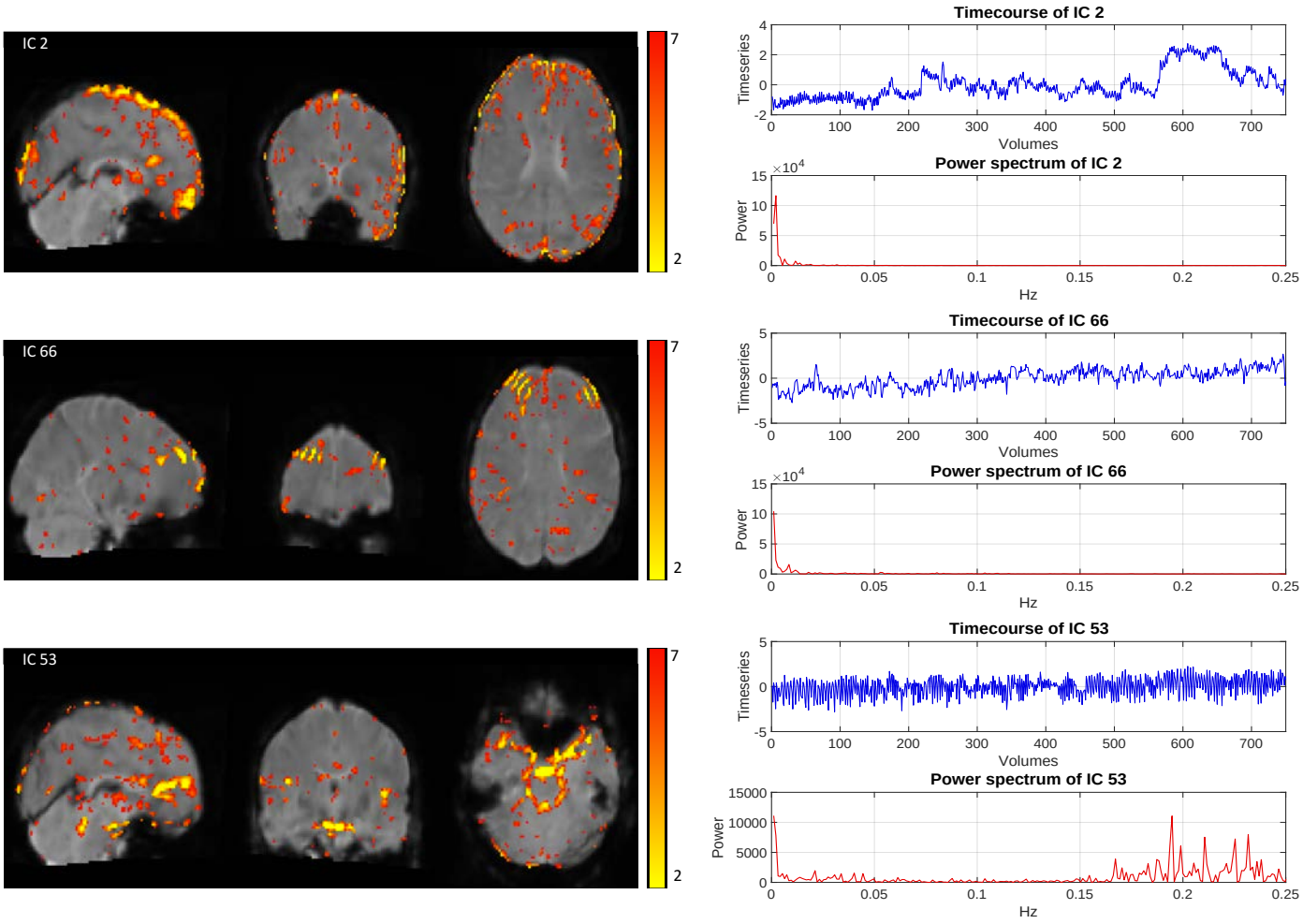

Figure 3.2: Graphic representation of some noise independent components coming from Melodic single subject. On the left side three spatial maps of subject 1 are showed, instead on the right the respectively timecourses and power spectrum are presented

In particular spatial maps of IC 2 highlights blood vessels, visible in the sagittal plane, and a ring near the edges of the brain resulting from a motion-related

source; IC 66 shows some stripes due to the effect of eyes rolling back; in the map (IC 53) the component reflects in the axial plane large arteries.
Timecourses of noise components can present large jumps and/or sudden change of oscillation pattern, as it can be seen in IC 2 timeseries. Regarding power spectrum noise sources are presented generally at high frequency as it can be seen in the power spectrum of IC 53, but cardiac and respiratory noise can often appear into BOLD low-frequency range (0.01 - 0.1 Hz) and this can be noticed in components 2 and 66.

Table 3.1 summarizes the results obtained from the cleaning-up of subjects' data. In particular the second column indicates the total number of noise com-

Subjects	**# noise components removed**	**explained variance removed**	**# components after clean up**
1	45	53.83	63
2	27	42.58	65
3	44	53.7	51
4	41	55.42	52
5	59	74.45	104
6	46	62.67	54
7	46	60.08	53
8	65	72.63	93
9	54	61.9	46
10	50	60.67	56
11	65	72.02	59
12	39	56.85	70
13	46	53.81	57
Mean value	48	60.05	63

Table 3.1: Results coming from the application of Melodic at the single subject level. In the first column the number of subjects is inserted; in the second and third one the number of noise components identified and removed and their respectively explained variance are showed; the last column represents, for each subject, the number of components estimated by Melodic after noise components are removed from patients data. The last row indicates the mean values of the results

ponents which for each subject are removed through command *fsl_regfilt*: on the average about half of components (48) have been removed from each data. In the third column the explained variance of all the removed components is specified. The last column reflects the number of components estimated by Melodic after subjects clean-up data. The mean value of this last column is 63 and it will be

used, as initial fixed number of group components, in the following group ICA analysis with GIFT.

3.2 Group spatial ICA

In order to decide which method is more performing with the available dataset for group-sICA, several comparisons between Melodic and GIFT are performed with similar input parameters. The testing parameters are represented on table 3.2.

	MELODIC	**GIFT**
Pre-processing	Normalization voxel-wise	• Intensity normalization • Variance normalization
Algorithm	FastICA	• FastICA • Infomax
Stability analysis	1 run	10 run

Table 3.2: Comparison between MELODIC and GIFT for group-ICA analysis. In GIFT two possibilities are tested in both Pre-processing and Algorithm type. Black dots reflect the possibility to chose one of the parameters

Regarding number of estimated independent components, it was fixed and its value is based on the model order selection criteria of both implementations of group sICA analysis. In Melodic the default technique of dimensions estimation is LAP, but there are available also the other methods. Instead GIFT provides only MDL method. This difference of criteria causes a different estimated number of components: Melodic estimates 101 components, GIFT 25 which results very low observing data components. Even changing Melodic's criteria to MDL the estimated number results very different to GIFT's ones (56 against 25), therefore the conclusion is that with the same criteria they work differently. Consequently to do a comparison between the two software, based on visual inspection the number of estimated components was fixed to 100.

Four comparisons were developed setting GIFT with pre-processing and Algorithm type varying during the tests while the other parameters of the table stayed fixed. The comparisons are based on exploring the respective Default Mode Network (DMN) and are developed between:

1. GIFT: variance normalisation, FastICA (setup1)
   Melodic: default parameters named in table 3.2 (setup2).

2. GIFT: variance normalisation, FastICA (setup1)
   GIFT: intensity normalisation, FastICA (setup3)

3. GIFT: intensity normalisation, FastICA (setup3)
   Melodic: default parameters (setup2)

4. GIFT: intensity normalisation, FastICA (setup3)
   GIFT: intensity normalisation, Infomax (setup4)

and they are showed respectively in figures 3.3, 3.4, 3.5 and 3.6.

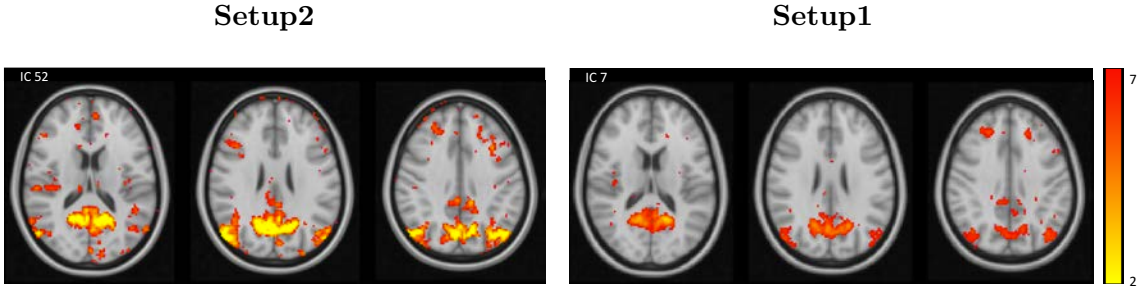

Figure 3.3: Comparison on Default Mode Network (DMN), at group level, between Melodic (Setup2) and GIFT which is run through Variance Normalization as pre-processing and FastICA as Algorithm (Setup1). Melodic results are reported on the left side, whereas GIFT's one are on the right side.

Observing the group spatial maps of the first three comparisons about DMN, it is noticed that Melodic (setup2) produces more intense but smaller sparse clusters, instead GIFT, performed with FastICA algorithm, gives as output well-defined and compact clusters with both variance and intensity normalization pre-processing (setup1 and setup3). Based also on the other spatial maps relative to different networks, Melodic doesn't hold this dataset, that is it seems not to be able to interpret data properly since that some networks result split in more

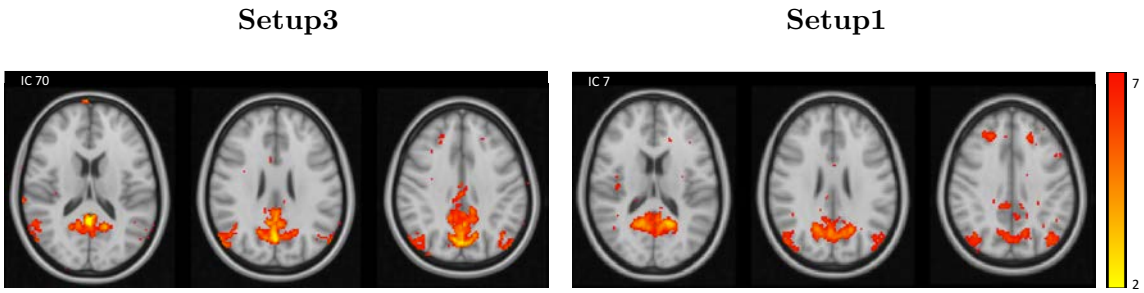

Figure 3.4: Comparison at group level on GIFT between different pre-processing. On the left Intensity normalization was used as pre-processing type (Setup3), instead on the right Variance normalization is used (Setup1). In both cases FastICA algorithm was chosen.

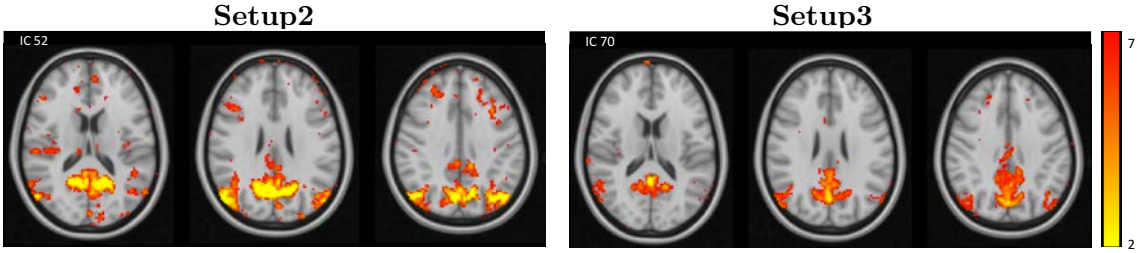

Figure 3.5: Comparison between Setup2 and GIFT which is run through Intensity Normalization as pre-processing and FastICA as Algorithm (Setup3). Melodic results are reported on the left side, whereas GIFT's one are on the right side. Spatial maps are extracted at group level and are compared respect to the same values range ([2 ; 7])

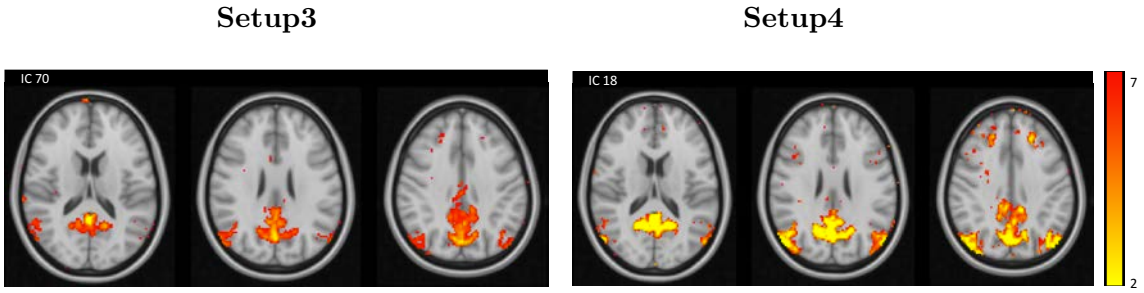

Figure 3.6: Comparison at group level on GIFT between different Algorithms: Setup3 with FastICA algorithm, Setup4 with Infomax. In both cases Intensity Normalization is used as pre-processing.

components.

Once GIFT has been chosen as method to do group-sICA analysis using the pre-processing intensity normalization, a last comparison between setup3 and setup4 (represented on figure 3.6) is made to understand which algorithm does a better estimate of independent components on available subject's data. Results from

both algorithms are very similar and in both cases signals are well-separated in sources, with Infomax producing more intense and compact clusters.

For these reasons group-sICA analysis is performed through setup4. Even in this case the components number has been fixed. To obtain an appropriate number of components, LAP criteria, performed by Melodic as default, was taken into advantage. In fact from the first tests it was noticed that, in case of this dataset, LAP seems to be the best estimator of components number. For this reason it has been used also for this selection. Hence the idea was to re-apply Melodic on data already cleaned to observe the new estimate of components number for each subject: as result 13 values were obtained, illustrated in the last column of table 3.1, then they were average obtaining 63 and this has been taken in consideration as number of component to be estimated. GIFT was applied on all subjects data using the dimensionality already obtained, but this mean value was not found to be representative of the entire group; therefore several tests were done with GIFT for group analysis, varying the number of components and increasing it to 100, choosing at the end an ICA decomposition dimensionality of 80.

Through group-ICA analysis performed by GIFT toolbox, 80 spatial ICA components and relative timecourses were estimated in the resting state fMRI data at both group and individual level. Some of the obtained spatial maps are reported in figure 3.7: it can be noticed that despise the cleaning through Melodic, there are still remarkable noise sources, as those highlighted on the right side of the figure.

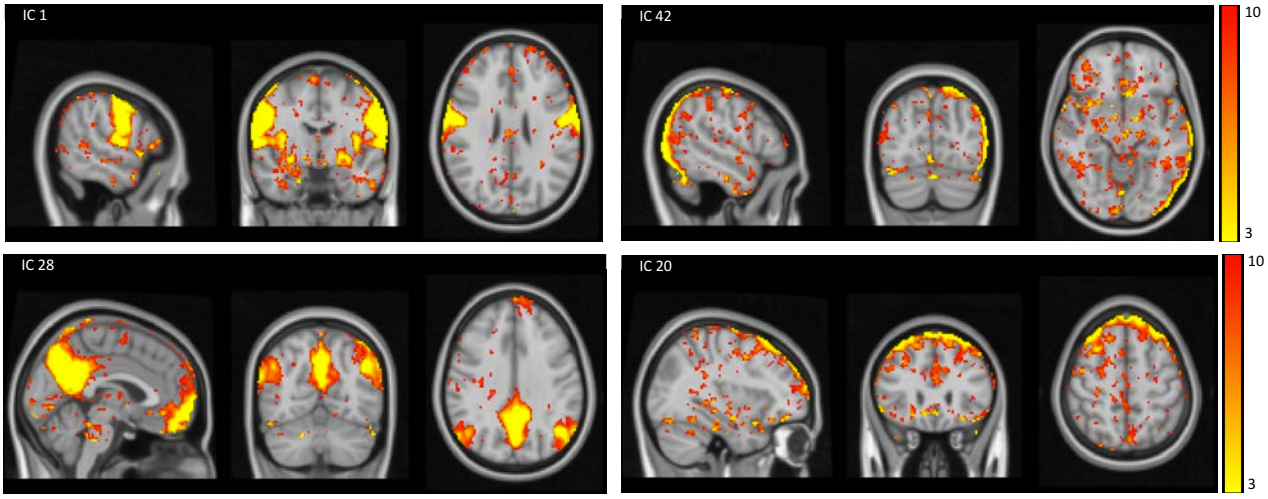

Figure 3.7: Examples of Group Spatial ICA components from GIFT. In particular two signal components are showed, on the left side, and two noise ones on the right

3.3 Temporal ICA

The timecourses of each subject obtained from the back-reconstruction of GIFT during the previous sICA analysis are concatenated and fed into FastICA algorithm to identify the temporal independent components. In this phase, as Glasser suggested, ICASSO procedure was used to estimate the appropriate number of components. In particular the index quality measure I_q is showed in figure 3.8. Each filled black circle represents the value of I_q associated to the relative component/cluster. A high value of I_q is related to a compact and tight cluster which reflects consequently a reliable component. The components with an index-quality measure $I_q > 0.5$ define how many of them have to be estimated: 53 components are over the threshold.

The component selection is based on a compromise. The method proposed by Glasser just described, has been performed on available dataset, but some issues have been detected: using the resulting 53 as components' number led some RSNs to converge on the same component, other times network and noise have appeared on the same component. The chosen dimensionality seems therefore not to be appropriated. As consequence a major number of component has been considered, in particular it has been increased up to 60. This choice is equivalent to analyse how many components have an $I_q > 0.47$ which is not so much different

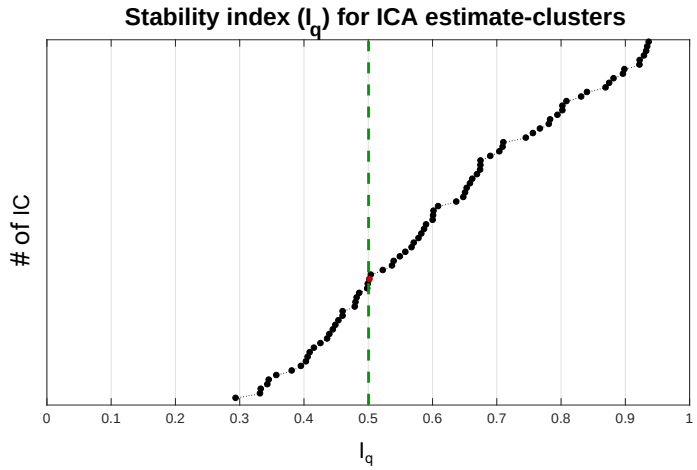

Figure 3.8: The quality indices Iq are showed in rank order of the clusters. Green dotted line is the threshold between clusters with $I_q > 0.5$ and those with $I_q < 0.5$. The red circle is the separator between the two groups.

to the previous threshold. Therefore increasing the number of components can be feasible without lowering extremely the quality of clustering.

Once tICA is completed, results are group and individual 60 spatial maps computed through the equations 2.17 and 2.18 and concatenated timecourses of the 60 components coming from FastICA. Examples of resulting group spatial maps are reported in figure 3.9. As it is expected, some IC clearly represent a network component, for example IC6, IC14 and IC32 are a default, a somatomotor and a visual network. Even several noise components seem to be clearly separated compared to signal ones. The three IC illustrate on the right side of figure 3.9 are certainty only noise-related sources.

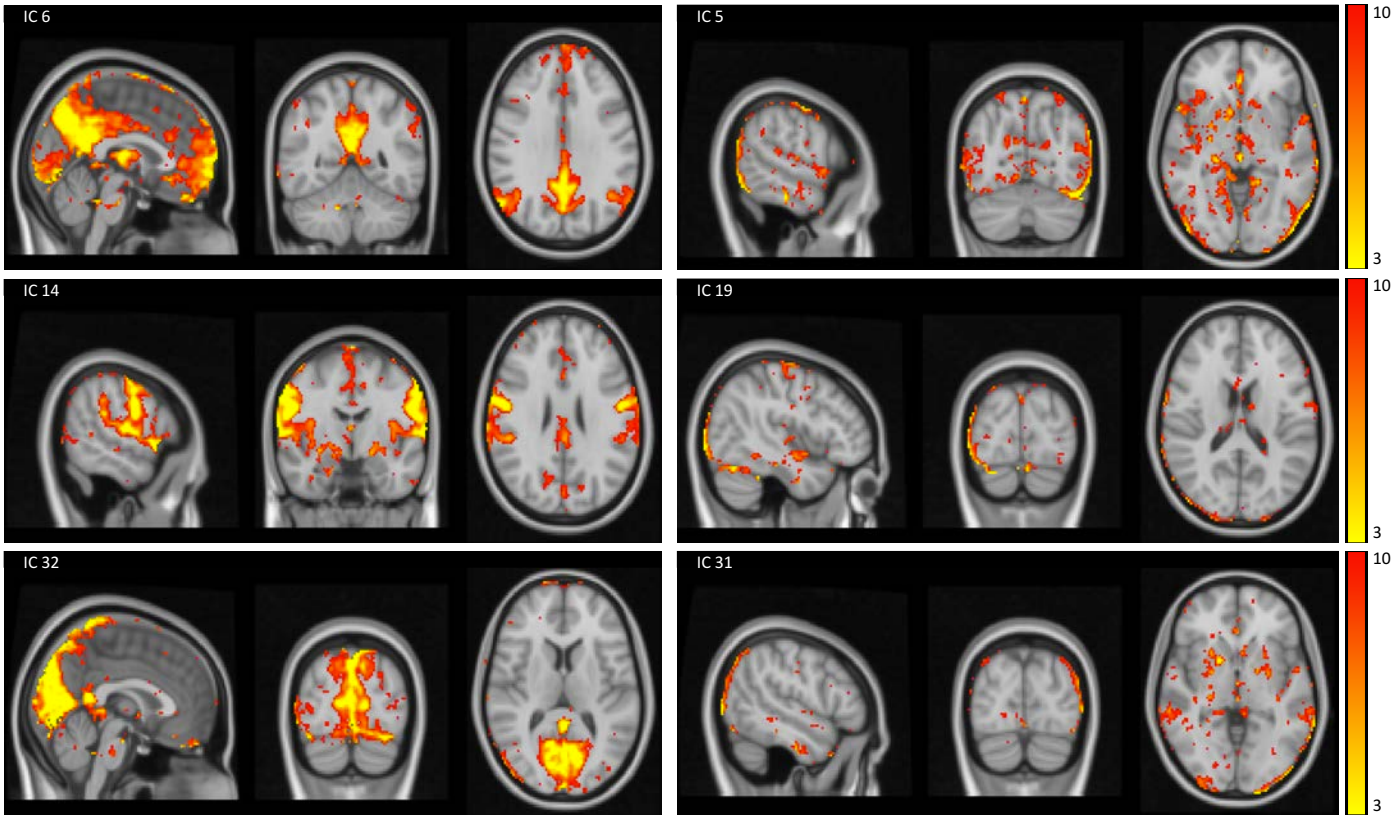

Figure 3.9: Examples of Group Temporal ICA spatial maps. Three group signal components (IC 6, IC 14, IC 32) are illustrated on the left. On the right side the components 5, 19, 31 reflect noise sources. The range of values is the same for all components ([3 ; 10])

3.4 Indices

3.4.1 Normalized Difference in Amplitude for DVARS dips

The first index for identification of motion-related noise components, $diff_{\text{AmpDVARS}}$, exploits the DVARS measure. DVARS is a metric that should reflect subject's motion. All traces are demeaned ($DVARS_0$) to allow comparisons between different subjects. From these traces it has been observed a difference in the amplitude of DVARS among subjects: all subjects except 13th could be observed starting from the same range of DVARS values ([-2 4]); on the contrary subject 13 presented a bigger range of values ([-5 15]), this means that the variance of the signal is completely different from the others. This strong variation of a subject compared to the others is due to the update of the scanner of magnetic resonance, therefore it is important to apply a certain normalization on DVARS data, in order they

could be compared appropriately.
As solution to this problem it was decided to normalize each DVARS trace for the mean intensity of images of the relative subject, resulting new traces named as $nDVARS$. Even the mean value has been removed, obtaining $nDVARS_0$. This method brought all subjects in a comparable range and appears as the more sensible metric to find out how subjects behaved during the acquisition.
Figure 3.10 shows for three subjects DVARS before and after normalization: subject 13, which is represented in the last row, now falls within variance of the others and hence he can be reasonable compared to other subjects.

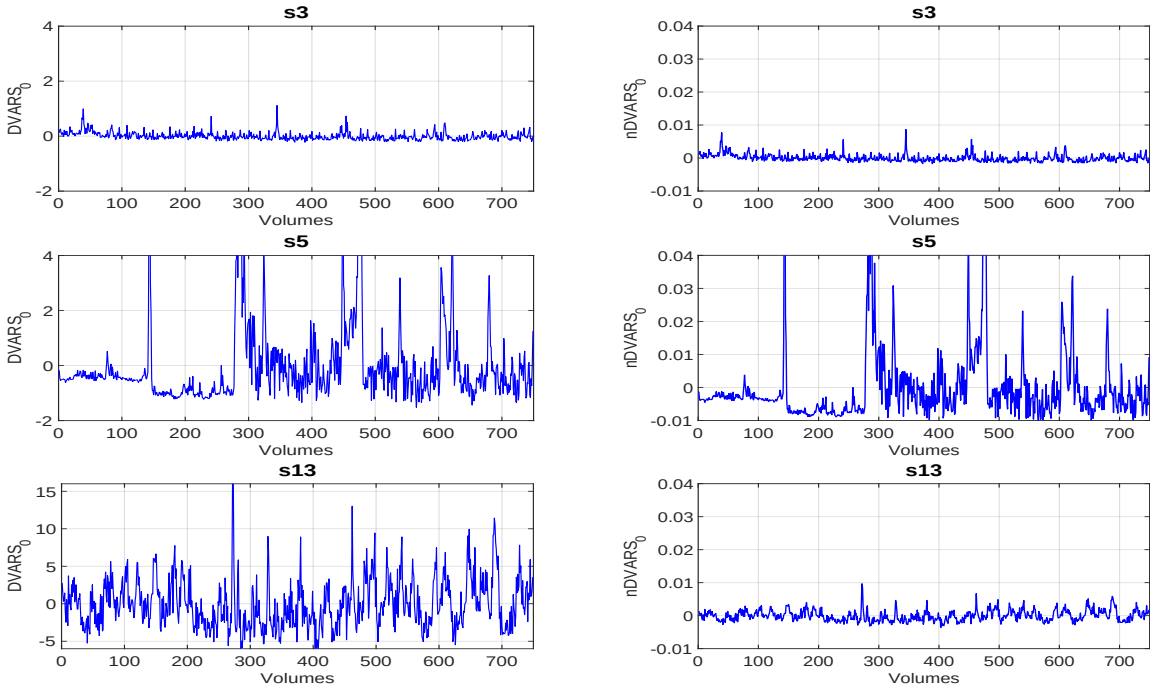

Figure 3.10: Comparison between $DVARS_0$ and $nDVARS_0$. The first one is illustrated on the left side and reflects DVARS plot in which mean value has been removed. Three example of representative subjects are showed: the first one moved not so much, in the second one it can be noticed a greater number and a major amplitude of peaks of motion; the last one represents an example of how the signal can change when there is a variation of the sequence. On the right the same DVARS traces have been demeaned, but also normalized for the mean intensity of the relative images ($nDVARS_0$)

In order to understand how much a subject moved during fmri data acquisition, in general the trend of DVARS trace and its peaks are inspected. In table 3.3 mean values and standard deviation of $nDVARS$ have been inserted for each subject. These $nDVARS$ are computed starting from data cleaned by Melodic single

subject. Subjects which moved a lot (for example subject 5, 8 and 11) provide to a standard deviation higher compared to others and they are characterized by very large and frequent peaks of motion or otherwise a variable pattern. Subjects that moved less, for example subject 3, 6 and 10, present a homogeneous trend with few and low spikes, so their standard deviation is lower and their values are generally small.

# Subjects	1	2	3	4	5	6	7	8	9	10	11	12	13
$\overline{\mathbf{nDVARS}}$ $_{\times 10^{-2}}$	3.52	2.77	2.98	2.82	3.14	3.32	2.63	2.52	2.99	3.59	2.40	2.74	2.53
nDVARS *std* $_{\times 10^{-3}}$	1.9	2.0	1.1	2.2	12.7	1.7	1.7	4.6	1.8	2.1	2.3	2.1	1.7

Table 3.3: Table of values of mean and standard deviation of nDVARS traces, computed after clean-up of Melodic single subject (s-sICA). In the second row the mean values are reported up to a constant multiplier equals to 10^{-2}. The last row represents the nDVARS standard deviation which is reported up to a constant multiplier equals to 10^{-3}.

Now the aim is to find DVARS spikes or dips remaining after the first clean-up procedure (*post s-sICA*) and to analyse tICA components' timeseries corresponding to peaks' instants/frames. Spikes and dips are needed for the computation of the metric $diff_{\text{AmpDVARS}}$ and they can be identify through a fixed threshold.
Several thresholds are tested and some examples of the application of the first chosen threshold, proposed by Glasser, are illustrated in figure 3.11: in each box, timecourse DVARS trace related to a subject is demeaned and then normalized for its maximum value, obtaining $gDVARS_0$. The threshold, represented with red dotted lines, is set to ± 25: all that is out of the band produced by the threshold is considered peak/dip.
Observing the graphs, it is noticed that a large amount of values is often brought outside the thresholds' band, but in reality those values are not all significant and so representative of movement. For example subjects 3, 6 and 10 have a lot of values over the threshold, but their $DVARS_0$ trace seem to have an homogeneous pattern, with no particular high peaks.
The threshold proposed by Glasser can't be adaptable with available dataset, its value is different from one subject to another and it results quite variable among

them, as consequence there are often too much values that are outside the band identified by the threshold.

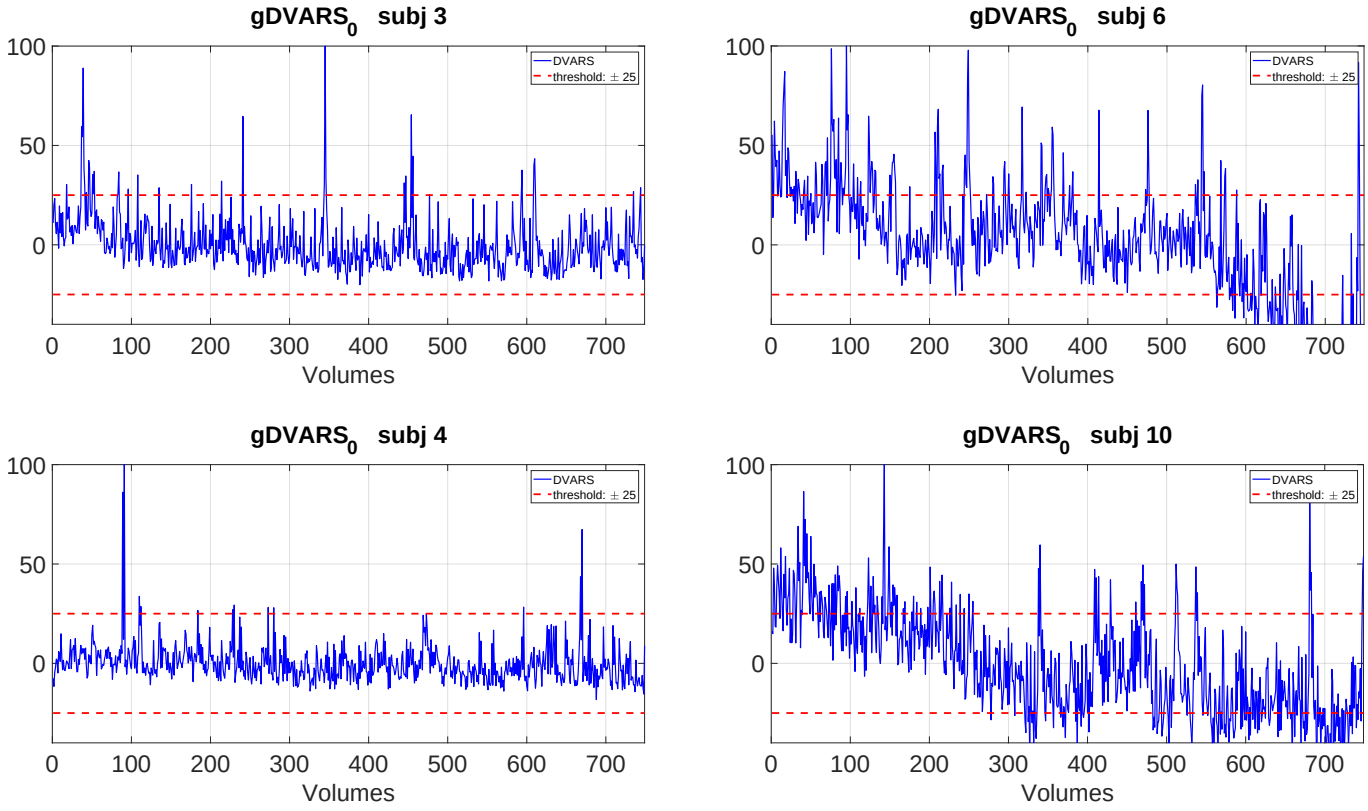

Figure 3.11: Examples of $gDVARS_0$ plots. The term g indicates the application of Glasser's threshold, i.e. all DVARS are normalized to the relative maximum value and the threshold has been fixed for all subjects to $\pm$ 25. The subscript 0 reflects the fact that traces are demeaned. The red dotted lines represent the chosen threshold of $\pm$ 25

The successive thresholds used for the same aim are computed considering $nDVARS_0$ of all subjects, so demeaning each of them and normalizing for the mean intensity of images of the specific subject. Then all DVARS are taking into account together to find one only threshold for all.

The threshold calculated through 10th percentile is showed in figure 3.12: for each subject their respective 75 higher values (peaks) of DVARS trace are figured in descent order. Green dotted line is the threshold obtained taking into account the 10th percentile of all 975 peaks (75 $\times$ number of subjects) and its value is 0.0117. Under this threshold the 10% of observations are situated.

The other thresholds are computed as a function of the standard deviation σ

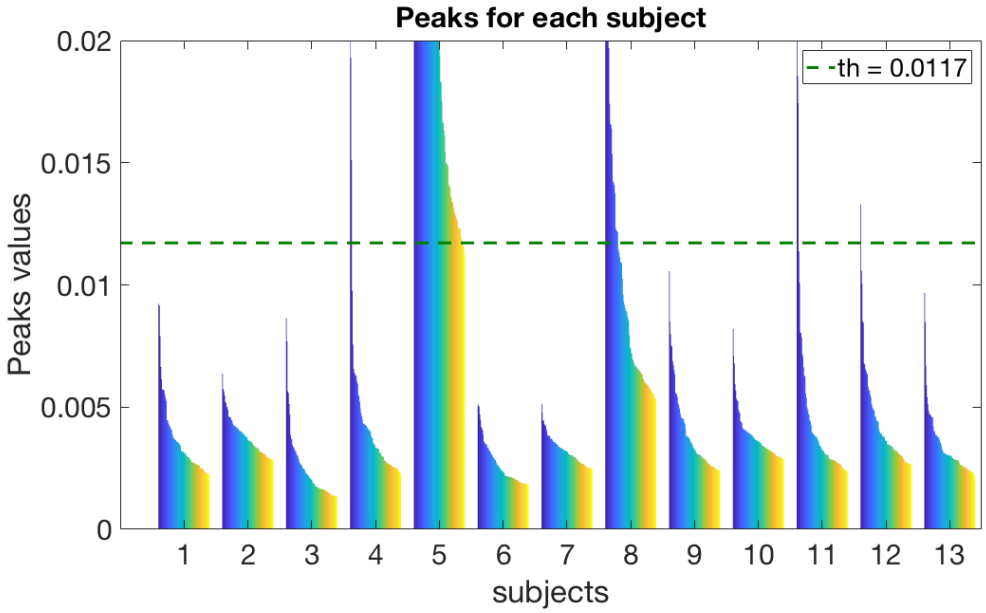

Figure 3.12: Histogram of higher 75 values (peaks) of each subject's DVARS. Green dotted line represents the threshold computed with 10th percentile

of DVARS of all subjects.

Three examples of subject DVARS traces with the 3 thresholds are showed in figure 3.13: in particular for subjects 4, 8 and 10 demeaned and normalized DVARS are represented with thresholds of 10th percentile, 2σ, 1.64σ and σ that are respectively figured in green, magenta, red and black dotted lines.

As it can be seen, those thresholds seem to be more appropriate respect to the first one represented in figure 3.11.

The values of all the five computed thresholds are reported in table 3.4. The second column, Thr_g, represent the threshold values proposed by Glasser, instead the other columns, Thr_α Thr_β, Thr_γ and Thr_θ reflect the values of the four thresholds computed in addition to those proposed in the reference paper [3]. These last four thresholds are calculated at group level and are constant for all subjects. On the contrary Thr_g is extremely variable and also from figure 3.11 would consider as spikes/dips too much DVARS frames.

The choice of the more appropriate threshold based on only observing DVARS plot of all subjects, but on the inspection of outliers number on traces and how it distributed among subjects.

Thr_g produced a number of frames outside the band of about 16.8% of the all

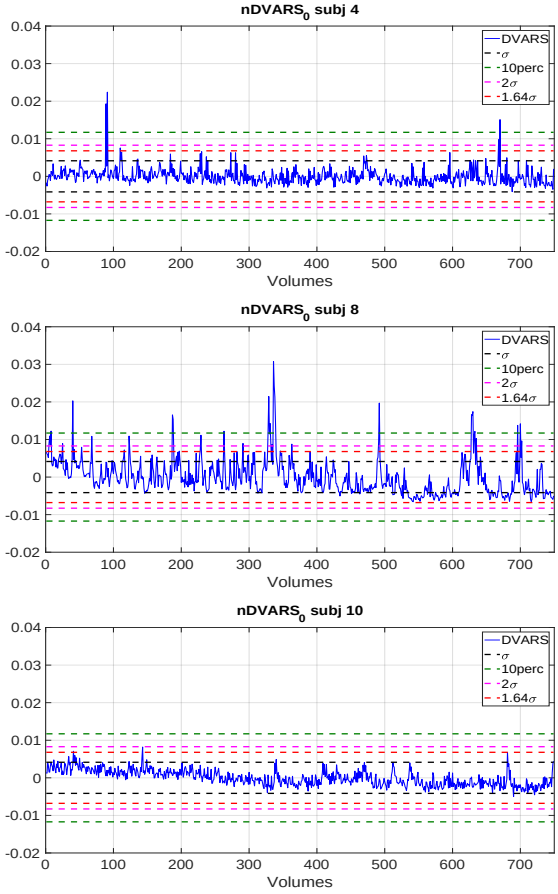

Figure 3.13: Examples of subject $nDVARS_0$ traces (demeaned and normalized by the respective mean intensity of the images). Four thresholds are showed and represent 10th percentile (green), 2σ (magenta), 1.64σ (red) and σ (black). All values outside the band defined by two symmetric thresholds are the so called spikes/dips

traces. For some subjects that moved less the number of outliers resulted too much big: for example subject 6 and 10 traces are homogeneous, with low values and without particular high peaks, but Thr_g highlighted respectively 251 e 257 values outside the band, so about 34% of total frames, as consequence these outliers numbers are too high. On the contrary for subjects which moved a lot during the acquisition as subject 5 and 8, the selected outliers are respectively 16 and 36, resulting probably fewer observing their DVARS traces. Therefore Thr_g has been easily excluded as method for threshold choice.
The other thresholds, Thr_α, Thr_β, Thr_γ and Thr_θ, produce a constant threshold which seems to be more appropriate for this dataset. They highlight an outliers

Subjects	Thr_g	Thr_α	Thr_β	Thr_γ	Thr_θ
1	0.3141	0.0117	0.00828	0.00679	0.00414
2	0.2264	0.0117	0.00828	0.00679	0.00414
3	0.2788	0.0117	0.00828	0.00679	0.00414
4	0.8290	0.0117	0.00828	0.00679	0.00414
5	4.7199	0.0117	0.00828	0.00679	0.00414
6	0.1636	0.0117	0.00828	0.00679	0.00414
7	0.1846	0.0117	0.00828	0.00679	0.00414
8	0.8848	0.0117	0.00828	0.00679	0.00414
9	0.3794	0.0117	0.00828	0.00679	0.00414
10	0.2934	0.0117	0.00828	0.00679	0.00414
11	1.0962	0.0117	0.00828	0.00679	0.00414
12	0.4566	0.0117	0.00828	0.00679	0.00414
13	4.6970	0.0117	0.00828	0.00679	0.00414

Table 3.4: Representation of thresholds' values for each subject. Thr_g is Glasser's threshold. The other thresholds, named in the following columns, are all those computed in this work and are respectively 10th percentile (Thr_α), 2 σ (Thr_β), 1.64 σ (Thr_γ) and σ as Thr_θ. While Glasser's threshold changes compared to subjects, the other are computed at group level and so they are fixed for all

number respectively of 0.99%, 2%, 3.4% and 8% compared to the total of traces. Observing subjects plots attempts have been made to understand which threshold could be suitable to identify frames with high spikes and without selecting those that couldn't reflect motion. For example from the three plots of figure 3.13 it was quite clear that green and black thresholds (Thr_α, Thr_θ), for opposite reasons, don't highlight appropriately spikes/dips.
Starting from all these informations, the choice fell on Thr_γ which allowed to select among all subjects a number of peaks/dips selected beyond the band equals to 335.

Once the classification between DVARS peaks/dips and non-peaks/non-dips is completed, the quantitative component-wise measure based on DVARS, $diff_{\text{AmpDVARS}}$, is computed through equation 2.30 for each component. The results of this computation is represented in figure 3.14. Red dotted line is the threshold equals to 0.945 and it has been calculated through equation 2.31, where the selected signal components are illustrated as the green diamonds, noise components as red

filled circles. These six components have been selected manually and are already illustrated in figure 3.9: the three signal components were easily identified as networks because of the presence of big and compact clusters, the three noise ones also were detected very quickly as manly the edges of the brain are highlighted. Observing figure 3.14, signal components are situated below the threshold as expected because they have been chosen the most credible ones among all the possible signals and less influenced by motion, so their value of $diff_{\text{AmpDVARS}}$ will be low.

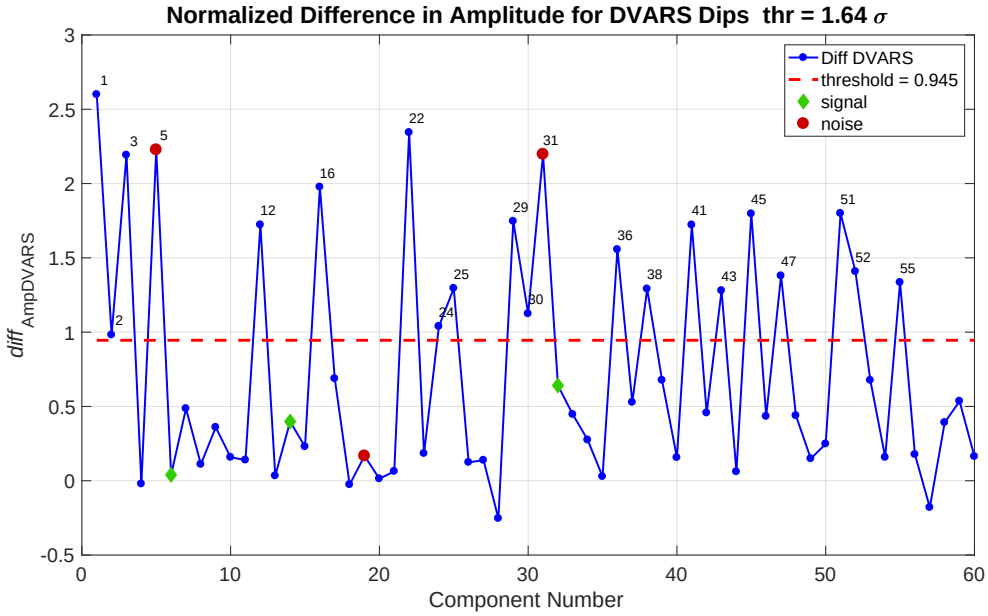

Figure 3.14: Difference in component amplitude (standard deviation σ of component timeseries) between frames with DVARS dips and those without DVARS dips normalized by the component amplitude across all frames. Red dotted line is the threshold that best discriminates between the components that had already been clearly identified as signal (green diamonds) or noise (red filled circles). The numbered components are those above the threshold

3.4.2 Variability between subjects: $\boldsymbol{Variability_{\mathrm{Amp}}}$, $\boldsymbol{Diff_{\mathrm{AmpDVARS}}}$

The other two evaluation indices are based on an analysis of amplitudes variability of component across subjects.

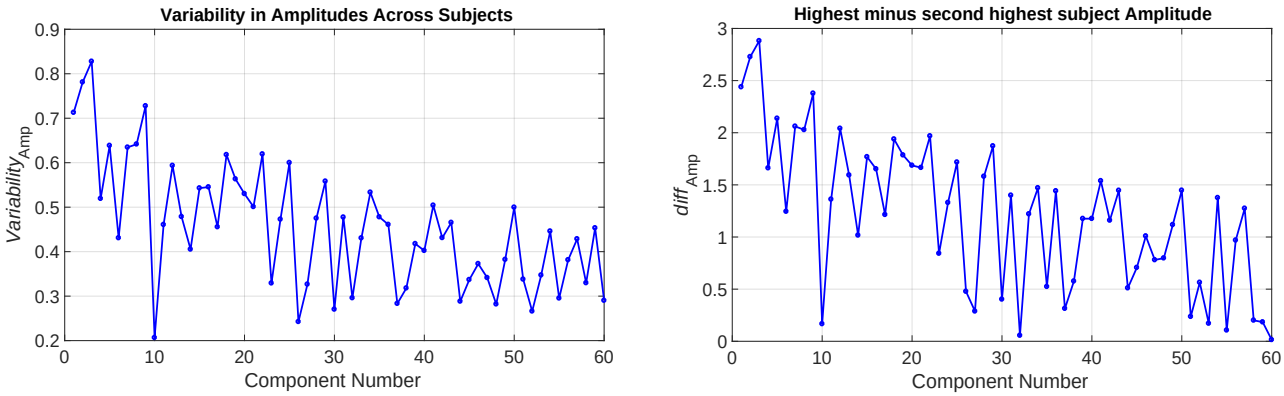

Figure 3.15: Comparison between $Variability_{Amp}$ and $diff_{Amp}$ metrics: variability in amplitude across subjects, represented on the left side, and difference between the two highest subjects amplitudes, illustrated on the right

Figure 3.15 illustrates the results obtained from equations 2.34 and 2.35 which describe the two metrics: the variability in amplitude across subjects for each component ($Variability_{Amp}$) on the left side and the difference between the two highest subjects amplitudes ($diff_{Amp}$) on the right side. The first one, for a given component, grows with the increasing of the component timeseries variability (standard deviation). The latter, for a given component, takes into account the dissimilarity of the two highest subjects amplitudes, highlighting those components that are particularly strong in a single subject.
Plots assume different range of values, but reveal a very similar trend. This lead to analyse the behaviour of the two indices and concluding that $Variability_{Amp}$ is little representative of group differences due to the reduced number of subjects: in the limit case the timeseries standard deviation of only one subject is very different from the others, the value of $Variability_{Amp}$ of a component raises significantly, showing the same behaviour of $diff_{Amp}$ whose aim is to expose the difference between two subjects amplitudes.

Figure 3.16 depicts the $diff_{Amp}$ measure plus the threshold (red dotted line) computed according to equation 2.31.

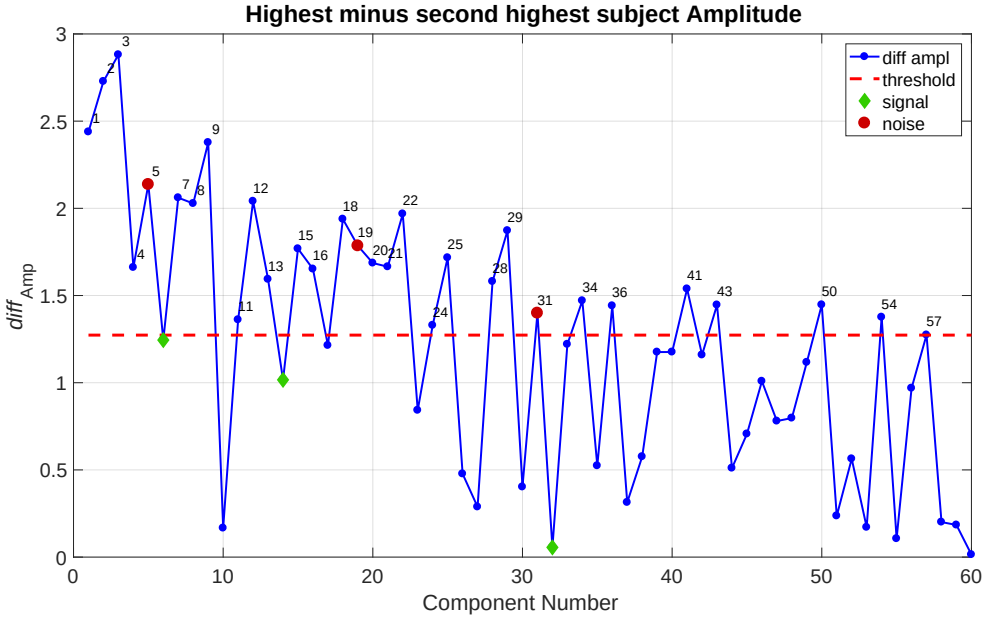

Figure 3.16: Difference between the maximum subject's component amplitude and the next highest subject's component amplitude normalized by the overall amplitude of each component. Red dotted line is the threshold that best discriminates between the components that had already been clearly identified as signal (green diamonds) or noise (red filled circles). The numbered components are those above the threshold

3.5 Identification of noise-related components

The two metrics $diff_{\text{AmpDVARS}}$ and $diff_{Amp}$ have been used for the identification of noise-related components. These components are those that result above both thresholds of the two plots. From the first plot, 21 components are above the threshold, while in the latter one, 30. The component common to both plots result 14 and their spatial maps can be seen in figure 3.17. These 14 components are removed from data, obtaining a total explained variance of those component equals to 41.47%.

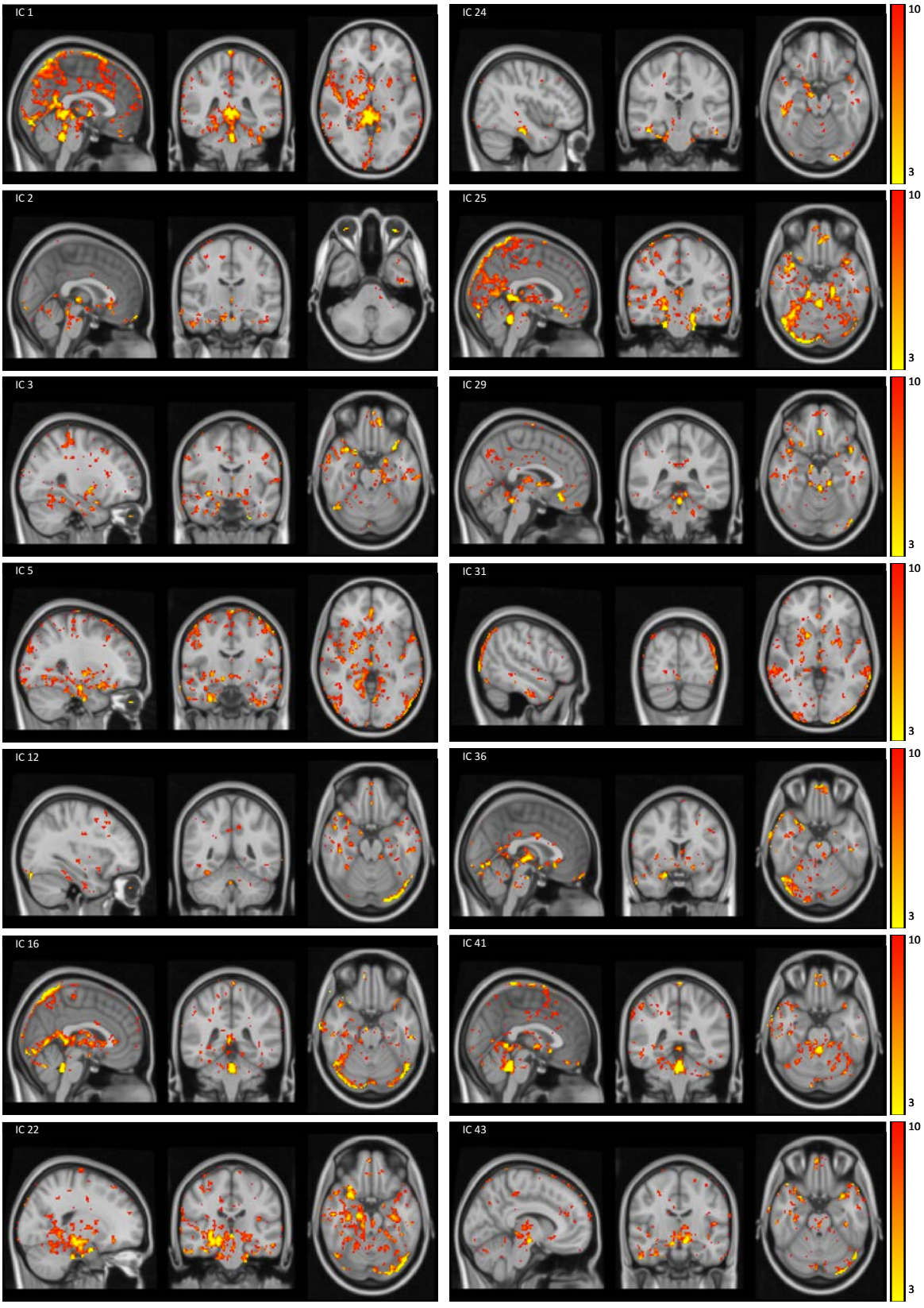

Figure 3.17: Temporal ICA components identified as noise. All spatial maps are reported in order and are saved with the same range of values ([3 ; 10])

3.5.1 Outlier Detection

The application on available dataset of the entire procedure described in this work (figure 2.4) and of indexes $diff_{\text{AmpDVARS}}$ and $diff_{Amp}$, with all the choices already justified, brought to the identification and removal of 14 tICA components classified as noise.

A further analysis has been that to verify if obtained results were somehow strongly influenced from some outliers of motion. In this case subject 5 was taken into account as he moved a lot during the acquisition compared to the others and this has been noticed starting form his DVARS traces. Hence attempts have been made to check if subject 5 have had a strong impact on results and how much this method is robust to outliers.

Figure 3.18 illustrates $nDVARS_0$ of subject 5: there are several high peaks that get to reach values near 0.14, in contrast to the others subjects DVARS that don't exceed 0.04.

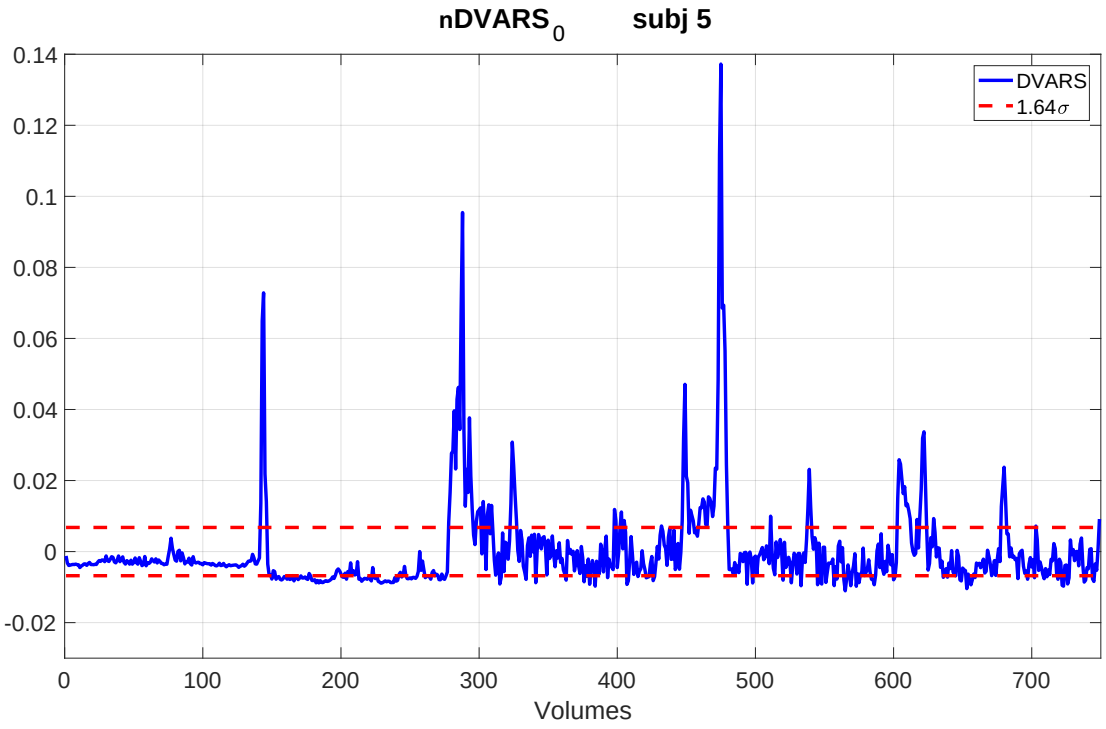

Figure 3.18: $nDVARS_0$ traces of subject 5 (demeaned and normalized by the mean intensity). Red dotted line is the threshold equals to 1.64 σ and representing about the 90% of data

This led to analyse obtained results after applying $diff_{\text{AmpDVARS}}$ and $diff_{\text{Amp}}$ for the identification of noise components, to verify if these are influenced from subject 5. Values of $diff_{\text{AmpDVARS}}$ are based on the partitioning of DVARS traces in spikes/dips and not-spikes/dips.

Hence the number of peaks is counted for each subject and result is represented in table 3.5: 76.4% over the total peaks comes from subject 5. Therefore the computation of thresholds has been rerun for DVARS plots, without considering subject 5.

# Subjects	1	2	3	4	5	6	7	8	9	10	11	12	13
# peaks over threshold	3	0	2	5	256	0	0	43	6	2	10	6	2

Table 3.5: Table of peaks over DVARS plot threshold (1.64 σ) for each subject

The new values of thresholds Thr_α Thr_β Thr_γ Thr_σ are reported on table 3.6 in second column. Last column reflects the values of the same thresholds, but computed before with all subjects. All threshold values lowered without considering subject 5 and this is expected as subject 5 DVARS is quite variable with some high spikes. Therefore the new thresholds are more stringent.

Threshold	**Value with 12 subjects**	**Value with all subjects**
Thr_α	0.00658	0.0117
Thr_β	0.00452	0.00828
Thr_γ	0.00370	0.00679
Thr_σ	0.00226	0.00414

Table 3.6: Representation of thresholds' values obtained without considering subject 5 in the second column, considering all subjects in the last column

The difference in thresholds' results can be seen also in figure 3.19 in which three subject DVARS traces are illustrated with all the computed thresholds.

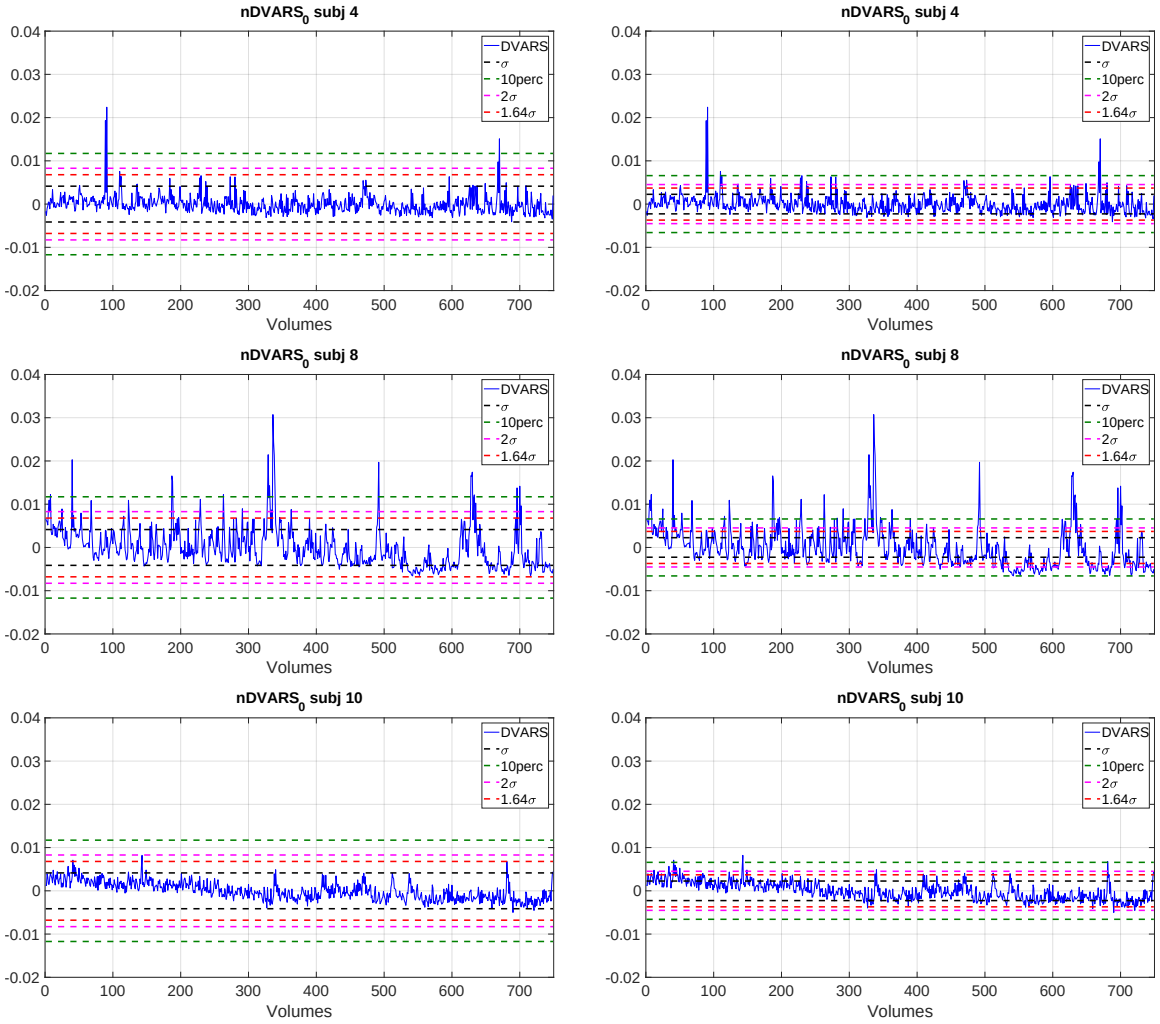

Figure 3.19: Examples of comparison between subject $nDVARS_0$ traces with all four thresholds performed in this work. On the left side three examples are presented, in which all thresholds were computed considering all subjects. On the right one, the same example are reported, but in this case the thresholds are computed on group excluding subject 5, resulting lower values.The four thresholds are 10th percentile (green), 2σ (magenta), 1.64σ (red) and σ (black)

The case of considering all subjects except patient 5 (right side of the figure) allowed to get lowered thresholds. For example the two cases can be compared considering the threshold Thr_β. In case with all subjects, Thr_β highlighted 335 spikes/dips above the band defined from the threshold, but most of them came from subject 5; in the second case, so without subject 5, peaks number for each subject is more homogeneous. In fact excluding subjects 8 and 3 (the first one moved a lot so reasonable most of his spikes are above the band, while the latter one is the one which moved little so the number of his peaks il very low) the number of peaks highlighted on average for each subject is 34 compared to all 750 values, so about 4.5% of the entire trace. This value is much more reasonable

with respect to case with subject 5 in which only 0.88% of values for each subjects were assigned as spikes/dips.

As before the focus now is to select the threshold more appropriate for peaks/dips identification. Even in this case the number of outliers has been inspected for all threshold. More specifically it has been analysed Thr_β Thr_γ Thr_σ, that are based on standard deviation, to understand if standard deviation could be appropriate measure to go on for thresholds computation.
Regarding this last aspect, all thresholds based on σ are computed on concatenated DVARS of the 12 subjects: observing the distribution of concatenated DVARS in figure 3.20 it has been found that is not properly a gaussian distribution because of the presence of a very long right tail.

The solution adopted in this work is to characterize a gaussian distribution based

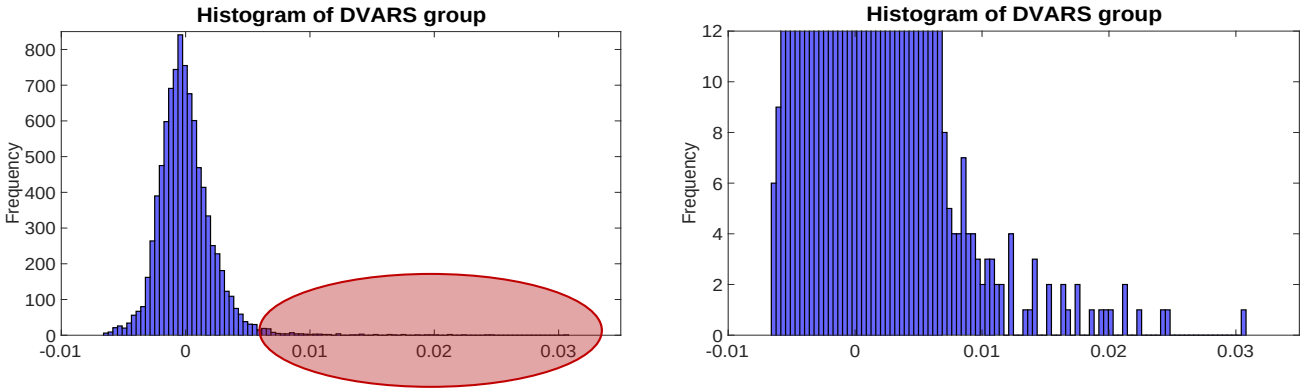

Figure 3.20: Distribution of concatenated DVARS without considering subjec 5. The figure on the right side is a zoom version of the left one, highlighting the long right tail circled in red

on reference subjects, that is those optimal subjects which don't move or moved not so much: in this case based on individual DVARS inspection with mean and standard deviation values, they are 2, 3, 6, 9, 10 and 13. The new distribution will have zero mean and a certain standard deviation (Σ). Now subjects DVARS are compared individually to this reference distribution which is illustrated in figure 3.21: everything that is outside 2Σ will be considered as outlier of motion. The value 2Σ is equals to 0.00352 and reflects the fact that data has the probability of 95% to fall inside the band derived from threshold.

In this way the new threshold to be applied for all DVARS traces is 2Σ. Figure 3.22 shows two examples of subjects DVARS traces in which threshold of 2Σ is

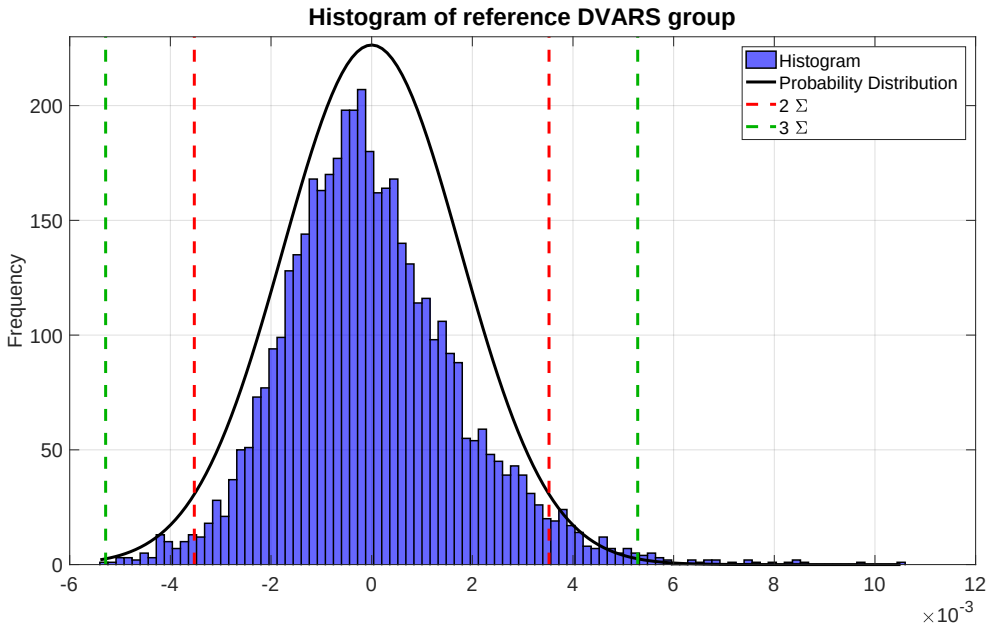

Figure 3.21: Histogram represents the reference distribution of concatenated DVARS. Black line is the reference probability gaussian distribution, red dotted lines are the threshold of 2 Σ (0.00352), instead green one are the threshold of 3 Σ

applied.

Through this threshold the classification of DVARS peaks/dips and non-peaks/non-dips is computed, obtaining for each subject a number of peaks as reported in table 3.7, with a total of 719 spikes and dips. From the table it is noticed that lots of

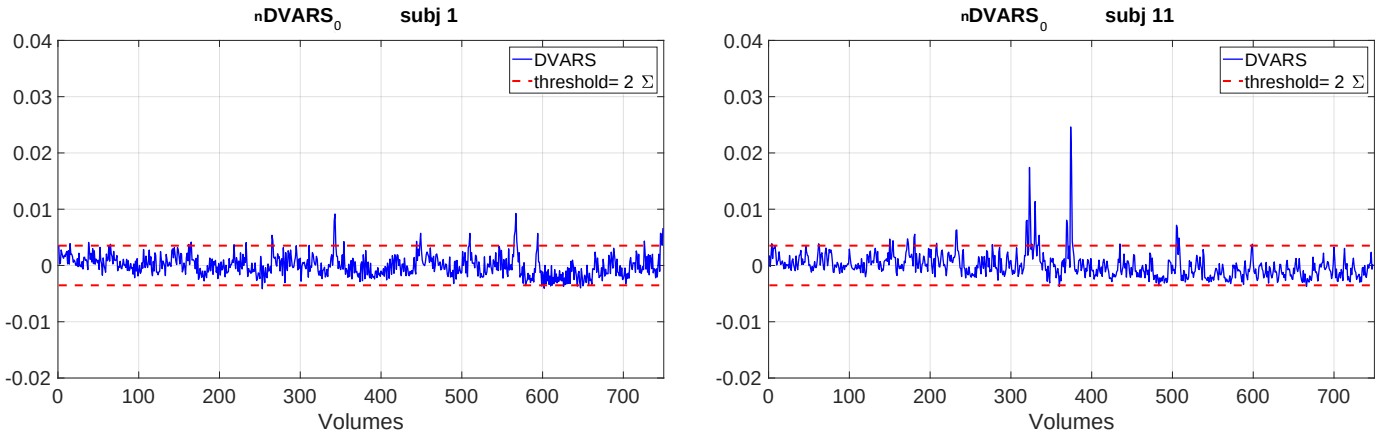

Figure 3.22: Example of DVARS traces with 2 Σ threshold. In particular DVARS of subject 1 and 11 are represented. Red dotted line is the threshold 2 Σ

identified spikes comes from subject 8: this is expected because his DVARS traces present many and wider peaks. A complementary consideration can be made on subject 3, whose DVARS has been already showed in figure 3.10: DVARS trace is quite homogeneous with few and low spikes, therefore it is reasonable that a low number of values has been identified as spikes.

# Subjects	1	2	3	4	5	6	7	8	9	10	11	12	13
# peaks over threshold	39	53	9	36	-	55	21	316	34	54	36	40	26

Table 3.7: Table of peaks over DVARS plot threshold (2 Σ) for each subject without considering subject 5

As before the quantitative component-wise measure based on DVARS is computed through equation 2.22 for each component. Figure 3.23 illustrates the two plots coming from this measure in the case of considering all subjects (figure on the left side) and of excluding subject 5 from the analysis (figure on the right). It can be noticed that not considering subject 5 significantly modifies $diff_{\text{AmpDVARS}}$ values.

Regarding $diff_{\text{Amp}}$ even in this case the focus is to analyse results obtained with all subjects, already showed in figure 3.16, and verify how much they are influences by subject 5. That can be seen in figure 3.24: on the left $diff_{Amp}$ plot is showed again, with the addition of the presence of pink stars that reflect components in which the maximum amplitude belongs to subject 5; instead on the right an histogram is created which count the number of times each subject assumes the maximum components amplitude. Observing this histogram, it is evident that subject 5 assumes the maximum amplitude in one-third of all components.

Therefore even $diff_{Amp}$ index should be significantly influenced by subject 5. To verify that, the index is recomputed, as already done for $diff_{AmpDVARS}$, without considering the subject 5. Figure 3.25 illustrates the two $diff_{Amp}$ plots in which the graph on the left takes into account all subjects, the right one is obtained excluding subject 5 from the analysis. In both figures red dotted threshold is computed, through equation 2.31, as the average value of the mean of three signal (components 6, 14, 32) and mean of three noise (5, 19, 31) components amplitude.

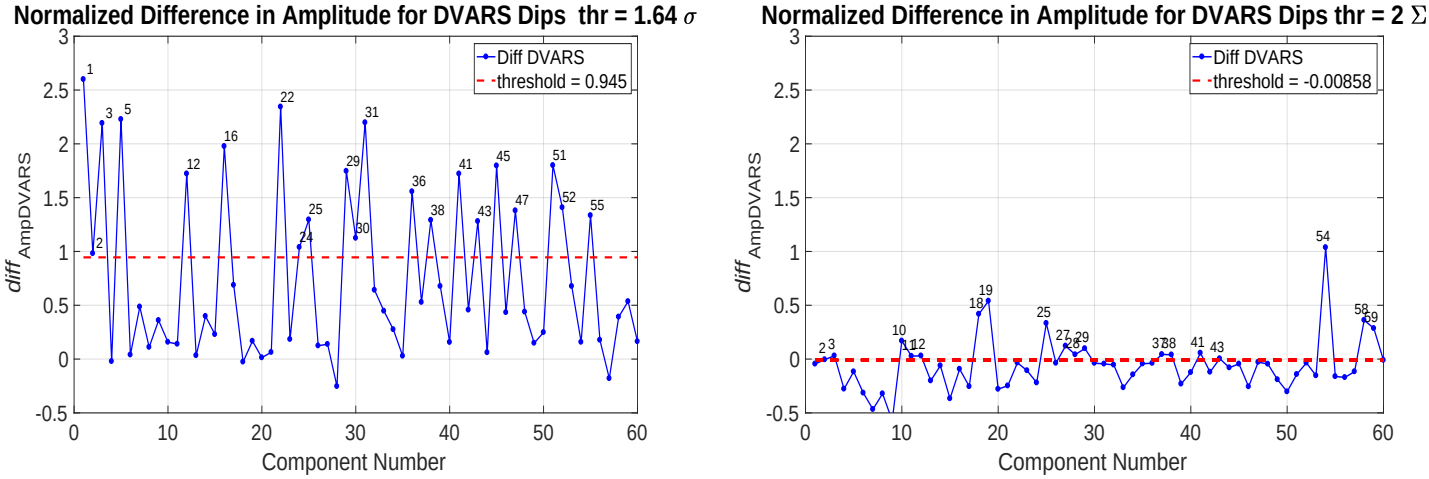

Figure 3.23: Comparison between DVARS Difference in component amplitude with and without subject 5 which are respectively represented on the left and right side. The first one is obtained after classification of spikes/dips non-spikes/dips through threshold of 1.64 σ, instead in the latter one the threshold computed without subject 5 is equals to 2 Σ. In both cases red dotted line is always calculated through equation 2.31 as the average value of the mean of the three signal and and mean of the three noise components. The numbered components are those above the threshold

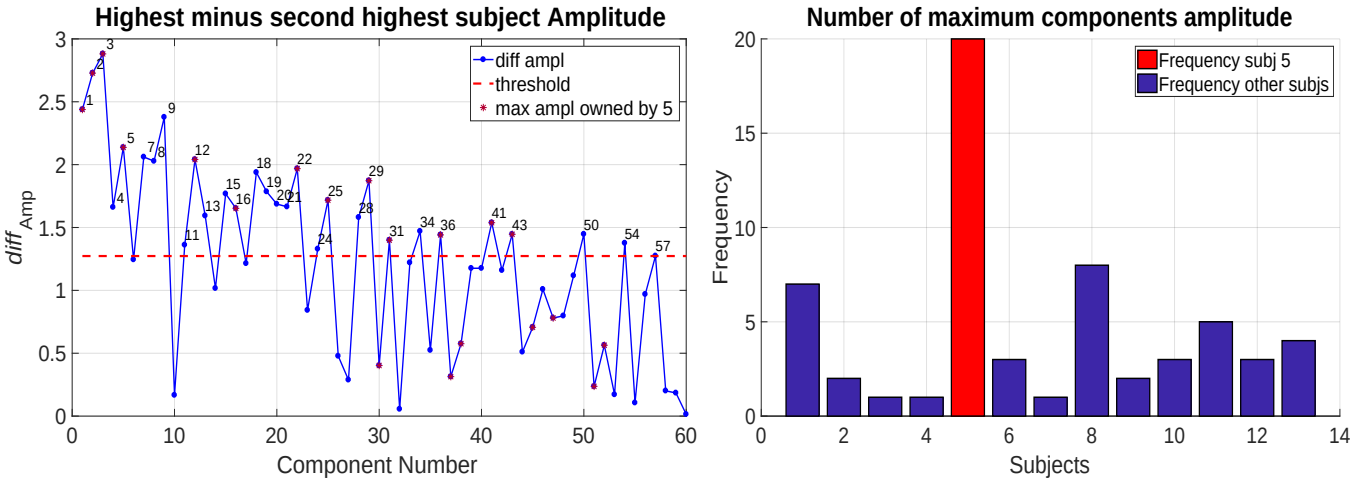

Figure 3.24: Representation of subject 5 influence on $diff_{Amp}$ plot. On the left side $diff_{Amp}$ is showed again, in which red dotted line is the threshold which best discriminated between that had already been clearly identified as signal or noise, pink stars reflects components with the maximum amplitude belonging to subject 5. On the right side the histogram of the maximum amplitude frequency is showed for each subject

Even for this index, its value changes significantly based on the presence of subject 5, in particular without subject 5 lots of values are lower (near zero which means

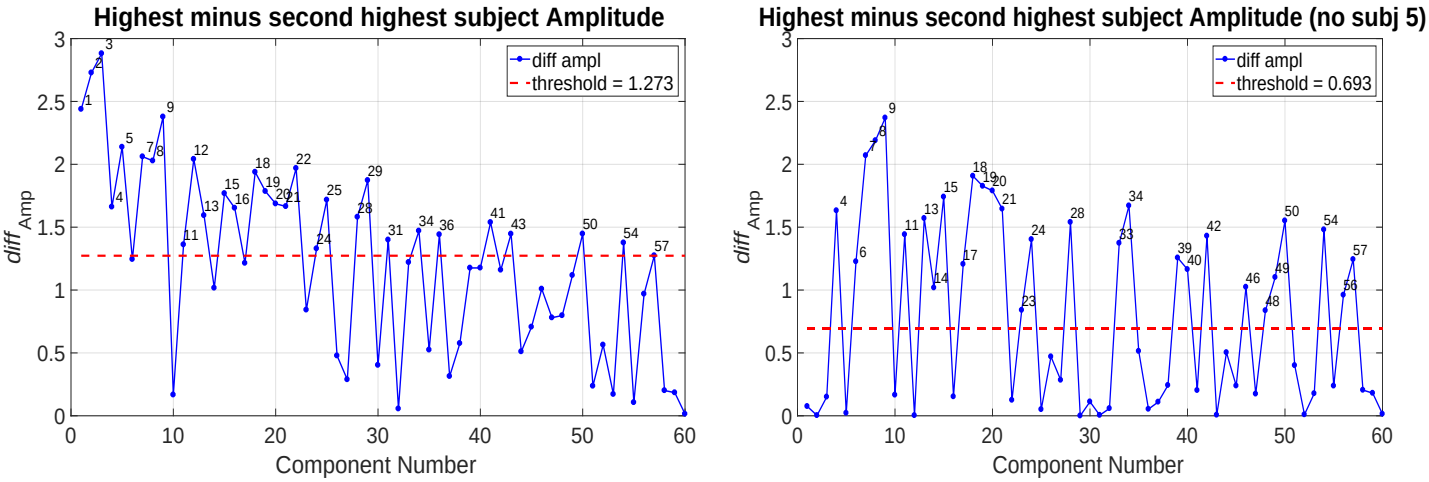

Figure 3.25: Comparison between $diff_{Amp}$ computed with and without subject 5 which are respectively represented on the left and right side. In both cases red dotted threshold is always calculated through equation 2.31 as the average value of the mean of three signal and and mean of three noise components amplitude. The numbered components are those above the threshold

that the difference between the two highest amplitude for some components are very similar), others instead are not influenced by subject 5 and stay more or less at the same level.

In summary, observing the previous results, it is noticed that both indices $diff_{AmpDVARS}$ and $diff_{Amp}$ are significantly modified based on the presence of subject 5. This brought the conclusion that the selected analysis for the identification of noise components is excessively influenced by the contribution of subject 5 components and so the findings are not very much plausible and credible.

3.5.2 Thresholds selection

The proposed final solution is to re-apply the temporal ICA through FastICA algorithm, without considering subject 5. As before, the number of estimated components is set to 60, obtaining new spatial maps and relative timecourses. The two metrics $diff_{AmpDVARS}$ and $diff_{Amp}$ are re-computed obtaining the results in figure 3.26 and 3.27. The first one is obtained classifying spikes using again as threshold 2Σ of the reference distribution. For both figures, red dotted line is always computed with equation 2.31 in which manually selected signal components (green diamonds) are 11, 13, 47, instead noise ones (red filled circles) are 10, 29, 45.

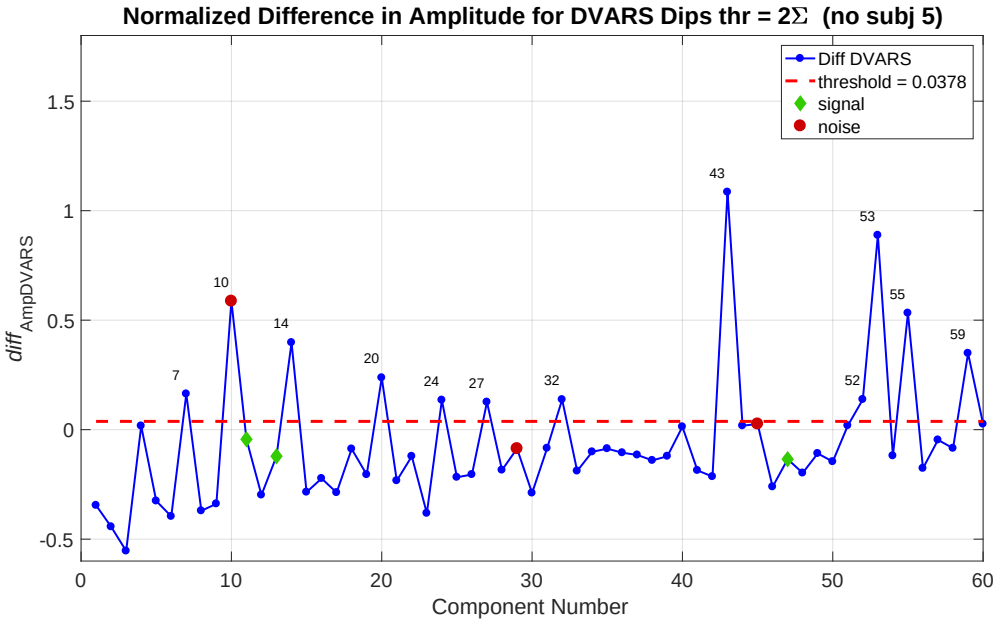

Figure 3.26: Difference in component amplitude between frames with DVARS dips and those without DVARS dips normalized by the component amplitude across all frames. All the analysis is done after the application of tICA without subject 5. Red dotted line is the threshold that best discriminates between the components that had already been clearly identified as signal (green diamonds) or noise (red filled circles)

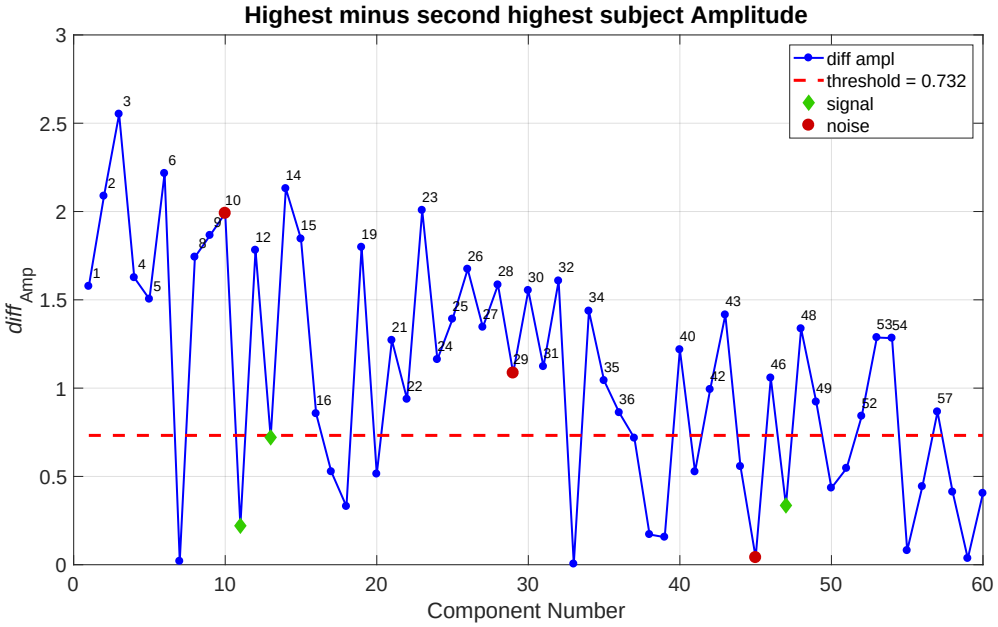

Figure 3.27: Difference between the maximum subject's component amplitude and the next highest subject's component amplitude normalized by the overall amplitude of each component. All the analysis is done after the application of tICA without subject 5. Red dotted line is the threshold that best discriminates between the components that had already been clearly identified as signal (green diamonds) or noise (red filled circles)

Further tests are performed changing twice the threshold illustrated in the red dotted line through equation 2.32 and 2.33. In this way, based on the different method to compute the threshold, for both plots $diff_{AmpDVARS}$ and $diff_{Amp}$ a different number of noise components will be obtained.
Table 3.8 represents the number of components to remove after tICA with and without subject 5 and with different thresholds. The values of Th_1, Th_2, Th_3 represent respectively equations 2.31, 2.32 and 2.33. It can be seen that the number of components to be removed above both thresholds of the two metrics and their total explained variance are less in cases of tICA without subject 5 compared to the one with all subjects. Th_1 is the lowest one and consequently causes a number of components to remove higher compared to the other cases (Th_2 and Th_3).
Since Th_2 and Th_3 remove a low number of components, and similarly the explained variance, the chosen threshold is Th_1.
The resulting plots of the new two thresholds, Th_2 and Th_3, are showed in figure 3.28 and 3.29.

	Threshold	**# comp over threshold** $diff_{\mathrm{AmpDVARS}}$	**# comp over threshold** $diff_{\mathrm{Amp}}$	**# comp over both**	**Explained Variance**
All subjects	Th_1	21	30	14	41.47 %
Subjects 5 Excluded	Th_1	12	39	8	9.91 %
Subjects 5 Excluded	Th_2	6	18	2	4.49 %
Subjects 5 Excluded	Th_3	6	21	3	5.20 %

Table 3.8: Table representing the number of components to remove after tICA with and without subject 5 and with different thresholds. The second row indicates results considering all subjects in tICA analysis, instead the following rows represent the results coming from exclusion of subject 5 in tICA analysis. In particular three different thresholds are used to obtain $diff_{\mathrm{AmpDVARS}}$ and $diff_{\mathrm{Amp}}$ plots: they are indicated with names of Th_1, Th_2, Th_3 and are computed respectively with equations 2.31, 2.32 and 2.33

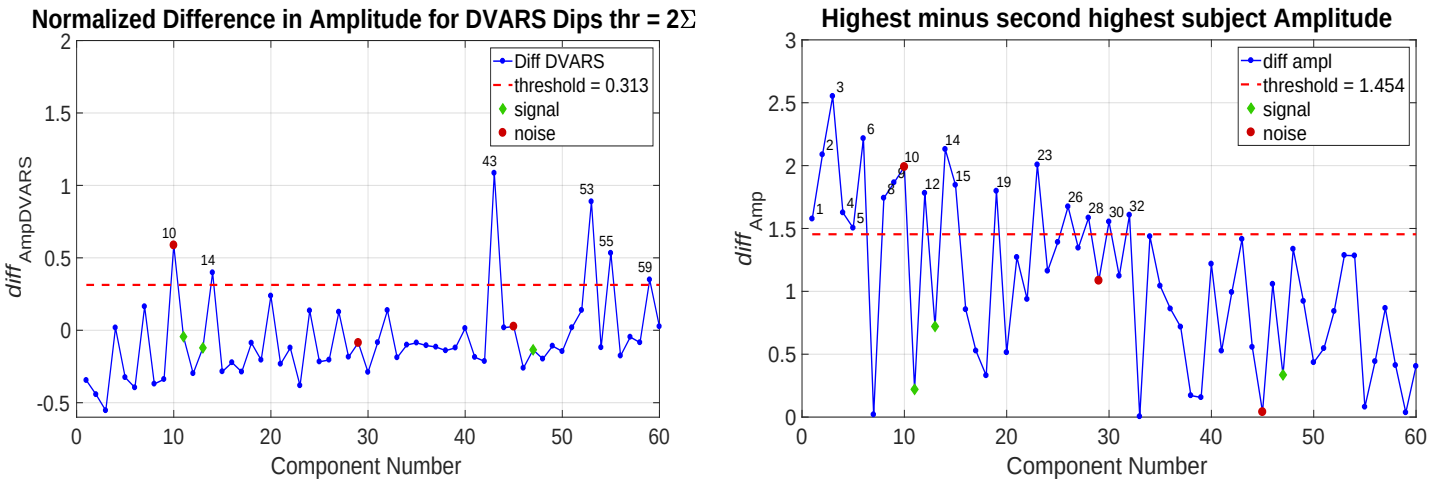

Figure 3.28: Representation of $diff_{AmpDVARS}$ (on the left) and $diff_{Amp}$ (on the right) computed without subject 5 in tICA analysis. Red dotted threshold (Th_2) is calculated through equation 2.32 as the sum of two values: the first one is the average value of the mean of three signal and mean of three noise components, the second one is the standard deviation of the 6 components. The numbered components are those above the threshold

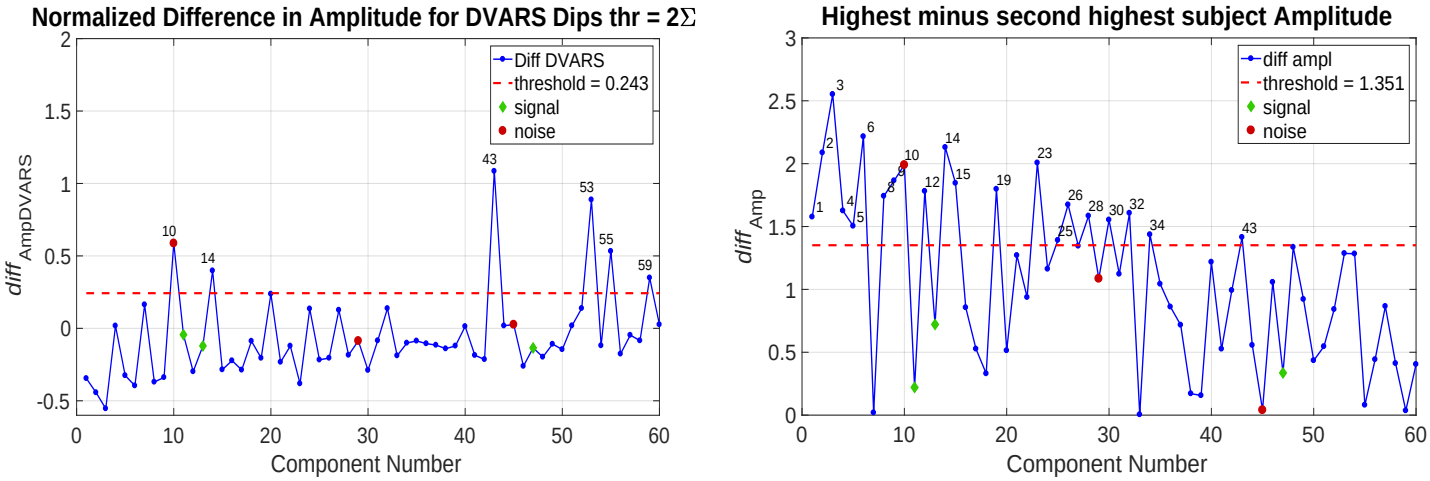

Figure 3.29: Representation of $diff_{AmpDVARS}$ (on the left) and $diff_{Amp}$ (on the right) computed without subject 5 in tICA analysis. Red dotted threshold (Th_3) is calculated through equation 2.33 as the sum of two means: the first one is the average value of the mean of three signal and mean of three noise components, the latter one is the mean between the resulting two standard deviations of three signal components and noise ones. The numbered components are those above the threshold

The spatial maps of the removed tICA components are showed in figure 3.30 in the two columns which respectively contains in order components 10, 14, 24, 27 and 32, 43, 52, 53. It can be noticed that all IC appear to be completely noise components. In fact most of them seems to be motion-relates components

as they manly highlight edges of the brain; others overlap with blood vessels (IC 10 shows clearly this characteristic), arteries or are mainly located within areas of air-tissue interface. In general all IC present a large number of small clusters, typical of noise sources.

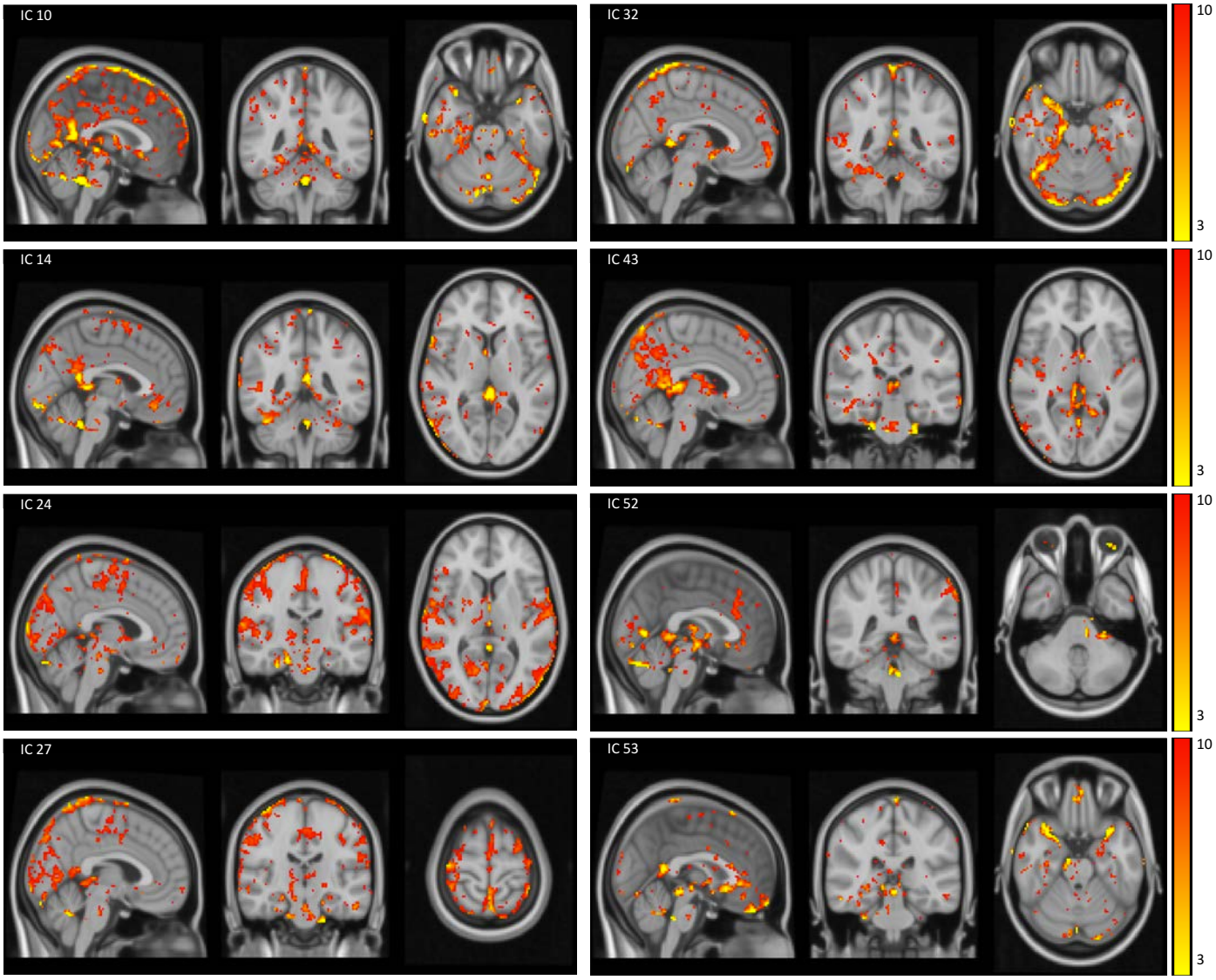

Figure 3.30: Group Temporal ICA spatial maps of the 8 components to be removed. Left column contains in order components 10, 14, 24, 27, whereas the right one contains 32, 43, 52, 53

In summary the principal choices adopted to develop the entire procedure of identification of motion-related noise components are resumed in table 3.9:

Steps	Final choices	Description
Processing	Denoising of Single Subject rs-fMRI through Melodic	This step has been performed to obtain initial data condition similar to Glasser's article. Each subject data has been fed into Melodic to identify 100 components. Of these components, noise ones have been identified and removed from data
Glasser Procedure	1. Group sICA 2. tICA	Group-ICA analysis has been performed by GIFT toolbox: the number of components to be estimated has been set to 80. As result spatial ICA components and relative time-courses were estimated at both group and individual level. Temporal ICA has been computed through FastICA algorithm and fixing the number of estimated components to 60. Subject 5 was excluded form tICA method
Noise Identification Indexes	1. $diff_{AmpDVARS}$ 2. $diff_{Amp}$	For calculate $diff_{AmpDVARS}$ it is necessary first identify peaks of $nDVARS_0$ plot: this has been done thresholding all traces to $\pm$ 2 Σ. In both plots of $diff_{AmpDVARS}$ and $diff_{Amp}$ a threshold has been chosen to identify and separate signal from noise
Thresholds for indexes	Th_1	The chosen threshold for both indexes plots is equal to Th_1 and it has been computed through 2.31, taking into account 3 signal components (IC 11, IC 13 and IC 47) and 3 noise (IC 10, IC 29 and IC 45)
Components Removal	Based on Th_1	All components above both thresholds of $diff_{AmpDVARS}$ and $diff_{Amp}$ are classified as noise

Table 3.9: Final choices to develop the entire procedure. In the second column most important parameters/choice are reported, while in the latter column a brief description is provided on how the several steps have been developed

3.6 Evaluation of Motion Related Noise Reduction Procedure

3.6.1 DVARS Comparison

DVARS comparison is the first method used to evaluate the entire procedure. To do that, for each subject three different DVARS measures are compared to each other. The first measure is computed starting from pre-processed data and it will be named as *pre s-sICA*. The second one, called *post s-sICA*, is performed from data cleaned by single subject sICA of Melodic. The last one is calculated after cleaning of tICA method, so it will be named as *post tICA*.
The first comparison is represented in figure 3.31 which shows some examples of DVARS traces computed pre s-sICA an post s-sICA, and below the difference between them in correspondence of frame with spikes/dips: a positive peak highlights a positive difference between pre and post s-sICA and hence a decrease of the peak.

From comparison between pre and post s-sICA it has been noticed a huge im-

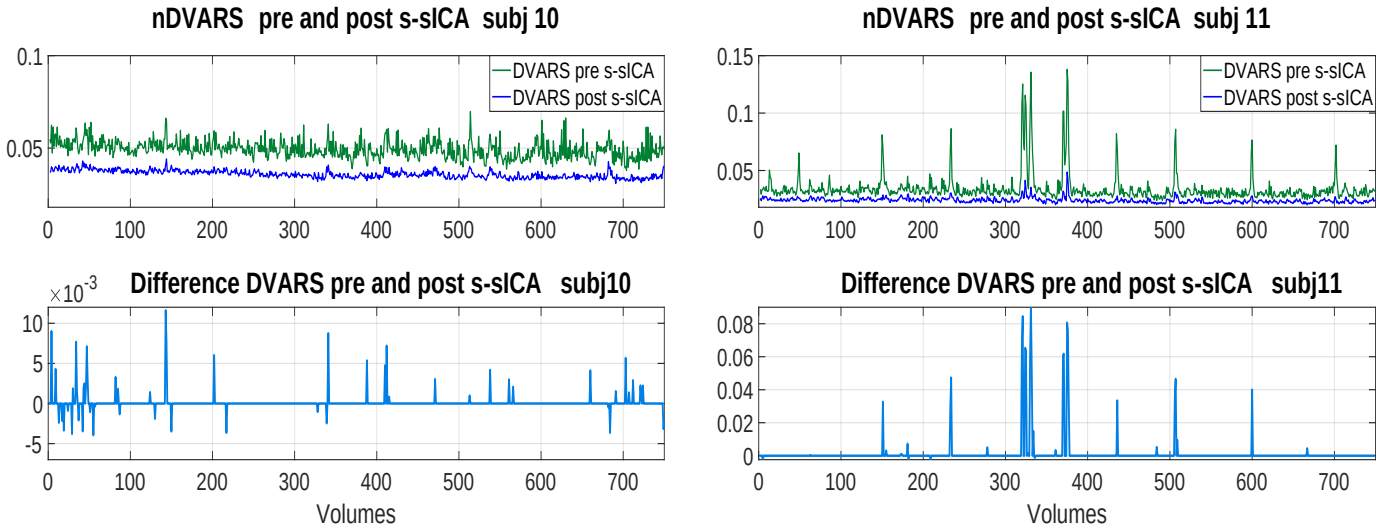

Figure 3.31: Examples of comparison of DVARS traces pre and post s-sICA (single subject sICA) which are respectively showed in green and blu lines. Each figure is composed of two subplots: the first one illustrates the two DVARS traces, the latter one shows the difference between the peak values of DVARS

provement on all DVARS. For subjects that moved a lot, characterised by high peaks, this improvement has been observed not so much at mean level, but rather at standard deviation level and on the inspection of spikes: in particular for sub-

ject 5 and 11 peaks have been strongly lowered, resulting a reduction of DVARS standard deviation respectively of 61% and 82% compared to the original one.
An example of that is illustrated on the right of figure 3.31: the major peaks of subject 11 that before reached values about 0.15, now are lowered to 0.05. This can be also seen in their second subplot in which the majority of differences between pre s-sICA peaks and those of post s-sICA are largely positive, with difference values reaching 0.08.
About subjects that moved less, such as subject 2, 10 and 13, DVARS improved further even though they were already characterized by homogeneous patter with few and low peaks: the mean value of DVARS decreased moderately, just like the standard deviation. An example of this case if presented on the left of figure 3.31 in which few spikes present in the trace of subjects 10 are slightly decreased, resulting a difference of peaks pre and post s-sICA characterized by one order less of magnitude compared to those of previous subjects.
In general, the majority of subjects obtained a significant reduction of mean DVARS, as it can be observed from the values reported on second and third row of table 3.10: its value, $\overline{nDVARS}$, has decreased about 20%-27% compared to the original mean value. S-sICA has been showed successful also for subjects as 8 and 12 which present few but high peaks: most of the peaks have been reduced, resulting to a drop of DVARS standard deviation of about 53%, as it can be seen on table 3.11 from values of these subjects before and after s-sICA.
On the other hand their mean value hasn't changed much.

The other comparison is performed between post s-sICA and post tICA. After the application of tICA some DVARS traces further improve, as it can be seen for subject 1 of figure 3.32, but in general the reduction of peak values is not so much visible: traces coming from tICA of subject 4 are not so different from those after s-sICA, and this is noticed also from the difference between peaks barely of an order of 10^{-3}.

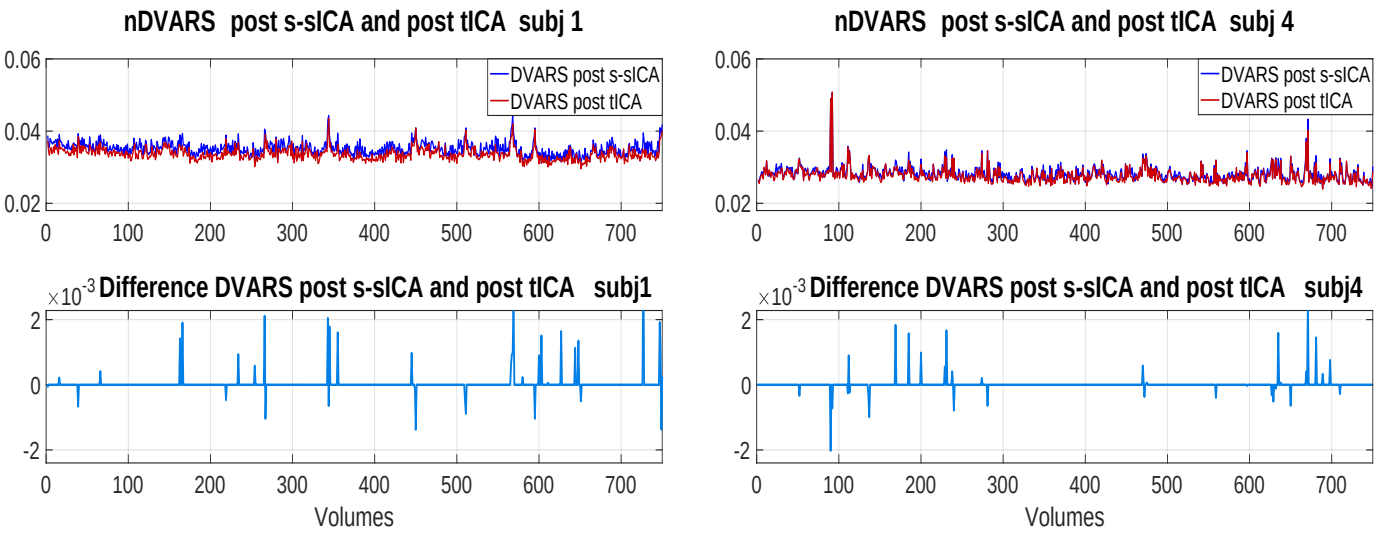

Figure 3.32: Examples of comparison of DVARS traces post s-sICA (blu lines) and post tICA (red lines). The term s-sICA indicates single subject sICA performed through Melodic. Each figure is composed of two subplots: the first one illustrates the two DVARS traces, the latter one shows the difference between the peak values of DVARS

Some examples of a complete representation of all the three comparisons are illustrated in figure 3.33 for three representative patients: in the first one it can be noticed a improvement of DVARS plot even after tICA, on the contrary in the other two examples the peaks reduction is evident only after post s-sICA, instead tICA seems not to modify so significantly the traces.

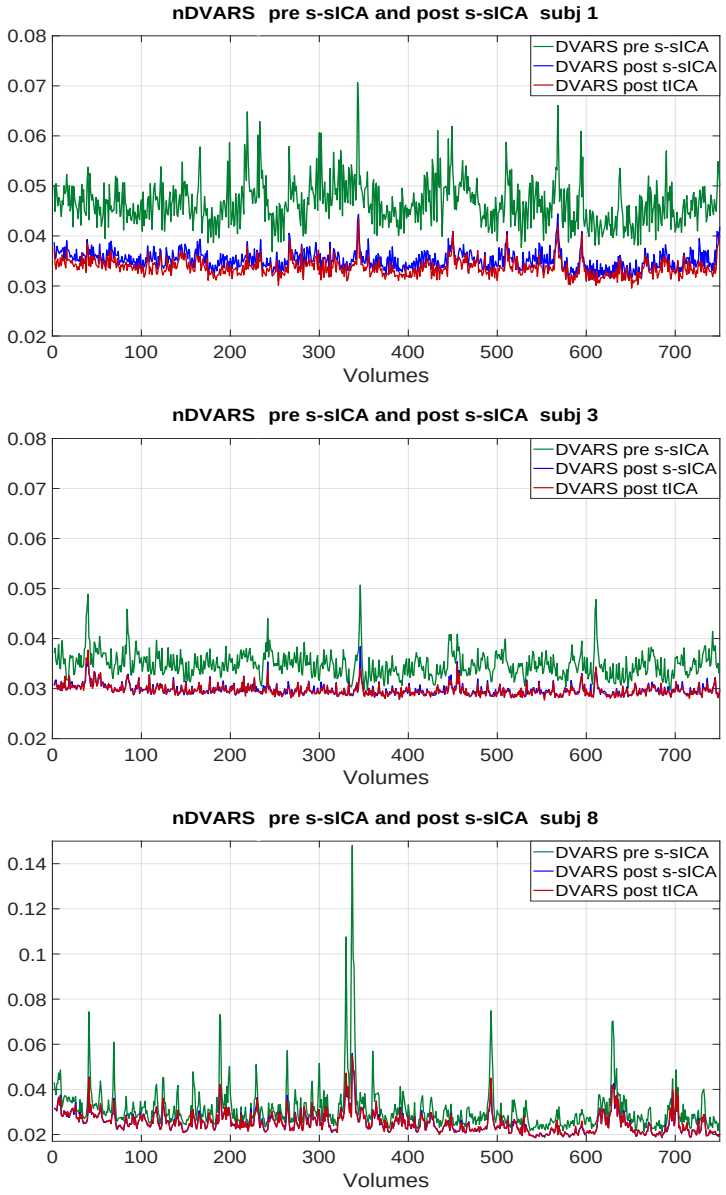

Figure 3.33: Examples of comparison of DVARS traces pre s-sICA, post s-sICA and post tICA which are respectively showed with green, blu and red lines. The term s-sICA indicates single subject sICA performed through Melodic

Tables 3.10 and 3.11 allow to verify quantitatively the evolution of DVARS traces between different steps, in particular for each patient of the three DVARS the mean and standard deviation values are reported.

Regarding the first table, it has been observed that mean value decreases significantly between $\overline{nDVARS}$ pre s-sICA and $\overline{nDVARS}$ post s-sICA, with a reduction ranging from 11% to 27%. A much smaller reduction appears instead between $\overline{nDVARS}$ post s-sICA and $\overline{nDVARS}$ post tICA: the variation of mean values is less significant compared to the previous comparison. Subject 1 is the one

# Subjects	1	2	3	4	5	6	7	8	9	10	11	12	13
$\overline{nDVARS}$ pre s-sICA $\times 10^{-2}$	4.66	3.19	3.48	3.61	3.92	4.07	3.35	3.12	4.12	4.93	3.41	3.08	3.32
$\overline{nDVARS}$ post s-sICA $\times 10^{-2}$	3.52	2.77	2.98	2.82	3.14	3.32	2.63	2.52	2.99	3.59	2.40	2.74	2.53
$\overline{nDVARS}$ post tICA $\times 10^{-2}$	3.37	2.74	2.97	2.77	-	3.29	2.64	2.52	2.99	3.58	2.38	2.75	2.50

Table 3.10: Table of values of mean of DVARS traces, computed pre s-sICA (second row), post s-sICA (third row) and post t-ICA (last row). All values are reported up to a constant multiplier equals to 10^{-2}

# Subjects	1	2	3	4	5	6	7	8	9	10	11	12	13
nDVARS *std* pre s-sICA $\times 10^{-3}$	4.4	2.6	2.5	3.3	32.5	3.2	3.1	10	3.5	4.9	12.5	4.5	3.5
nDVARS *std* post s-sICA $\times 10^{-3}$	1.9	2.0	1.1	2.2	12.7	1.7	1.7	4.6	1.8	2.1	2.3	2.1	1.7
nDVARS *std* post tICA $\times 10^{-3}$	1.7	2.0	1.1	2.2	-	1.6	1.7	4.6	1.8	2.1	2.4	2.2	1.7

Table 3.11: Table of values of standard deviation of DVARS traces, computed pre s-sICA (second row), post s-sICA (third row) and post t-ICA (last row). All values are reported up to a constant multiplier equals to 10^{-3}

in which mean value is significantly improved, with a difference of about 4.3% between the two means. On the other hand for the other subjects $\overline{nDVARS}$ doesn't seem too much altered. The same conclusion results in the observation of standard deviations: they stay constant in most of the subjects.

In order to quantify the impact of the two steps (s-sICA and tICA) on pre-processed data, it is taken into account the difference between peaks illustrated in the subplots of figures 3.31 and 3.32, then for each of the two comparisons, a sum of the peaks difference is calculated, obtaining figure 3.34: red line represents the sum of DVARS spikes difference between pre and post s-sICA, blue one reflects that between post s-sICA and post tICA. Observing the result, the application

of the first step s-sICA produced a remarkable decreasing of peaks value, in particular for subjects 8 and 11 that moved a lot during acquisition. The step of tICA, instead, produced a little and almost null improvement for the majority of subjects, in total the reduction of spikes is about 2.8% of the one produced by s-sICA step.

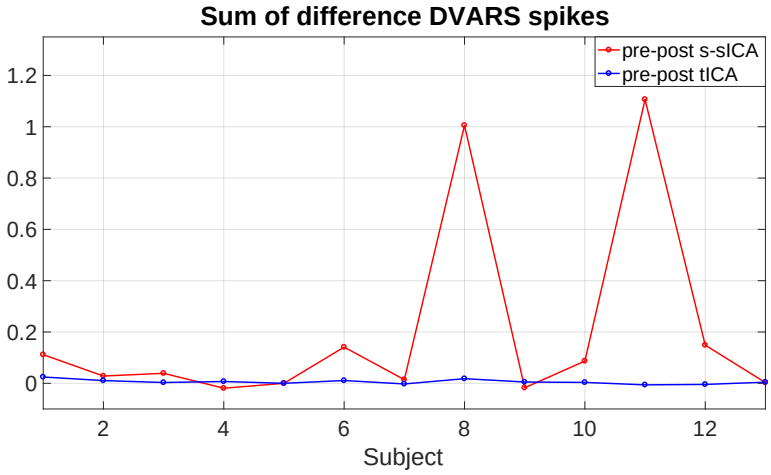

Figure 3.34: Sum of DVARS peaks difference between pre and post s-sICA (in red line), pre and post tICA (in blue line). Subject 5 has already been removed from the analysis, so the value of the two plots for subject 5 is zero.

3.6.2 **QC-RSFC**

Another index for evaluation of procedure of motion-related noise removal is QC-RSFC and to use it, functional connectivity matrices have to be calculated.
All computed FC matrices show the correlation between 27 rs-networks identified manually from the 60 group spatial maps of group sICA with GIFT. These RSN were labelled taking into account of article of [28] and are identified as 3 subcortical (SC), 3 auditory (AUD), 5 somatomotor (SM), 5 visual (VIS), 4 default (DMN), 6 cognitive (COG) and 1 cerebellar (CB). FC matrices are represented with the networks ordered as in figure 3.35. Pairwise correlation between 27 rs-networks' timeseries results in $27 \times (27-1)/2 = 351$ connectivity values for each subject.

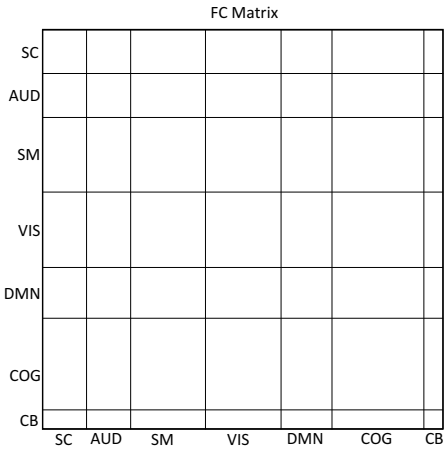

Figure 3.35: Structure of FC matrix. Networks are grouped into the following functional domains: subcortical (SC), auditory (AUD), somatomotor (SM), visual (VIS), default-mode (DMN), cognitive (COG) and cerebellar (CB) networks.

To quantify QC-RSFC measure, firstly it is necessary to compute for each subject FC_S and FC_{T+G} matrices, obtained as represented in figure 2.10. Then all FC_S are stacked in a single matrix and correlated to the vector of mean values of subject-wise framewise displacement (FD), resulting a correlation matrix and p-value matrix illustrated in the left side of figure 3.36. The same calculation has been applied for FC_{T+G} obtaining the two matrices on the right side of figure 3.36. Observing the two QC-RSFC matrices on the first row, it can be noticed that tICA application modified some node connectivity strengths, but p-value matrix assumes in both cases high values for most nodes, making results less

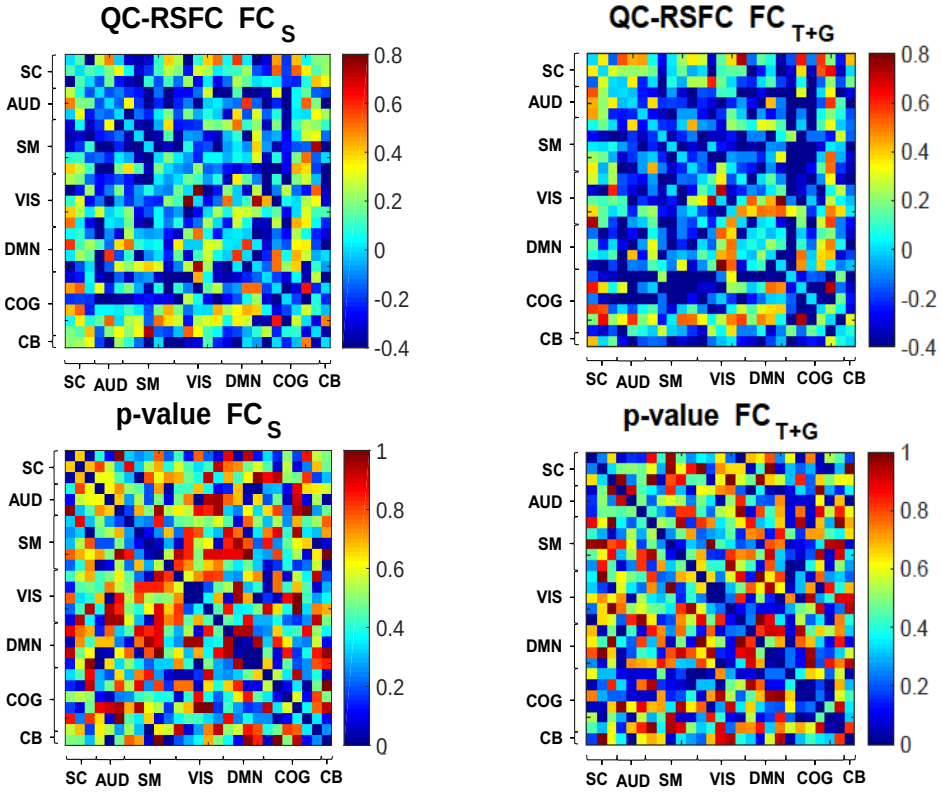

Figure 3.36: FC and p-values resulting from QC-RSFC measure. The two matrices on the left represent the FC and p-value matrices obtained from application of QC-RSFC on pre-tICA FC (FC_S). Instead on the right is showed those computed on post-tICA FC (FC_{T+G})

significant. In fact after FDR correction there is no statistically significance for both QC-RSFC matrices.

In order to verify possible modifications of connectivity strengths between rs-networks in the different steps of the entire procedure, the statistical analysis is performed and provides the use of t-tests between FC pairs. Before t-test can be applied, FC matrices has to be computed. In particular for each subject five FC matrices are computed with the procedures illustrated in figure 2.10. Two examples of resulting matrices are showed in figures 3.37 and 3.38. Observing FC of subjects 6 and 10 firstly it can be noticed that there is an evident similarity between FC_{M+G} and FC_{M+G+C}, as well as between FC_S and FC_{S+C}, where in both second terms the only additive step is the application of censoring.

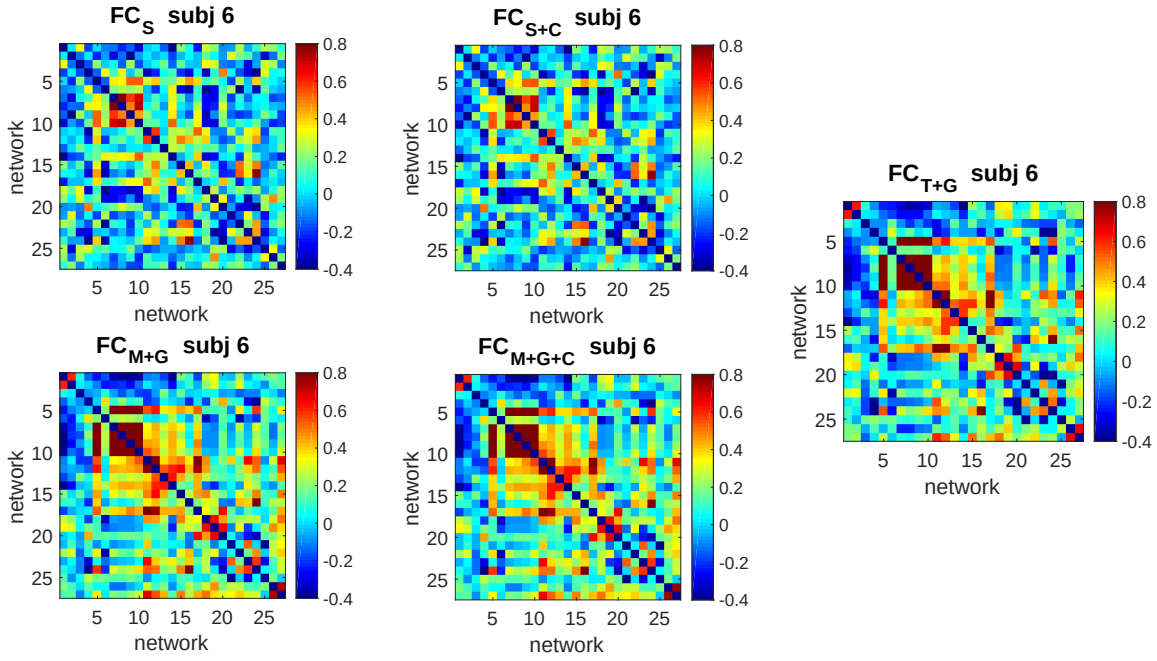

Figure 3.37: FC matrices of subject 6

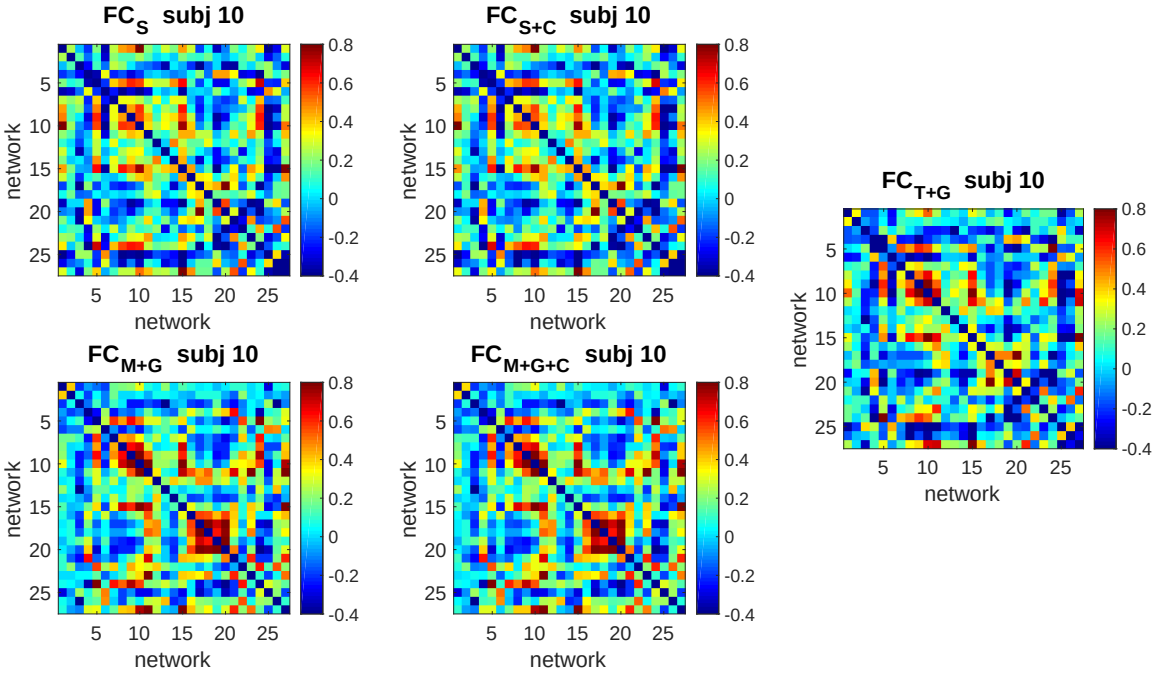

Figure 3.38: FC matrices of subject 10

Moreover FC_{T+G} tends to have the same pattern of FC_{M+G} and FC_{M+G+C}, rather than that of FC matrices obtained without GIG-ICA method. All these considerations are present also in the other subjects' FC.
Another aspect is that the difference between FC_S and FC_{M+G} is expected only if GIG-ICA method has a strong impact on results.
In this case it is observed that these two kind of matrices show different connectivity strength, with FC_{M+G} appears to have higher contrast than FC_S. The same observation can be derived also for the pair (FC_{S+C}, FC_{M+G+C}).
For the five type of matrices the mean value is computed among the subjects, obtaining results in figure3.39. These matrices confirm the observations highlighted at subject level: FC_{T+G} presents a pattern very similar to those of FC_{M+G} nad FC_{M+G+C}. From all FC mean it can be observed strong correlation between somatomotor networks, whereas other important connectivity strengths in default networks and in visual ones are more visible in FC matrix in which GIG-ICA was performed. In general in the most of subjects these strengths are present, even if slightly pronounced in FC of subjects 2, 4 and 12.

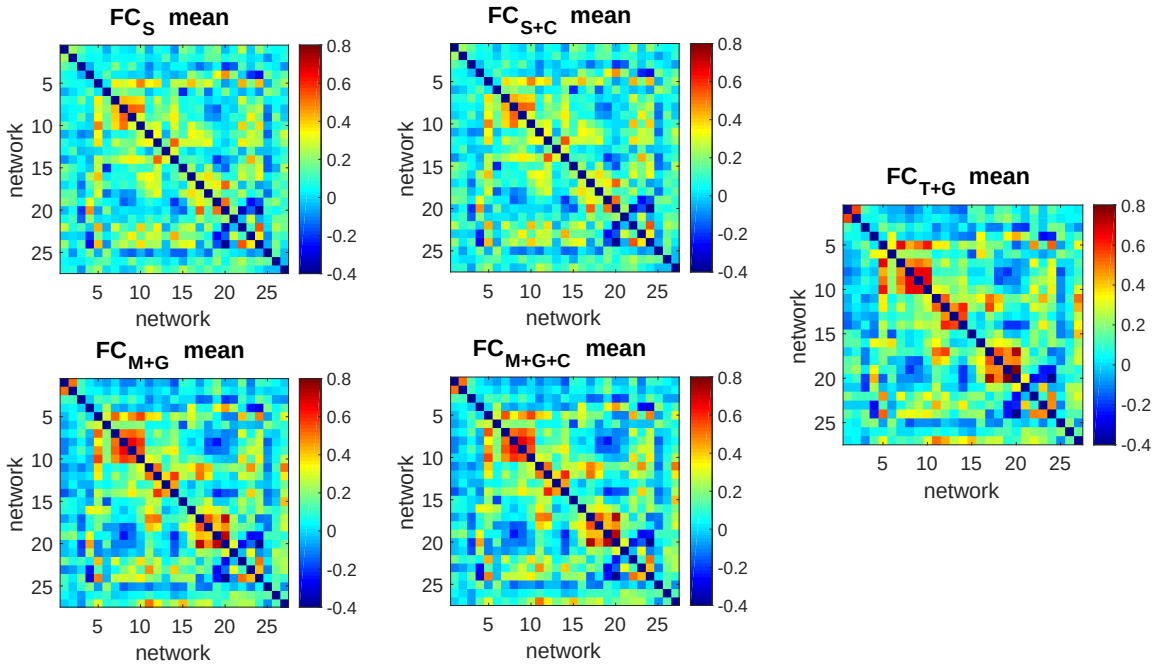

Figure 3.39: Mean FC matrices among subjects

Once all FC are available for each subject, the focus is to perform the statistical

analysis on functional connectivity through t-tests. Five comparisons, listed in paragraph 2.3.2, have been done and for each comparison between two different type of matrices t-test is performed for each entries, so 351 t-tests. As results a p-value matrix and a t-test matrix, which has been corrected for multiple comparison through FDR correction, are obtained.

Findings of comparison ① are showed in figure 3.40: the first matrix is the result of t-tests between the two groups FC_{S+C} and FC_{T+G} with FDR correction. The last matrix represents the p-value matrix. When in correlation matrix a yellow node appears means that there is a significant statistically difference between the two groups, instead blue nodes reflect a non significance. Observing the result below, several entries of the first matrix show a significant statistically difference, suggesting a difference between FC_{S+C} and FC_{T+G} and consequently tICA application seems to have changed some connectivities between rs-networks.

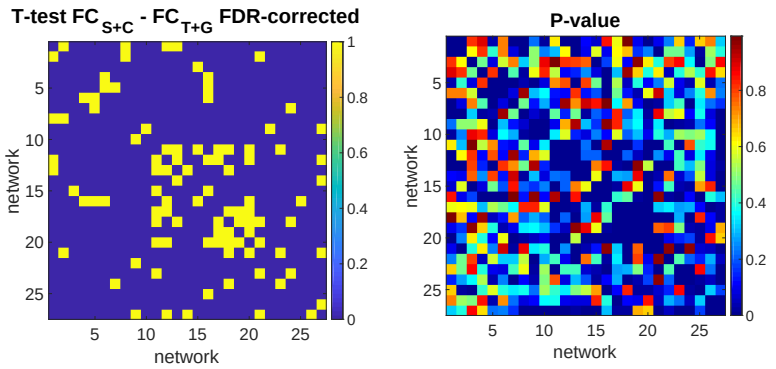

Figure 3.40: T-Tests on comparison between FC_{S+C} and FC_{T+G} that represents the comparison ①. Two images are reported: the first indicates the result of t-test between the two groups of matrices with FDR correction, the latter instead is the p-value matrix

The comparison ② has been performed because it is expected that if GIG-ICA application has a different impact on data compared to the case in which it isn't applied, then the comparison between FC_{M+G} and FC_S should not produce any significances, in fact they should present the same pattern. Instead from results in figure 3.41 it is noticed that several matrix entries, after FDR correction, are statistically significant; as consequence these differences are due to GIG-ICA method application in only one of the two groups of matrices.

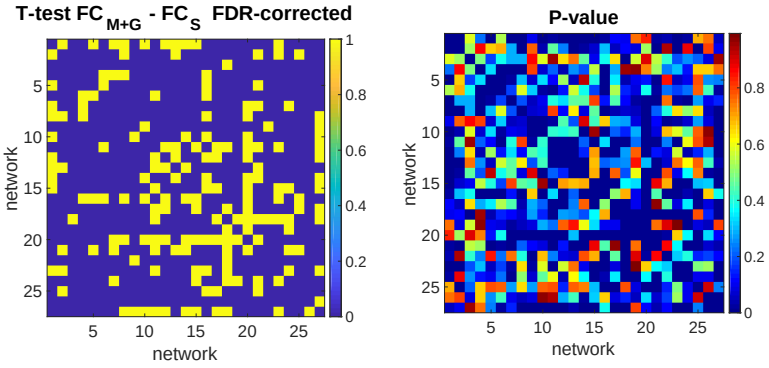

Figure 3.41: T-Tests on comparison between FC_{M+G} and FC_S that represents the comparison ②. Two images are reported: the first indicates the result of t-test between the two groups of matrices with FDR correction, the latter instead is the p-value matrix

The comparison ③ represents the t-tests applied between FC_{M+G+C} and FC_{T+G} and it is showed in figure 3.42. From the results in figure no statistically significance is present, therefore as consequence the two groups of matrices have connectivity strengths values very similar.

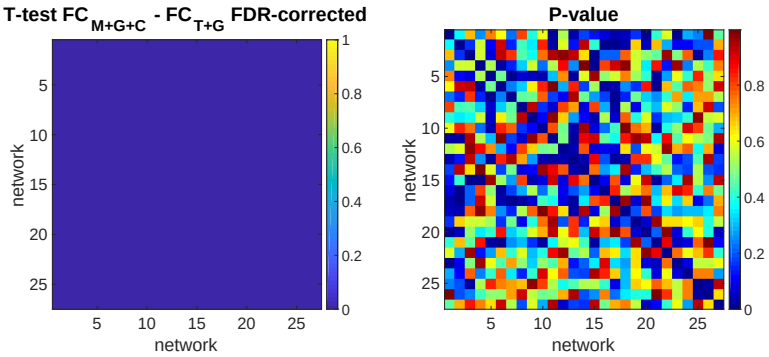

Figure 3.42: T-Tests on comparison between FC_{M+G+C} and FC_{T+G} that represents the comparison ③. Two images are reported: the first indicates the result of t-test between the two groups of matrices with FDR correction, the latter instead is the p-value matrix

The comparison ④ which represents the difference FC_{M+G} and FC_{M+G+C} produced no statistically significant, indicating therefore how the application of censoring didn't modify considerably connectivities between the 27 rs-networks obtained with the same procedure for the two groups (cleaning-up of Melodic and GIG-ICA application).

Also in the last comparison there is no remarkably statistically difference between FC_{M+G} and FC_{T+G}, consequently tICA procedure doesn't seem to have changed rs-networks connectivity.

From t-test matrices it is resulted that reasonable comparisons are between pairs of FC matrices both computed with or without GIG-ICA method. Therefore the result of comparison ① is not indicative of a possible variation due to tICA in FC connectivity strengths. Moreover it was found, through the other comparisons, that tICA didn't modify rs-networks connections with respect to what standard s-sICA or s-sICA+censoring obtain, in fact no statistical differences are showed in comparisons ③ and ⑤.
In light of this, the comparison performed previously between QC-RSFC of FC_S and that of FC_{T+G}, to see the impact of tICA at motion level, is not reasonable because in itself FC_S and FC_{T+G} are not comparable. Hence now to verify in terms of motion a possible difference between FC_{T+G} and what is given from the-state-of-art, i.e. censoring, QC-RSFC has to be computed starting from FC_{M+G+C} and then the result compared to those previously obtained with FC_{T+G}. The two QC-RSFC matrices with the respective p-values are reported in figure 3.43.

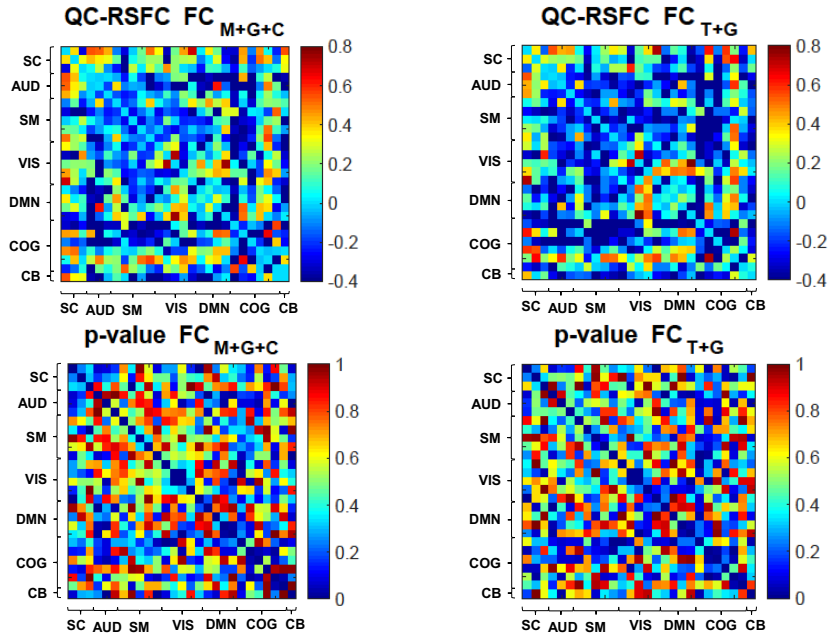

Figure 3.43: FC and p-values resulting from QC-RSFC measure. The two matrices on the left represent the FC and p-value matrices obtained from application of QC-RSFC on FC_{M+G+C}. Instead on the right is showed those computed on FC_{T+G}

QC-RSFC matrices are very similar, therefore at motion level tICA seems not to have modified significantly the connectivity strengths between the subjects FC and the mean vector of FD. Moreover after FDR correction no entries of matrix remains, indicating that there isn't any statistically significance.

4
Discussion

In this work of thesis, an attempt has been made to implement a new method introduced by Glasser and colleagues [3] for the cleaning-up of fmri data from global noise. In this case their method was used to try to remove sources related to subjects motion in rs-fmri data.
Hence at first a standard pre-processing for fmri data has been applied and includes slice timing, readout distortion correction, motion correction and coregistration. Next a pipeline has been developed and it can be resumed in two phases as described in figure 2.4: the first phase concerns a manual cleaning of rs-fmri data, individually for each subject, through sICA with Melodic; the latter one, instead, reflects the implementation of Glasser procedure which consists of a group approach with group sICA followed by the use of tICA.

Regarding the first part, Melodic has been used to perform single subject sICA, in which the number of estimated components was fixed to 100 after a visual inspection on results. Once 100 spatial maps and relative timecourses were obtained, a components classification has been made to identify noise components and then remove them from each subject. This classification was made manually because the low number of available subjects didn't allow to use classifiers as FIX which needs to be trained with part of available data.

For the second part of pipeline, group sICA was implemented through GIFT, after several comparisons between this toolbox and Melodic. GIFT allowed to

obtain spatial maps with large and well defined clusters, moreover it automatically reconstructed maps and timeseries of components to single subject level thanks to the back-reconstruction. With GIFT, ICASSO was used to run several times the algorithm for ICA for researching a better local minima. In fact the basic principle of most ICA algorithms is to start in some initial point, and then make steps in a direction that decreases the cost function, until one finds a point in which the cost function is locally minimized. Depending on the point where the search was started (the "initial condition"), the algorithm will find different local minima.
As before the number of components has been fixed. To do that, the solution provides to use Melodic to re-estimate from each single subject the number of components of pre-processed cleaned data, then from resulting 13 values a mean values has been computed obtaining 63. Hence GIFT has been tested several times, fixing at first the number of components to 63 and increasing it until the more appropriate choice for available data has been 80 components.
Therefore 80 group spatial maps and timecourses were obtained from GIFT and, through back-reconstruction already implemented in the toolbox, also results at individual level were produced.

After group sICA, tICA was performed giving as input to FastICA algorithm the timeseries previously obtained from back-reconstruction. Even in this case the choice was to fix the number of estimated components: ICASSO was taken into account, as showed in figure 3.8, and it selected as more appropriate number 53. So tICA was run with the number identified from ICASSO, but it has been noticed that several components' maps seemed to include more networks at once, therefore the number has been increased up to 60. As results tICA produced 60 group and individual spatial maps and timecourses.

At this point to identify and remove possible subjects motion-related components, three indexes proposed by Glasser were used and named as $diff_{AmpDVARS}$, $Variability_{Amp}$ and $diff_{Amp}$: the first one is based on DVARS measure computation as motion index, instead the others two attempt to highlight the variability of components among subjects.
DVARS traces are not comparable among subjects and this has been noticed thanks to the fact that subject 13 presented a DVARS with a range completely different from the others. Therefore to allow comparisons between these traces

the proposed solution was to demean each of them and normalize for the mean value of images intensity of the relative subject.
One of the critic choice in this phase of work was the identification of a threshold to define the so called DVARS peaks/dips which should reflect possible movement of subjects. At first the threshold proposed by Glasser's paper was applied, but it didn't seem appropriate for this dataset: Glasser uses a threshold computed at individual level for each subject, but from obtained results this cannot be a valid method because for subjects which moved less during the acquisition the result was a too low threshold and therefore highlighted erroneously lots of peaks as motion.
The solution was to try and apply other kind of thresholds, computed at group level, which have been considered more appropriate and are 10th percentile and thresholds based on standard deviation of concatenated DVARS. Thr_{γ}, equals to 1.64 σ has been chosen after an inspection of spikes on different subjects.
Once spikes have been selected, plot of $diff_{AmpDVARS}$ has been computed and then also the other two metrics, resulting figures 3.14 3.15. From results it is seen that the second index isn't significant in available dataset, in particular because of the reduced number of subjects this index comes down to describe what the third index represents. For this reason $Variability_{Amp}$ has been excluded as metric for the successive analysis.

Plots obtained from $diff_{AmpDVARS}$ and $diff_{Amp}$ present a threshold to discriminate what is signal or noise and the idea is that all components above both thresholds will be classified as motion-related noise sources and consequently will be removed from data. So the choice of these thresholds is crucial. The way in which illustrated thresholds should be computed was not specified by Glasser. So, based on the fact that these thresholds have to well separate signal and noise, they have been calculated as the average between the mean value of three signal sources and mean of three noise sources: these six components have been manually selected between all the 60 group spatial maps, trying to identify three components that clearly reflected networks and three that clearly represented only noise presence. The selection of 6 components is justified from some considerations. First of all it not easy identify many components that distinctly belong to one of the two groups, consequently choosing too much components for threshold computation would bring to a more time consuming analysis without the security

of a correct and definitely result; on the other hand instead, choosing too few components doesn't allow to obtain a credible threshold. This choice of threshold calculation seemed appropriate even if a strong limit is that a different choice of the 6 components could produce threshold values quite different. Once selected the thresholds, 14 components have been selected as noise and then removed.

Analysing with more detail indices used for identification of motion-related components it has been discovered a remarkable dependence on subject 5: this subject moved a lot during the acquisition and all performed analysis turned out to rely almost entirely on its components.
To solve the problem, subject 5 was removed from analysis, so tICA has been re-run without it and again the indexes have been computed.
Regarding the identification of DVARS spikes, it was noticed that the usage of thresholds based on standard deviation of concatenated DVARS was not so adequate because the distribution of concatenated traces isn't gaussian, but presents a long right tail. The solution adopted in this work is to characterize a gaussian distribution based on reference subjects, that is those optimal subjects which moved not so much. The new distribution will have zero mean and a certain standard deviation Σ and based on this Σ a new threshold has been computed, in particular it was set to 2Σ because it reflects the probability of about 95% for a sample to fall inside the interval produced from 2Σ.
The computed indices $diff_{AmpDVARS}$ and $diff_{Amp}$ produced as results figures 3.26 and 3.27. This time it has been tried to calculate plots' thresholds in different ways, but since they removed few components, and consequently a very low explained variance, it was decided to keep valid the initial threshold method, Th_1, which seems more robust.

As result 8 components were removed from data and, observing their spatial maps, they effectively seem to reflect only a noise source.
After that, attempts have been made to find out some metrics for evaluation of entire procedure and hence to verify that new data are effectively characterized by no motion.
Firstly DVARS traces have been computed for the different steps of procedure: in this way it was possible to see visually if spikes/dips of DVARS are disappeared or their values are decreased. From results it can be noticed that after the application of single subject sICA with Melodic there is a relevant variation of DVARS

which decrease their spikes, so this technique is sensitive enough to motion effect; the second step instead, i.e application of tICA, doesn't seems to be particular effective in the reduction of movement as spikes didn't decreased so much and in some cases actually they got worse, underlining ever more peaks related to motion.

Another index used for procedure evaluation is QC-RSFC, is a more robust metric based on the computation of FC matrices. All FC of this work have been obtained considering exclusively the 27 rs-networks identified at group level.
The correlation between the mean vector of FD and first the group of FC_S matrices, then with FC_{T+G} produced two correlation matrices and p-value matrices. Results showed some variations of connectivities between the two comparisons, but non relatively significant due to high value of p-value matrices. So this result can't bring to any conclusion about the effectiveness of tICA on motion components removal.

In order to verify possible differences between FC computed before and after tICA, a statistical analysis has been performed through t-tests between the group of matrices FC_{S+C} and FC_{T+G}. The two kind of matrix were obtained with different procedures as seen in figure 2.10, in particular the latter one is obtained from data cleaned after tICA in which GIG-ICA method was applied. The principal concern was that GIG-ICA could modify results compared to the case in which GIG-ICA didn't be applied because it uses different informations coming from the entire group.
For this reason the statistical analysis is enlarged to five groups of FC matrices as illustrate in figure 2.10. In particular two of them have been computed starting from cleaned data due to single subject sICA with Melodic (FC_{M+G} and FC_{M+G+C}), other two have been get after group sICA with GIFT (FC_S and FC_{S+C}) and then FC_{T+G} produced from data cleaned after tICA.
Five comparisons have been obtained from these matrices groups and for each of comparison t-tests have been calculated as many as the entries of a FC matrix. For each comparison 2 plots are illustrated: a t-test matrix corrected for FDR and a p-value matrix.
From results it can be deduced that comparison ① brought significant statistically differences between FC_{S+C} and FC_{T+G}, consequently tICA seems to have had some effects on available signal.

Even in comparison ② there are significant statistically differences: the two groups of matrices should instead produce correlations between rs-networks very similar, because FC_{M+G} reflects network correlations computed starting from data after cleaning of Melodic and after GIG-ICA method, while FC_S shows the correlations resulting after group sICA. So the only difference between these two groups is the application of GIG-ICA in only one of the FC groups.
Therefore GIG-ICA method effectively modifies results because it is based on maps and timeseries reconstruction starting from the prior of group maps, and so this affects also functional connectivity. The finding is that comparison ① is inconclusive since doesn't take into account two FC groups with both GIG-ICA analysis.
Therefore to verify if tICA actually modifies connectivities between rs-network, comparison ③ is the one that has to be observed because both the FC groups in consideration use GIG-ICA and so the two groups can be reasonably compared. Results of ③ shows that there aren't any statistically significant differences between FC_{M+G+C} nad FC_{T+G}, this means that at connectivity level between rs-networks the application of tICA on available dataset hasn't modified networks.
Comparisons ④ regards two FC groups (FC_{M+G} and FC_{M+G+C}) in which the only difference is the application of censoring in one of them: from the results there is no statistical difference detected in rs-networks correlations.
Comparisons ⑤ didn't show once again any statistical differences between before and after tICA application. These results were evident also only visually from comparison of the 5 FC in several subjects as showed in figure 3.37 and 3.38 for subject 6 and 10: FC obtained after tICA presents a patter very similar to those of FC_{M+G} and FC_{M+G+C}.

Hence from evaluation indexes used in this work, it seems that tICA hasn't had any impact on fmri signal compared to the usage of the first step of manual cleaning made through Melodic, and so it hasn't be able to remove remaining noise sources related to motion. This finding is in contrast with what Glasser obtained with his data, in particular from the results he states that his procedure, in spite of some limits that could be resolve in the future, managed to separate and remove noise sources compared to neural signal. This discrepancy between thesis results and Glasser's ones can be due to several factors. First of all available dataset is characterized by a greatly reduced number of subjects and, as Glasser said in

his paper, this can be a heavy influence: his method is designed to work with high spatial and temporal resolution fMRI data at the group level with a large number of subjects [3]. Moreover it is essential using tICA from data with a high number of timepoints because it couldn't do perform well, in fact this method is particularly applicable to large datasets.
Another important consideration is that Glasser and colleagues dispose of much more information about subjects, for example they benefit from the usage of respiratory belt and a heart rate monitor to acquire physiological data and hence perform a more detailed analysis on noise sources. So they could take advantage of more indexes compared to this work of thesis, as RVT (Respiration Volume per Time) or monitoring of subjects sleep, that were used to help identifying noise components, not only those related to motion.
One crucial difference with Glasser's article is that all the choices that leaded us to identify and remove 8 motion-related tICA components, such as the way to obtain thresholds used for computation of indexes $diff_{AmpDVARS}$ and $diff_{Amp}$, are mostly likely different compared to reference paper because was not provide a detail explanation of the several steps. The calculation of these thresholds has been certainty critic because a different choice of the 6 components from which thresholds are computed cause a variation of the thresholds' values and so a possible difference in the number of components to be removed. Despite all differences with reference article, the aim of this thesis is quite different from Glasser's one because the focus here is to remove only motion-related sources. Unfortunately this aim doesn't seem to be reached for available dataset.

4.1 Relation with the state-of-the-art

About Glasser's article, a debate has been emerged between Glasser and another important researcher, Jonathan D. Power, which in recent months published an article discussing Glasser's results [44]. One of the topic of discussion is that the entire classification has been performed manually and, because there are no neural records to anchor decisions to classify as signal or noise a certain component, it is fundamental that this identification is done appropriately. In particular his critic focused on respiratory signals that are considered from both articles those prevalent in fMRI data. Power states that Glasser exploited physiological

data obtained through a respiratory belt and a heart rate monitor as measures useful for final identification of noise components, but these data haven't been inspected and any data quality has been assured: according to Power instead it is really important assessing personally physiological data because in these cardiac and respiratory traces is possible to find peaks that allow to understand what is happening to patients [45].
Measures of respiratory and cardiac cycles are not available for dataset of this work, so this problem does not concern.

Through his article, Power tried to verify if the hand-classification of tICA components as noise or signal has been correct. The fact that all the identification is done manually is a strong limit, observed also in this thesis because despite component identification is based on thresholds of plot $diff_{AmpDVARS}$ and $diff_{Amp}$, these thresholds have been necessary computed through visual inspection of some components, and hence part of classification still remains manual.
Analysing in detail Glasser data and results, Power observed that sources separation is "flawed" [44] because sometimes global signals have been assigned to both noise and signal components. This consideration brought him to the conclusion that the observed problem is due to an incomplete removal of noise or to a inappropriate identification of some neural signals.
In this thesis work these investigations on signals cannot be performed but from indexes used for procedure evaluation it has been established that tICA didn't significantly modified signals obtained after single subject cleaning and so didn't manage to completely remove noise sources, in this case, related to motion.

The possible erroneous separation between the two kind of sources has been detected by Power also observing some components assigned as neural signals. In particular, taking into account of a relation highlighted in some studies [46] [47] between regressors accounting for respiratory signals and a sensorimotor distribution, it is possible that some components identified as signals, which show a sensorimotor distribution, have proprieties of respiratory signals and so they are erroneously interpreted as neural sources. Since Power supports that a link between respiratory signals and head motion exists [48] [45], the checking of some components classified as sensorimotor signals to have respiratory signals propriety has been done evaluating how much these components' amplitude is related to subjects' movement, hence observing if their value in $diff_{AmpDVARS}$ is high. Power

found out some signal components having this characteristic.
Regarding this last aspect, removed components from this thesis work are those above both thresholds of $diff_{AmpDVARS}$ and $diff_{Amp}$ plots. Observing the first plot, it has been noticed that components with higher $diff_{AmpDVARS}$ values have been already identified as noise, so in this work the problem argued by Power is not present.

Starting from received criticisms, Glasser published a new article [49] in which he agreed for some aspects with Power's analysis, for example in the fact that the classification of components presented in his paper might be reviewed in order to find out one more effective and toward an automation of the tICA approach to make it widely accessible.
However regarding Power most important critic, i.e. the fact that tICA didn't completely separate signla and noise sources, Glasser emphasised that in most of the cases the global noise has been entirely removed from sICA+tICA framework minimizing the removal of neural signal. Glasser showed that, in case of task, the events highlighted by Power of a simultaneous identification of noise and signal in different parts of the brain, actually occur in correspondence of neural activity induced by the task in task-positive brain areas; hence the fact that all portions of epochs, which temporally match with respiratory noise, are artefacts may lead one astray.
Glasser disagrees also with the statement relative to a link between respiration and motion, saying that these two kind of artefacts not necessary are linked and can be strongly dissociated, showing that through the inspection of some subjects' data at the disposal.

All these consideration will be remain at the heart of future debates that could leads to a deeper, experimental and theoretical basis for fMRI data denoising, in order to better understand how to exploit tICA. The discussion between Power and Glasser focused mostly on problem of sources related to respiration, therefore about that any considerations cannot be brought from this thesis, but starting from tICA procedure applied to available dataset some limits have been highlighted previously explained.
Despite the procedure didn't produce expected results with the available dataset, tICA still remains a promising approach for removing global noise from fMRI data and this concept has been underlined from both researchers.

5
Conclusions

The aim of thesis's work is to verify if the new procedure developed by Glasser [3] can be usefulness to remove motion-related noise sources for rs-fMRI data. In fact these sources have proved to be very critical in resting state as they induce changes in the signal intensity, causing presence of peaks or drop of the signal. Glasser's paper is intended to clean data of physiological, motion and MR physics related artefacts through a procedure which uses a combination of spatial and temporal ICA. In this work the focus is on identification and removal of noise sources related only to motion starting from rs-fMRI data of 13 glioma patients. During the implementation of this method, several problems have been detected. First of all, as Glasser highlighted in his article, the entire procedure relies on manual classification of ICA independent components at group level. In fact in this work the identification of noise components occurred through the use of some indexes, $diff_{AmpDVARS}$ and $diff_{Amp}$, in which a threshold has been necessary for components classification. These thresholds are computed through visual inspection of 6 components and therefore the setting of the appropriate threshold is crucial: a different choice of these components and hence a variation of the threshold could lead to different results.
Even the computation of the index $diff_{AmpDVARS}$ has been elaborate, as it is based on the identification of spikes/dips which characterize subject DVARS traces. The method proposed by Glasser for the selection of peaks hasn't been effective in

available dataset; therefore several kind of thresholds have been explored, in order to find out the more appropriate. So even in this case, a different choice of the DVARS thresholds causes a different number of peaks which leads to a difference in $diff_{AmpDVARS}$ values.
An important limit highlighted with this work is that the entire procedure depends heavily on the presence of outliers. This has been proved as in available dataset there is the subject 5 which moved a lot compared to the others: observing the results, it has been noticed that all the analysis and the choices made to get motion components rely almost exclusively to this particular subject. In order to perform properly the procedure and obtain credible outcomes, the proposed solution was to exclude subject 5 from tICA analysis. Since in this thesis the method has been performed to remove motion-related noise, obviously Glasser method should be improved in the future from this point of view, in order to include subjects considered outliers.
In general a crucial choice in ICA analysis is the setting of estimated components number. In this case this problem has been revealed for both sICA and tICA. Regarding tICA, ICASSO toolbox was exploited, as proposed by Glasser, to obtain the more appropriate dimensionality, but for this dataset it was not sufficient to ensure the optimal number of components: it produced a sub-clustering of the information, so further investigations have necessarily been requested.

In the attempt to assess the effectiveness of entire procedure, two different approaches have been employed: DVARS and QC-RSFC.
From comparisons between the three DVARS traces (pre s-sICA, post s-sICA, post tICA) it is emerged that standard application of group sICA affects motion, in particular spikes of DVARS traces are considerably reduced for both subjects who moved a lot and subjects who moved less. In fact the mean value of DVARS lowered about of 11%-27%. Moreover for some subjects that moved a lot, as subject 5 and 11, the radical reduction of peaks led to an important decrease of the standard deviation of DVARS, respectively of 61% and 82%. The additive tICA step instead produced a minimal drop of peaks: mean values and standard deviations of DVARS traces remained more o less approximatively unchanged, only subject 1 has obtained a significant improvement, with a mean value lowered of 4.3%. This brought to the conclusion that possible tICA effects cannot be observable at motion traces level.

For this reason tICA has also been evaluated in terms of functional connectivity FC. QC-RSFC computed pre and post tICA have highlighted some differences that nevertheless are not significant as proved from high value assumed by p-value matrices. As consequence of that, tICA didn't have any impact at motion level. In order to quantify the influence of tICA, the statistical analysis has been developed through t-tests between pairs of FC matrices identified for each subject. However no significant statistically difference has been revealed from the comparison between FC obtained from tICA (FC_{T+G}) and those obtained with the standard approach (FC_{M+G+C}), in which single subject sICA and censoring has been performed. Therefore also at functional connectivity level tICA has not resulted in modifying connectivity strengths of rs-network.

In summary from specified methods for evaluation of the entire procedure, it is established that tICA hasn't had any impact on fmri signal and it hasn't be able to remove noise sources related to motion. Moreover it doesn't seem to produce a real improvement compared to results generated by the state-of-the-art in this field.
This result is in contrast with what Glasser and colleagues exposed, but it is important to bear in mind that available dataset is characterized from a greatly reduced number of subjects compared to Glasser's one; additionally they take into advantage of data coming from fmri at both resting and task level while in this work dataset used for analysis comes from resting state fmri. Moreover they dispose of much more information about subjects, for example they benefit from the usage of respiratory belt and a heart rate monitor to acquire physiological data and hence perform a more detailed analysis on noise sources.

Glasser's method turned out to be very tricky to perform and, because of the complexity of its formalization, has token a long time to be completed also due to limits already described. Despite that, from results and the development of the procedure, some important considerations have been revealed. A relevant result concerns about GIG-ICA method, which exploits group spatial maps as prior. From t-tests performed on pairs of FC matrices it has been found out that GIG-ICA modifies the signal and has a strong impact on results. Therefore in order to perform reasonable comparisons between FC computed after tICA (FC_{T+G}) and another FC matrix, it is appropriate that the two terms of comparison are both obtained using GIG-ICA method.

Another important consideration refers to DVARS measure. What it has been observed is that in order to compare DVARS of different subjects, not only the mean value of each dvars has to be removed, but also a certain normalization of DVARS traces has to be performed. This finding has been noticed because one of the available subject data presented a trace with a completely different range compared to the other subjects due probably to the update of the scanner of magnetic resonance.
In order to solve the problem, the proposed solution has been to normalize each DVARS for the mean intensity of the images of the relative subject.

The small number of subjects could have had a great impact on the results obtained: probably with more patients' data some problems highlighted previously could be solved, for example the method for choosing the thresholds that characterized DVARS would have been more robust, or the results from QC-RSFC could reveal a statistically significant difference.
Therefore to confirm the obtained results, future development should be based on the use of a larger dataset and on availability of physiological signals; in this way a more reliable evaluation will be reached.

A

FastICA Algorithm

FastICA is an algorithm introduced by Hyvärinen in 1999 [31] and used in the component analysis for the separation of source signals. It allows to compute, one by one, all independent non-gaussian components that created observed dataset. FastICA is based on a fixed-point iteration scheme to maximize the non-gaussianity of observed data through the usage of a non-gaussianity measure as the approximation of negentropy:

$$J(y) \propto [E\{G(y)\} - E\{G(\nu)\}]^2 \tag{A.1}$$

where G is a non-quadratic function, y is a non-Gaussian random variable standardized (zero mean and unit variance), ν is a standardized Gaussian variable and $J(y)$ is the negentropy which by definition represents the variation of entropy so that it is equal to zero if it is applied to a gaussian variable, otherwise non-negative. Because J goes to zero for gaussian variables, the focus is to maximize it.
FastICA learning rule finds a direction, i.e. a unit vector w such that the projection $w^T x$ maximizes the non-gaussianity measured by the approximation of negentropy $J(w^T x)$. So after data are pre-whitened, the following steps are performed [30]:

1. Choose an initial (e.g. random) weight vector w_i, which is the vector for an

individual i-th component.

2. Define $w_i^+ = E\{xg(w_i^T x)\} - E\{g'(w_i^T x)\}w_i$, where g is the derivative of G.
3. Update $w_i = \frac{w_i^+}{\|w_i^+\|}$.
4. If not converged, repeat the procedure starting from second step. The word convergence means that the previous and the actual values of w_i point in the same direction, i.e. their dot-product is (almost) equal to 1.

The variable w_i represents a column-vector of the un-mixing matrix W, w_i^+ is a temporary variable used to calculate w_i, g' is the derivative of g and E is the expected value (mean).
The described procedure allows to estimate one independent component, so to estimate n of them, the algorithm has to be applied n times using the vectors $w_1, w_2, ..., w_n$. To avoid that different w_i vectors converge to the same maximum of non-gaussianity, each new w_i that is computed must be made orthogonal to the previous w_i vectors through the following computation:

$$w_i^+ = w_i - \sum_{j=1}^{i-1} w_i^T w_j w_j$$

The new w_i is obtained as:

$$w_i = \frac{w_i^+}{\|w_i^+\|}$$

In this way the new estimated component will be different from those already calculated.

B

Infomax Algorithm

Infomax is another algorithm proposed by Amari et al. [50], with which the estimate of independent components is done by focusing on minimizing the mutual information.
This measure can be described, for a pair of random variables, starting from entropy as:

$$\begin{aligned} I(X;Y) &= H(X) - H(X|Y) \\ &= H(Y) - H(Y|X) \\ &= H(X) + H(Y) - H(X,Y) \end{aligned}$$

where $H(X)$ $H(Y)$ are the entropy respectively of X and Y, $H(X|Y)$ is the conditional entropy (the entropy of X conditional on Y taking a certain value y) and $H(X,Y)$ is the joint entropy of X and Y. Observing the previous equation, it is noticed that this index is equal to zero for independent variable and in general not negative, therefore maximizing the non-gaussianity of the source signals means to minimize the mutual information.
To compute the un-mixing matrix W and estimate the source signals, Amari et al. used mutual information equation and, after some manipulations, created and proposed Infomax algorithm which is composed of the following steps:

1. Initialize $W(0)$ (e.g. random)
2. $W(t+1) = W(t) + \eta(t)\ (I - f(Y)Y^T)\ W(t)$
3. If not converged, repeat the process starting from the second step

where t represents a given approximation step,$\eta(t)$ a general function that specifies the size of the steps for the un-mixing matrix updates (usually an exponential function or a constant), $f(Y)$ a non-linear function usually chosen according to the type of distribution (super or sub-Gaussian), I the identity matrix and T the transpose operator.

C

ICASSO

An important problem of most ICA algorithms used for components estimation is that they are stochastic: their results may be somewhat different in the different runs of the algorithm. In fact the basic principle of ICA algorithms is to start in some initial point and find out a point in which the cost function is locally minimized. Depending on the initial point, the algorithm will find different local minima. Thus for a chosen ICA algorithm, the outputs of a single run should be interpreted with some reserve. Therefore it is reasonable to run the estimation algorithm many times, using different initial points, and assessing which of the components are found in almost every run: this has been implemented in ICASSO.

It is a software package developed by Himberg et Al. [37] with the aim to investigate the ICA reliability analysis. It is based on estimating a large number of candidate independent components by running a chosen ICA algorithm (for example FastICA) many times, and visualizing their clustering in the signal space. Each estimated independent component is one point in the signal space. If an independent component is reliable, ideally every run of the algorithm should produce one point in the signal space that is very close to the real component. So, reliable independent components correspond to clusters that are small and well separated from the rest of the estimates, unreliable components correspond to points which do not belong to any cluster. ICASSO consists of the following

steps:

1. Parameters for the ICA estimation algorithm are selected. For example in case of FastICA algorithm, the orthogonalization approach (symmetric or deflationary) and the non-linearity are chosen.

2. ICA algorithm is run a chosen number of times. Each time, the data is bootstrapped and/or the initial point of the optimization is changed. In the first case the initial condition for the run of the algorithm is kept the same in every run, but the data is re-sampled by bootstrapping every time. In the latter one the algorithm is run M times for the same data, so that for each run the algorithm starts from a new random initial condition.

3. The estimated components are clustered according to their mutual similarities. As default the agglomerative clustering with average-linkage criterion is selected.

4. The clustering is visualized as a 2-D plot. The user investigates how the estimates are concentrated in the clusters. The clustering of the estimated components is expected to yield information on the reliability of estimation. A compact, tight cluster emerges when a similar estimate is repeatedly obtained despite the randomization. The user can examine the quality of the clusters and rank them accordingly.

5. The user can retrieve the estimates belonging to certain clusters for further analysis and visualization.

Regarding the third step, the agglomeration method produces as output the tree-like hierarchy or dendrogram, which is intuitively appealing in the sense that all clusters implied by lower levels of the tree are always subsets of clusters at the higher levels.
To direct the attention of the user to those clusters that seem to be the most compact and interesting, a cluster quality index Iq is created during this step: it reflects the compactness and isolation of a cluster.
It is computed as the difference between the average intra-cluster similarities and

average inter-cluster similarities, and its expression is the following:

$$I_q(C_m) = \frac{1}{|C_m|^2} \sum_{i,j \in C_m} \sigma_{ij} - \frac{1}{|C_m| \ |C_{-m}|} \sum_{i \in C_m} \sum_{j \in C_{-m}} \sigma_{ij}\sigma_{ij} \qquad \text{(C.1)}$$

where C represents the indices set of all the estimated components, C_m and C_{-m} are respectively the set of indices belonging and not belonging to the m-th cluster, $|C_m|$ is size of the m-th cluster.

References

[1] J. D. Power, "Spurious but systematic correlations in functional connectivity mri networks arise from subject motion." *NeuroImage*, vol. 59, no. 3, pp. 2142–2154, 2012.

[2] L. Griffanti, G. Salimi-Khorshidi, and C. Beckmann et Al., "Ica-based artefact removal and accelerated fmri acquisition for improved resting state network imaging." *NeuroImage*, vol. 95, pp. 232–247, 2014.

[3] M. F. Glasser, "Using temporal ica to selectively remove global noise while preserving global signal in functional mri data." *NeuroImage*, vol. 181, pp. 692–717, 2018 Nov.

[4] C. Beckmann, "Probabilistic independent component analysis for functional magnetic resonance imaging." *Trans. Med. Imag.*, vol. 23, no. 2, pp. 137–152, 2004.

[5] Roy and Sherrington, "On the regulation of the blood-supply if the brain." *Journal of Physiology*, 1890.

[6] S. Ogawa, "Brain magnetic resonance imaging with contrast dependent on blood oxygenation." *Proceedings of the National Academy of Sciences of the United States of America*, vol. 87, pp. 9868–9872, 1990.

[7] B. Biswal, F. Yetkin, V. Haughton, and J. Hyde, "Functional connectivity in the motor cortex of resting human brain using echo-planar mri." *Magnetic Resonance in Medicine*, vol. 34, pp. 537–541, 1995.

[8] H. Lv and Z. Wang et Al., "Resting-state functional mri: Everything that nonexperts have always wanted to know." *AJNR Am J Neuroradiol*, vol. 39, no. 8, pp. 1390–1399, 2018.

[9] M. D. Fox and M. Corbetta et Al., "Spontaneous neuronal activity distinguishes human dorsal and ventral attention systems." *Proceedings of the National Academy of Sciences*, vol. 103, no. 26, pp. 10 046–10 051, 2006.

[10] J. L. Vincent and I. Kahn et Al., "Evidence for a frontoparietal control system revealed by intrinsic functional connectivity," *Journal of Neurophysiology*, vol. 100, no. 6, pp. 3328–3342, 2008.

[11] D. Tomasi and N. D. Volkow, "Functional connectivity density mapping," *Proceedings of the National Academy of Sciences*, vol. 107, no. 21, pp. 9885–9890, 2010.

[12] J. Hérault and B. Ans, "Circuits neuronaux à synapses modifiables : décodage de messages composites par apprentissage non supervisé." *C.-R. de l'Académie des Sciences*, pp. 525–528, 1984.

[13] J. Hérault, C. Jutten, and B. Ans, "Détection de grandeurs primitives dans un message composite par une architecture de calcul neuromimétique en apprentissage non supervisé." *Actes du Xème colloque GRETSI*, 1985.

[14] V. Kiviniemi, J.-H. Kantola, and J. Jauhiainen et Al., "Independent component analysis of nondeterministicfmri signal sources." *Neuroimage*, vol. 19, pp. 253–260, 2003.

[15] C. Caballero-Gaudesa and R. C. Reynolds, "Methods for cleaning the bold fmri signal," *NeuroImage*, vol. 154, pp. 128–149, 2017.

[16] L. Griffanti, O. Dipasquale, and M. Lagana' et Al., "Effective artifact removal in resting state fmri data improves detection of dmn functional connectivity alteration in alzheimer's disease," *Frontiers in Human Neuroscience*, vol. 9, p. 449, 2015.

[17] Bijsterbosch, "Introduction to resting state fmri functional connectivity." *Oxford Univ*, 2017.

[18] M. A. Graya and L. Minati et Al., "Physiological recordings: Basic concepts and implementation during functional magnetic resonance imaging," *Neuroimage*, vol. 47, pp. 1105–1115, 2009.

[19] M. Zaitsev, J. Maclaren, and M. Herbst, "Motion artifacts in mri: A complexproblem with many partial solutions," *Jouranl of Magnetic Resonance Imaging*, vol. 42, pp. 887–901, 2015.

[20] K. Friston and S. Williams et Al., "Movement-related effects in fmri time-series," *Magnetic Resonance in Medicine*, vol. 35, no. 3, pp. 346–355, 1996.

[21] J. D. Power, "Recent progress and outstanding issues in motion correction in resting state fmri." *NeuroImage*, vol. 105, p. 536–551, 2015.

[22] R. Pruim, M. Mennes, J. Buitelaar, and C. Beckmann, "Evaluation of ica-aroma and alternative strategies for motion artifact removal in resting state fmri." *NeuroImage*, vol. 112, pp. 278–287, 2015.

[23] B. B. Avants, "A reproducible evaluation of ants similarity metric performance in brain image registration." *NeuroImage*, vol. 54, no. 3, pp. 2033–2044, Feb 2011.

[24] Smith, "Advances in functional and structural mr image analysis and implementation as fsl," *NeuroImage*, vol. 23, no. 2, p. 208–219, 2004.

[25] A. Yushkevich, J. Piven, C. Hazlett, R. Smith, S. Ho, J. J. Gee, and G. Gerig, "User-guided 3d active contour segmentation of anatomical structures: Significantly improved efficiency and reliability." *NeuroImage*, vol. 31, no. 3, pp. 1116–28, 2006.

[26] V. Fonov, A. C. Evans, K. Botteron, and C. R. Almli et Al., "Unbiased average age-appropriate atlases for pediatric studies." *Neuroimage*, vol. 54, no. 1, pp. 313–327, 2011.

[27] M. Jenkinson, C. F. Beckmann, and T. E. Behrens et Al., "Fsl." *NeuroImage*, vol. 62, pp. 782–790, 2012.

[28] E. A. Allen, "Tracking whole-brain connectivity dynamics in the resting state." *Cerebral Cortex*, vol. 24, no. 3, pp. 663–676, 2012.

[29] L. Griffanti, "Hand classification of fmri ica noise components." *NeuroImage*, vol. 154, pp. 188–205, 2017.

[30] A. Hyvärinen, "Independent component analysis: Algorithms and applications. neural networks." *Neural Networks*, vol. 13, no. 4-5, pp. 411–430, 2000.

[31] Hyvarinen, "A fast fixed-point algorithm for independent component analysis." *Neural Computation*, vol. 9, no. 7, pp. 1483–1492, 1997.

[32] V. Calhoun, "Spatial and temporal independent component analysis of functional mri data containing a pair of task-related waveforms." *Human Brain Mapping*, vol. 13, no. 1, pp. 43–53, 2001.

[33] "https://fsl.fmrib.ox.ac.uk/fsl/fslwiki."

[34] Z. Ge, "Process data analytics via probabilistic latent variable models: A tutorial review." *Industrial Engineering Chemistry Research*, vol. 57, pp. 12 646–12 661, 2018.

[35] "http://mialab.mrn.org/software/gift."

[36] Glasser, "A multi-modal parcellation of human cerebral cortex." *Nature*, vol. 536, no. 7615, pp. 171–178, 2016.

[37] H. J., "Validating the independent components of neuroimaging time series via clustering and visualization." *NeuroImage*, vol. 22, no. 3, pp. 1214–1222, 2004.

[38] C. Liu, J. JaJa, and L. Pessoa, "Leica: Laplacian eigenmaps for group ica decomposition of fmri data," *NeuroImage*, vol. 169, pp. 363–373, 2018.

[39] V. D. Calhoun, "A review of group ica for fmri data and ica for joint inference of imaging, genetic, and erp data." *NeuroImage*, vol. 45, pp. 163–172, 2009.

[40] "http://mialab.mrn.org/software/gift/docs/v4.0b_gica_manual.pdf."

[41] R. Fisher, "Statistical methods for research workers." 1928.

[42] Y. Du, "Comparison of iva and gig-ica in brain functional network estimation using fmri data." *Front. Neurosci.*, vol. 11, p. 267, 2017.

[43] Y. Benjamini and Y. Hochberg, "Controlling the false discovery rate: A practical and powerful approach to multiple testing." *Journal of the Royal Statistical Society B.*, vol. 57, no. 1, pp. 289–300, 1995.

[44] J. D. Power, "Temporal ica has not properly separated global fmri signals: a comment on glasser et al., 2018," *Neuroimage*, vol. 197, pp. 650–651, 2019.

[45] J. Jonathan D Power, M. Plitt, and T. Laumann et al., "Sources and implications of whole-brain fmri signals in humans." *Neuroimage*, vol. 146, pp. 609–625, 2017.

[46] R. Birn, J. Diamond, and M. Smith et Al., "Separating respiratory-variation related fluctuations from neuronal-activity related fluctuations in fmri." *Neuroimage*, vol. 31, pp. 1536–1548, 2006.

[47] R. Birn, M. Smith, T. Jones, and P. Bandettini, "The respiration response function: the temporal dynamics of fmri signal fluctuations related to changes in respiration." *Neuroimage*, vol. 40, pp. 644–654, 2008.

[48] J. Jonathan D Power, M. Plitt, and S. Gotts et al., "Ridding fmri data of motion-related influences: Removal of signals with distinct spatial and physical bases in multiecho data." *Proc Natl Acad Sci*, vol. 115, pp. 2105–2114, 2018.

[49] M. Glasser, T. Coalson, J. Bijsterbosch, and S. Harrison et al., "Classification of temporal ica components for separating global noise from fmri data: Reply to power," *Neuroimage*, 2019.

[50] Amari, "A new learning algorithm for blind signal separation." *Advances in Neural Information Processing Systems*, vol. 8, pp. 757–763, 1996.